UNIVERSITY OF THESSALY

SCHOOL OF ENGINEERING

DEPARTMENT OF MECHANICAL ENGINEERING

EXTREMUM SEEKING CONTROL FOR TRAFFIC CONGESTION CONTROL

by

AMORGIANOS PANAGIOTIS-SPYRIDON

Submitted in partial fulfillment of the requirements for the degree of Diploma
in Mechanical Engineering at the University of Thessaly

Volos, 2022

Approved by the Committee on Final Examination:

Advisor	Dr. Konstantinos Ampountolas, Associate Professor, Department of Mechanical Engineering, University of Thessaly
Member	Dr. Dimitrios Pantelis, Professor, Department of Mechanical Engineering, University of Thessaly
Member	Dr. Costas Papadimitriou, Professor, Department of Mechanical Engineering, University of Thessaly

Date Approved: [09/26/2022]

Acknowledgements

Firstly, I would like to thank my professor Dr. Konstantinos Ampountolas for being helpful and inspiring throughout all this valuable time he offered on my effort. I would like to thank my dear friends Tasos, Mike and Chara for being by my side in every way I needed them, all this time I was conducting my thesis.I would like to specially thank my mother and father, without whose guidance and support I would not be here.

EXTREMUM SEEKING CONTROL FOR TRAFFIC CONGESTION CONTROL

AMORGIANOS PANAGIOTIS-SPYRIDON

Department of Mechanical Engineering, University of Thessaly,2022

Supervisor: Dr Konstantinos Ampountolas
Associate Professor

Abstract

Urban traffic light control is a challenging problem that emerged the recent years, concerning many researchers all over the world. Inefficient traffic light control may lead to congestion phenomena which impact severely not only the economy but also the environment and peoples' health. Controlling a traffic network system efficiently, is an arduous task since the system is governed by unknown varying dynamics, disturbances are sudden and sometimes unmeasurable, and measurements obtained are subject to high noise. Extremum Seeking is an adaptive control technique that does not require a model or any a priori knowledge of the system's dynamics, therefore it is suitable for application on a traffic network. In this thesis, Extremum Seeking is utilized in an open loop scheme to estimate the unknown prevailing critical occupancy, that maximizes the system's throughput. This estimate is destined to be utilized from a perimeter controller as its reference set point. The proposed scheme is simulated with real data exhibiting a Network Fundamental Diagram (NFD), which were collected from the Central Business District (CBD) of Chania.

Key words: Network Fundamental Diagram (NFD), Extremum Seeking Control (ESC), Perimeter Controller

ΕΛΕΓΧΟΣ ΕΥΡΕΣΗΣ ΑΚΡΟΤΑΤΟΥ ΓΙΑ ΕΛΕΓΧΟ ΚΥΚΛΟΦΟΡΙΑΚΗΣ ΣΥΜΦΟΡΗΣΗΣ

ΑΜΟΡΓΙΑΝΟΣ ΠΑΝΑΓΙΩΤΗΣ-ΣΠΥΡΙΔΩΝ

Τμήμα Μηχανολόγων Μηχανικών, Πανεπιστήμιο Θεσσαλίας, 2022

Επιβλέπων Καθηγητής: Δρ. Κωνσταντινος Αμπουντωλας
Αναπληρωτής Καθηγητής

Περίληψη

Ο έλεγχος των αστικών φωτεινών σηματοδοτών είναι ένα δύσκολο πρόβλημα που εμφανίστηκε τα τελευταία χρόνια και απασχολεί πολλούς ερευνητές σε όλο τον κόσμο. Ο αναποτελεσματικός έλεγχος των φωτεινών σηματοδοτών μπορεί να οδηγήσει σε φαινόμενα κυκλοφοριακής συμφόρησης που επηρεάζουν σοβαρά όχι μόνο την οικονομία αλλά και το περιβάλλον και την υγεία των ανθρώπων. Ο αποτελεσματικός έλεγχος ενός συστήματος κυκλοφοριακού δικτύου είναι ένα δύσκολο έργο, δεδομένου ότι το σύστημα διέπεται από άγνωστη μεταβαλλόμενη δυναμική, οι διαταραχές είναι ξαφνικές και μερικές φορές μη μετρήσιμες και οι μετρήσεις που λαμβάνονται υπόκεινται σε υψηλό θόρυβο. Ο Ελεγχος Ευρεσης Ακροτατου είναι μια προσαρμοστική τεχνική ελέγχου που δεν απαιτεί μοντέλο ή οποιαδήποτε εκ των προτέρων γνώση της δυναμικής του συστήματος, επομένως είναι κατάλληλη για εφαρμογή σε ένα δίκτυο κυκλοφορίας. Στην παρούσα διατριβή, ο Ελεγχος Ευρεσης Ακροτατου χρησιμοποιείται σε ένα σύστημα ανοικτού βρόχου για την εκτίμηση της άγνωστης επικρατούσας κρίσιμης πληρότητας, η οποία μεγιστοποιεί την απόδοση του συστήματος. Αυτή η εκτίμηση προορίζεται να χρησιμοποιηθεί από έναν περιμετρικό ελεγκτή ως σημείο αναφοράς του. Το προτεινόμενο σύστημα προσομοιώνεται με πραγματικά δεδομένα που παρουσιάζουν ένα θεμελιώδες διάγραμμα δικτύου (NFD), τα οποία συλλέχθηκαν από την κεντρική επιχειρηματική περιοχή των Χανίων.

CONTENTS

TABLE OF FIGURES

1. INTRODUCTION

1.1 Motivation

Urban transportation is essential to contemporary civilization, yet it confronts mounting challenges due to rising population density and automobile ownership. Multiple major cities experience traffic congestion, which is affecting many domains of our society, including being costly. Cities are becoming hotter while transportation times for people and commodities are larger than they could be, because of the saturation of urban networks or even of some crucial parts of them. According to [1] in 1994, traffic congestion in several large urban areas of the United States had already cost an average of US$640 per driver per year due to transportation delays. Moreover, driving delays lead to higher emissions of carbon dioxide and particulate matter such as fine particles ($PM_{2.5}$), which impacts severely the environment and the people. In [2] the authors suggest that a $10\,{}^{\mu g}/_{m^3}$ raise in ($PM_{2.5}$) levels originating from vehicles' combustion engines, caused a 3.4% raise in day-to-day mortality while, authors in [3] suggest that, extended exposure to fine particles ($PM_{2.5}$) can cause atherosclerosis, thrombosis, and vascular remodeling. The issues stated above could be diminished by decreasing the traffic congestion in urban areas. This thesis aims at contributing to the solution of this problem, by proposing Extremum Seeking Control as an estimation algorithm that seeks, online, for the optimal occupancy value of the network. This estimation is then actuated by a perimeter controller.

1.2 Introduction to Literature Review

1.2.1 Traffic Congestion Problem

The traffic congestion problem has been attempted to be solved following several approaches. A slower time-scale approach focuses on infrastructure's further development. Expansion of road networks aim at increasing the networks' capacity in vehicles, but as modern cities become more densely populated, it is becoming an increasingly sophisticated and expensive venture. Nonetheless, expansion of road networks is challenging and needs proper research and planning. The Pigou-Knight-Downs paradox, as described in [1], suggests that, increasing road's capacity in vehicles can attract more drivers, thus failing to avoid the congested regime. Therefore, this approach needs to be investigated thoroughly in terms of its effect on travel times before its implementation is decided. Building infrastructure is necessary, but it shall be accompanied by sophisticated traffic light controller programs, to utilize its potential.

Numerous researchers have been investigating how traffic light controllers can tackle the problem of underutilization of the existing infrastructure. Urban traffic light controllers' purpose is to ensure that collisions between conflicting flows are avoided, while Travel Time Spent (TTS) and Total Travel Distance (TTD), are minimized and maximized, respectively. Efficient traffic light control systems can be of great benefit towards a network's performance, without long time construction requirements and at a relatively low cost. Because a traffic network of an entire city

is a very complex dynamical system which is usually disturbed by unexpected events (e.g., creation of bottleneck due to collided vehicles), a pre-fixed signal plan is not able to maintain good performance and avoid congestion. Therefore, researchers over the last years focused on online, model or non-model-based traffic light controllers such as: Perimeter Control [4],[5], SCATS [6], and self-organizing traffic lights (SOTL) [7]. Perimeter Control, through which, this thesis addresses the traffic congestion problem, is a traffic light controller relied upon the existence of a Network Fundamental Diagram (NFD) within a protected area. Essentially, a Perimeter Controller, adjusts the accumulation of vehicles inside the network, towards a reference set point, in which the (NFD) exhibits maximum flow. The controller can achieve it by regulating, the percentage of vehicles waiting at the entrance links, that will finally enter the protected area. The optimal accumulation of vehicles of an NFD is subject to various unpredictable factors, making the a priori selection of a reference set point inefficient. This problem drastically calls for an adaptive control technique, resetting, in real-time the critical occupancy value, by utilizing sensor measurements of flow and occupancy. In [8], a Kalman filter-based estimation algorithm is proposed to tackle this problem, while in this Thesis, an Extremum Seeking algorithm is proposed for estimating the critical occupancy.

1.2.2 Extremum Seeking Control

Extremum seeking control is an adaptive, model-free technique dating back in 1922 [9], making it the first adaptive control technique developed. It attracted researchers' interest mainly after its stability guarantees, proven in 2000 in [10]. Extremum Seeking Control is a perturb and observe method, where an excitation signal is perturbing the input with an additive sinusoid, and then it observes the objective criterion's output to estimate the gradient. The next step of the algorithm is headed towards the extremum and is proportional to the estimated gradient. The scheme's purpose is to seek for the gradient of an extremum (which is zero), thus minimizing or maximizing the objective function. It has been utilized to control numerous applications of hard-to-model systems, such as: Anti-lock Braking System (ABS) [11],[12], Maximum Power Point Tracking (MPPT) of Photovoltaics [13] and Wind Energy Conversion Systems (WECS) [14],[15] while it has even been applied on an industrial scale, on a biochemical wastewater treatment process called CANON [16], or to minimize the thermoacoustic pressure oscillations of industrial combustors [9]. Finally, Extremum Seeking has also been proposed to control traffic lights in [17] and [18]. See Chapter 3, for a general overview of ESC's methodology.

1.3 Thesis Organization

The rest of this thesis is divided into four chapters, from Chapter 2 to 5.

Chapter 2 covers literature review, beginning from ESC's background and evolution throughout the last century. Then, a thorough investigation of ESC's applications and modifications is presented.

In Chapter 3 the theory and methodology of Extremum Seeking Control as well as of its generalization, Slope Seeking Control, are presented

Chapter 4 is divided into two parts. The first part, from Chapter 4.1 to Chapter 4.4 contains a series of Numerical examples beginning with a simple application of ESC to an LTI system and an application of SSC to an LTI system. Then ESC is applied to an LTV system without input and output dynamics and in 4.3.2 an example with input and output dynamics, inspired by the benchmark example of Krstic in [9], is presented. In 4.4, a uni-cycle model is modeled on Simulink in order to simulate the Antilock Braking System with an Extremum Seeker. In 4.5, ESC is utilized as an estimation algorithm firstly for seven static objective functions (one for each day of the week) and then on an open loop scheme, estimating the critical occupancy values based on data collected from the CBD network of Chania.

The conclusions of this study are presented in Chapter 5, accompanied by propositions for further investigation of the topic.

2. LITERATURE REVIEW

In this chapter, a literature review of Extremum Seeking is presented. At first ESC's background and evolution are presented beginning from Leblanc in 1922 [9], up until its proof of convergence from Krstic and Wang in [10], and the latest breakthroughs concerning the method. Then, follows a presentation of various applications for which ESC has been utilized, industrial or not, but also various extensions of the original scheme that were mostly proposed the years following its mathematical underpinning [10]. Finally, an analysis is performed on the work of Kutadinata, [17] where an augmented ESC scheme is applied to three distinct traffic light controllers (Perimeter controller, SCATS, SOTL). This is the first work ever, to implement ES on urban traffic light controllers, and it has showcased promising results.

2.1 Background

Extremum Seeking Control (ESC) (or peak seeking) is an Adaptive Control, model-free technique which dates back at 1922 [9] and is considered as the first method of adaptive control. The decades following its "birth" Extremum Seeking Control (ESC) has not been a significant pole of attraction for the scientific community up until the 1940s. Researchers in the USSR made significant steps towards its development but under the shadow of the 2nd world war these works remained untranslated and were only available in Russian, therefore the International Control Community was not particularly attracted at the time. A little later, in the 1950s Extremum Seeking Control experienced its revival through some outstanding works such as the publication of Draper and Li in 1951 cited in [16], in which the nowadays called "classical" Perturbation Based-Extremum Seeking Control method was utilized in order to maximize the power output of an airplane's combustion engine. The proposed scheme is seeking for the optimal ignition timing of the engine which maximizes the output in real-time, while the system is subject to uncertainties, varying conditions and disturbances. This work has been cited by plenty of Control researchers [16] as the work that brought back the interest of the Control community by highlighting ESC's efficiency as a non-model-based technique. Combined with the increasing complexity of engineering problems, ESC started to attract researchers again in the 1960s, and there were even published books (some of them exclusively) about extremum seeking such as [19], and others which are cited in [9]. These two decades the scientific community proposed many new schemes and applied them in numerous problems, thus expanding the available information on ESC. Despite this, the researchers' interest shifted towards model reference adaptive control methods and ESC went through a dormant period for the following years up until the work of Krstić and Wang [10]. The proof of local convergence in [10] encouraged researchers to study and publish about ESC, therefore widening the spectrum of its variations. Perturbation Based-Extremum Seeking Control (PESC), Slope Seeking Control [9], Sliding Mode Based Extremum Seeking Control [20] and Lyapunov-based Extremum Seeking Control [21] are some of the variations proposed by researchers the last years.

2.2 Applications

Extremum-Seeking has been applied to many complex systems since it comes with ease of implementation and guaranteed convergence with the only restriction that the dynamics be open-loop stable. To begin with, ESC has been widely used and researched for implementation on Wind Energy Conversion Systems (WECSs) in [14], [15], [20], [22], and on arrays of solar panels in [13], [23], as a Maximum Power Point Tracking (MPPT) method aiming at maximization of the power output compared to the theoretical maximum. Another popular application of ESC is on Anti-lock Braking Systems (ABS), which may be the most widely known of its applications, with numerous extensions and novel schemes proposed such as those in [9], [24], [11], [12] all with the purpose of avoiding slipping under hard braking conditions and thus retaining the vehicle's controllability. Moreover, ESC has been applied to Mode-Locked fiber lasers by Brunton, Fu and Kutz in [25]. In order to provide maximum energy pulses, a multi-parameter Extremum Seeking Control algorithm is utilized for tuning four optical components which in their turn they will maximize a properly designated objective function. The objective function introduced is the raw energy output divided by the kurtosis of the pulse spectrum, so that the algorithm favors coherent energy solutions. Simulations results suggested that the proposed scheme can track the required tuning that maximizes the objective function even though it is subject to significant disturbances from the fiber Birefringence. In [26], an ESC algorithm is proposed to control a thermal environment in real time. Model based techniques for buildings climate control are costly and require too much effort both to design and construct them but also to frequently update the models to compensate for the uncertainties arising such as weather changes or activities inside the building with thermal imprint. For the reasons stated above, the authors in [26] chose to address this issue via perturbation-based ESC which is a model-free method, suitable for hard-to-model cases. The simulations conducted, confirmed that ESC is efficient in controlling thermal environments since it does not have the drawbacks of model-based techniques. Many researchers have published work on engines' optimization performance via ESC such as in [27] where the authors propose an ESC scheme aiming at maximum fuel efficiency, which is approximated by cylinder pressure sensors, by adjusting the spark timing online. Another interesting approach to the fuel efficiency problem is the one proposed in [28] where the authors employ an objective function primarily based on brake specific fuel consumption (BSFC) estimations in order to achieve maximum efficiency with respect to a set of emission constraints. The conducted experiments on a Euro-VI heavy-duty truck engine suggest that the proposed scheme is robust enough to withstand real world disturbances while optimizing the fuel efficiency with respect to the imposed emission levels. In [29], the authors applied three extremum seeking control schemes in fuel cell hybrid electric vehicles to reduce hydrogen consumption by retaining the system's operating point within the high efficiency region. A first order Extremum Seeker, a high pass filter-based Extremum Seeker and a bandpass filter-based Extremum Seeker were scrutinized. They were all found to track the optimum operation point of the system with respect to the battery's constrained conditions, and to dynamically adapt the output power, so that the battery's state of charge is retained in an a priori

set range. The proposed schemes' performance was evaluated through experimental implementation. Other applications of ESC, include minimum power demand formation flights [9], optimization of aircraft control [30] and maximization of compressor pressure rise [9]. In [31] ESC was utilized for maintaining desired illumination levels, while optimizing the energy consumption in hybrid lighting offices, in [32] for control of Tokamaks, tuning a fractional order PI controller in [33], biochemical wastewater treatment process in [16] and even optimal function of an ellipsoidal trajectory orientation using muscle effort in [34].

2.2.1 Bioreactors

ESC has been applied in bioreactors for a mass structured cell population balance [16] ,[35]. The underlying dynamics of this process are governed by a nonlinear partial integral-differential equation bounded by a nonlinear condition accounting for the cell population growth and a nonlinear ordinary integral-differential equation describing the substrate consumption. In this case the controlled input is the feed substrate concentration through which the algorithm steers the input value towards the desired set point that maximizes the value of a cell density objective function. A Lyapunov-based Extremum Seeking Control technique is proposed in order to estimate the unknown state and to track the unknown optimum value. The Lyapunov function and the design parameters are selected in such manner that a persistent of excitation condition is satisfied and it has also been shown mathematically that the proposed ESC scheme guarantees exponential convergence to within a small region of the system's maximum cell density.

2.2.2 Solar Panels and Photovoltaics

Extremum seeking Control has been also applied to an array of solar panels in [36], in order to track the optimizing power condition for which the output power is maximized. In this application the input is the set current which is adjusted in order to track the maximum power point. The proposed ES controller, instead of utilizing, the classical in ES, perturbation by injection of sinusoidal signal, it perturbs the input using the inverter ripple. Simulations were conducted, applying this novel, ripple-based Extremum Seeking scheme to experimental data, obtained from a rooftop in Princeton, NJ and it was shown that even in days where the irradiance follows an unpredictable trajectory, because of the partially shaded conditions (clouds covering the sun etc.), the proposed ESC scheme manages to track down the theoretical maximum power point very efficiently and thus it is achieving real time convergence to the optimal output for the solar panels array.

The control of solar panels array has been also approached through a Lyapunov based switching scheme in [16], [21]. While the traditional ESC scheme enters a region of the optimal value without converging to the optimal point itself, the Lyapunov based switching scheme (Lyap-ES) on the other hand converges to the optimal value by exponentially decaying the perturbation signal since the system has reached to a small region around the extremum. Thus, the Lyap-ES addresses one of the main challenges of traditional extremum seeking which is the elimination of the limit cycle and the convergence to the extremum point itself, asymptotically. The proposed scheme is applied to the maximum power point tracking (MPPT) problem in photovoltaics, and it has been assessed via simulation by utilizing experimentally measured environmental data. From the simulation results, it derives that Lyap-ES produces larger energy conversion efficiencies than the common MPPT methods.

Another challenge that has retrieved from studying the maximum power point tracking (MPPT) for solar arrays is the existence of suboptimal solutions. The reference-to-output map may not have only one Global maximum power point (GMPP) but also some local maximum power points (LMPP). The global MPP is the one the algorithm should track in order to achieve the maximum feasible power output. In [13], the author proposes a new perturbed based Extremum seeking control (PESC) scheme which is able to avoid getting stuck in one of many local maximum power points (LMPP) as opposed to most of the common MPP tracking algorithms that haven been proposed in the past decades. The (PESC) scheme proposed utilizes a feedforward control of the dither gain according to the 1st derivative of the photovoltaic power. Unlike other schemes the one proposed in [13] detects and tracks the GMPP in one step, thus increasing its tracking speed. Moreover, while the system is on steady-state regime, an outstanding 99.9% (and higher) accuracy is achieved with this technique. The simulation results under partially shaded conditions indicate that the proposed (GPESC) scheme can efficiently be applied to maximize the power output of a photovoltaics array.

2.2.3 Wind Energy Conversion Systems

Wind energy conversion systems (WECS) have also been approached by extremum seeking based Maximum Power Point Tracking (MPPT) methods in different variations. Similarly, to the photovoltaics (MPPT) approach, in (WECS), the algorithm's purpose is to keep the system's operating point at the neighborhood of the optimal Power Coefficient C_p value by controlling the tip speed ratio λ, which is the ratio between the speed of the blade tips and the wind speed. In [22], the authors implement the MPPT method for the output maximization problem in wind energy system but instead of utilizing the perturbation based ESC in its classical form, the wind turbulence is employed as search disturbance. The phase lag between the normalized signals C_p and λ, which are obtained from measurements of the electrical power, the wind speed and the rotational speed, are utilized to define the actual distance between the current operating point and the maximum point of the $C_p(\lambda)$ curve. This is achieved by computing the Fast Fourier Transform (FFT) of both signals and thus, after the phase information is extracted, the mean phase lag $\theta(t)$ is computed. Simulations were conducted in the partially loaded region for a wide range of wind speed. The proposed scheme is efficient even though there is lack of information about the plant's dynamics. Because of that, there are no guarantees that the scheme will be able to converge to the optimal λ_{opt} and therefore eliminate the steady-state error. What makes the proposed scheme attractive is the absence of information about the system's parameters and state and that the input's variations are slow, thus minimizing the fatigue of the mechanical components and extending their life expectancy.

As it was observed in [22], the proposed ESC scheme was sensitive to wind speed fluctuations and more specifically the method seemed to be less effective for low turbulence levels. Later, in [37] it was shown that plain ESC algorithms are not robust enough when implemented in Wind Energy Conversion Systems (WECS). The algorithm climbs very slowly towards the optimum when there is low wind speed, while it climbs abruptly when the wind speed is higher. The authors' proposition in [37] for counter measuring this problem was a saturation nonlinearity in order to moderate the effect of the wind speed fluctuations. The same problem was also approached in [14] where the author proposed a simple but efficient modification. Instead of using the power output feedback,

the logarithm of the power output is employed as the feedback. In contrast to the proposition in [37], the logarithmic power feedback does not require additional tuning. As it is stated in [14], when the logarithm of the power is used, the relevant slope is independent of the wind. Simulations were conducted for both power feedback and log-of-power feedback and were based on a simple differential equation model. The results support the proposed theory, since the ESC algorithm with log-of-power feedback produced almost identical settling times for all three wind speeds simulated. Therefore, the modified ESC scheme is more robust to wind speed and presents consistent performance.

In [15], the author proposed a new MPPT method for WECS which does not demand sensor measurements of the wind's or tip's speeds. This method utilizes only the voltage and the current as its parameters. The method is particularly attractive because, unlike most MPPT methods, it tracks the maximum power point of WECSs and not of their wind turbines therefore the output power of WECS is maximized. The proposed technique was simulated, and the results indicated small convergence time and efficiency of more than 98.5%.

2.2.4 Anti-lock Braking System

Finally, one of the most well-known and deeply investigated applications of extremum seeking control is the Anti-lock braking system (ABS). ABS is a crucial active safety component for passenger vehicles that has been widely employed in numerous car models since Mario Palazzetti, Giancarlo Michellone and Giovanni Tabasso invented the modern ABS system for automotives in 1971 in the Fiat Research Center [38]. Nonetheless, its ancestor, the Dunlop Maxaret anti-skid braking system was introduced in the early 1950s and had been broadly utilized in the British aviation.

The braking process' performance depends on countless varying factors such as the vehicle's speed, the applied braking pressure, the condition of the wheels, the road's surface and the friction between them. Most of those factors cannot be measured by the vehicle or any of its sensors and therefore they compose a nonlinear process with high uncertainty. The purpose of the Anti-lock braking system is to prevent the wheels from lockups and skidding in slippery conditions which would not only decrease the deceleration of the vehicle, but it would also make the steering of it under heavy breaking situations impossible. Therefore, the objective of the ABS scheme is to maximize the friction coefficient which is proportional to the friction force or in other words minimize the stopping distance. The input this system needs to extremize in order to achieve maximization of the objective function is the wheel slip λ. The ABS has been approached in numerous forms besides the traditional Extremum Seeking Control [9]. From the work of [39] about tyre dynamics it has been revealed that for varying external inputs, the force response of the tire presents a time lag. Because ABS controllers command very abruptly the brakes and therefore the tyres, such an impact must be taken seriously into consideration. A response to that has been given in [12] where two different time anticipation methods are embedded in a modified five phase Anti-lock braking algorithm. Both the open-loop pressure steps and the Pressure derivative profiles compensate for the time delays at a satisfying degree as shown in the experimental results. Another study in [11], confronts the undesirable drop in lateral tyre forces that appears while the system attempts to maximize the breaking forces. In order to address this issue, the algorithm is adjusted so that it analyzes the steering input information to determine the operational zone of the search

algorithm. Simulations were conducted for both the modified ABS algorithm which enhances the lateral stability and for the ABS algorithm which only prevents the longitudinal slip. The comparison between them showed that the enhanced scheme has a slightly larger stopping time, however the vehicle's lateral stability has improved significantly thus offering the vehicle enhanced capability of turning under abrupt braking situations. Moreover, the extremum seeking control scheme without steady-state oscillation (ESCWSSO) which has been proposed in [24] was applied in Anti-lock braking system and was compared to the traditional perturbation-based ESC scheme and sliding-mode-based ESC scheme. The simulation results showed that under the same circumstances the proposed scheme behaved more efficiently by stopping the vehicle within the shortest time. Although the sliding-mode-based scheme reached higher braking torque than the proposed scheme, it appeared very large oscillations which call for higher requirements on actuators.

2.3 ESC for traffic congestion

Extremum Seeking Control has also been utilized for tuning or estimating parameters of three types of traffic light controllers in [17], modified as a Nash Equilibrium Seeking scheme. The road network in this work, is considered as a non-cooperative game, where the agents are the intersections, or neighborhoods (set of neighboring intersections) whose purpose is to solely maximize their own output ignoring the system's overall performance. Meaning, that an agent may command increased external flow to alleviate the congestion locally (maximize its performance measure), thus, possibly creating congestion to a neighboring agent. Nonetheless, the author manages to ease the task of assigning frequencies to each intersection compared to [40], where the authors proposed a Nash Equilibrium Seeking scheme which required unique frequency for each agent. Instead, the author of [17], exploited the decaying effect that a road network (in accordance with many physical systems) exhibits spatially, by re-using dither frequency signals to agents far enough from each other in order to reduce the system's computational load while making the assigning task easier. The proposed scheme was combined with Perimeter Controller [4],[5], SCATS [6], and self-organizing traffic lights (SOTL) [7] and they were simulated on SUMO in a simple handmade road network. In the perimeter controller's case, the internal network's intersections are governed by SOTL, which was shown in [6], to homogenize the region in terms of congestion, therefore exhibiting a robust NFD. Simulations results, shown a significant increase in performance compared to the controllers working on pre-set, fixed parameters, especially for the perimeter controller which showcased an impressive performance enhancement of 29%.

3. METHODOLOGY

In this chapter, the theory and methodology of the Perturbation Based Extremum Seeking Control (PESC) are investigated. A common ESC block diagram is presented, as well as the analytical proof of convergence for the linear time invariant case. Then, a generalization of the method, called Slope Seeking Control (SSC) is presented and analyzed together with its corresponding block diagram. In SSC, instead of seeking for the extremum, the method tracks the gradient it is commanded to seek. An intuitive analysis of how the method works (PESC and its generalization SSC) also takes place in this Chapter.

3.1 Perturbation Based – Extremum Seeking Control

Perturbation based Extremum Seeking Control (PESC) is the foundation of Extremum Seeking Control (ESC) by being its classical and most common method. It was introduced from Leblanc in order to optimize the power transfer from an overhead power - line to a train. It has been studied for many years since then and it has been tested in many applications. It relies on a sinusoid to perturb the system's input and in some cases this sinusoidal excitation can as well be an already existing disturbance of the plant. Then, the controller observes the corresponding output and decides whether the input was perturbed towards the direction that extremizes the output. If that is

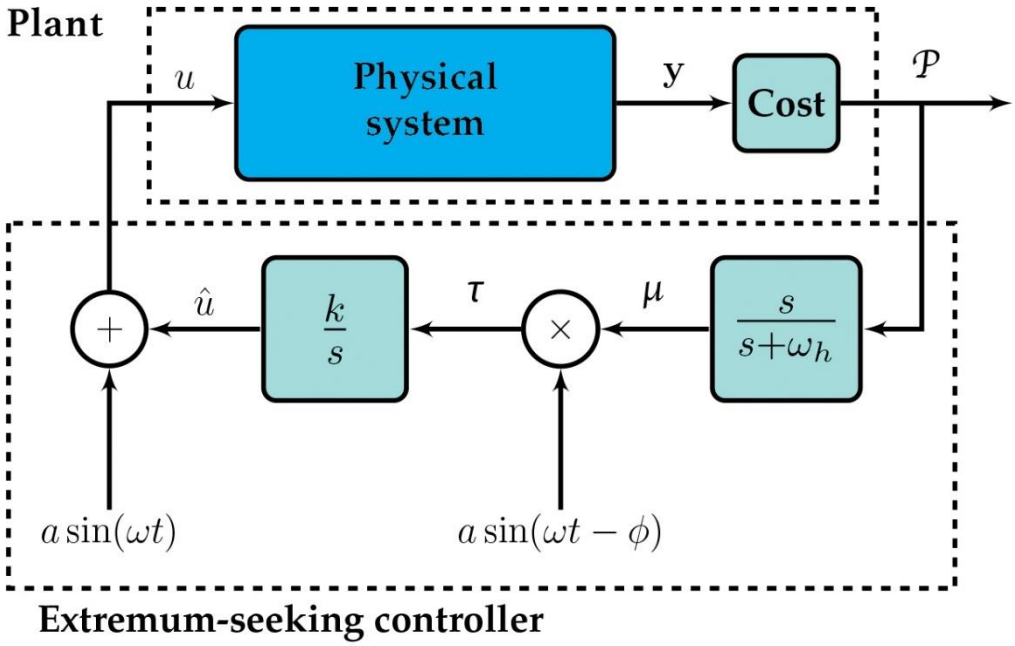

Figure 3. 1:Extremum Seeking Control block diagram

the case, the next step will also be to that direction, and it will be proportional to the estimated gradient of the objective function for the current operating input value. Otherwise, the algorithm is steered to the opposite direction with a step, again, proportional to the estimated gradient. Extremum Seeking is an Adaptive control method which tracks the extremum (maximum or

minimum) of an objective function P. The values of the cost function P are usually provided by some sensor measurements however the final value of P depends on the input signal and the underlying dynamics. A common extremum seeking control block diagram is shown in Figure (3.1).

The purpose of the Extremum Seeking Control scheme is to minimize (or maximize) a quadratic objective function. Under Taylor's approximation, any C^2 function can be approximated locally by eqn.

$$P(u) = P^* + \frac{P''}{2}(u - u^*)^2 \quad (3.1.1)$$

Where, for $P'' > 0$ negative integration gain $k < 0$ is selected, while for $P'' < 0$, positive $k > 0$ is selected. Overall, the scheme's purpose is to track the optimal value u^* for which the objective function is optimized. $\hat{u}$ stands for the estimate of the unknown variable u^*. A sinusoidal perturbation is added to $\hat{u}$ resulting in signal u

$$u = \hat{u} + asin\omega t \quad (3.1.2)$$

Signal u passes through the plant resulting in a cost function P which is oscillating, around some mean value (the current operating point).

$$P(u) = P^* + \frac{P''}{2}(\hat{u} + asin\omega t - u^*) \quad (3.1.3)$$

The output P is passing through a washout high-pass filter resulting in a zero mean output perturbation (signal μ) by excluding the mean Direct current component. A representation of a simple high-pass filter in the frequency domain follows:

$$HPF = \frac{s}{s + \omega_h} \quad (3.1.4)$$

Where, s is the Laplace variable and ω_h is the filter cutoff frequency

Thus, the information about the objective function's gradient has already been separated from the DC component of the map, $P^*(u)$.The high-pass filer is not required but it enhances the scheme's performance [30] therefore it is included.

The high-pass filtered signal μ is then demodulated by a sinusoidal perturbation which might as well be phase-shifted. Multiplication of signal μ with the input sinusoid results in signal τ

$$\tau = \alpha \sin(\omega t - \Phi)\,\mu \quad (3.1.5)$$

It is noted that when the input signal is greater than the optimal value $u > u^*$, the output perturbation is out of phase thus resulting in a mostly negative signal τ which drags the input u towards the extremum. If the input signal is smaller than the optimal value $u < u^*$, the output

perturbation, colored red, is in phase and the produced signal τ is mostly positive as shown in Figure (3.2).

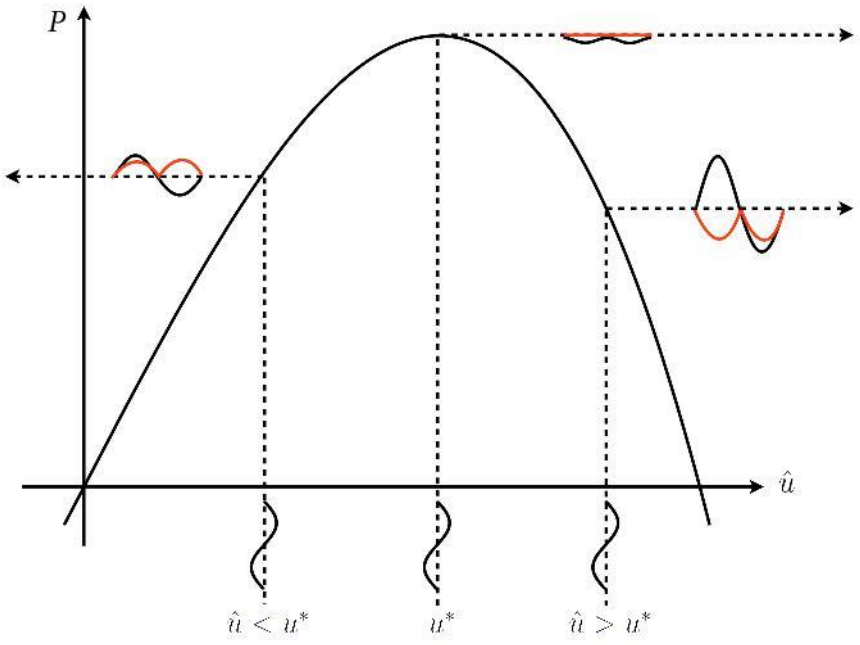

Figure 3. 2: Schematic illustrating extremum-seeking control acting on a static quadratic criterion P(u).

Signal τ essentially estimates the gradients of the objective function in the current operating point and thus steer the algorithm towards the optimal value rapidly when the gradient is larger and slower when the gradient is smaller. This can easily be noticed for plants with constant dynamics, where the cost function P is only a function of the input signal u. Substituting, equation (3.1.2) in the cost function P gives

$$P(u) = P(\hat{u} + \text{asin}(\omega t)) \quad (3.1.6a)$$

Assuming that perturbation amplitude a is small and expanding the cost function $P(u)$ to the perturbation amplitude, yields.

$$P(u) = P(\hat{u}) + \left.\frac{\partial P}{\partial u}\right|_{u=\hat{u}} \cdot \text{asin}(\omega t) + O(a^2) \quad (3.1.6b)$$

Averaging signal $\tau = \alpha \sin(\omega t - \Phi)\mu$, and substituting the leading order term in the high pass filtered signal which roughly is $\mu \approx \left.\frac{\partial P}{\partial u}\right|_{u=\hat{u}} \alpha \sin(\omega t)$, over one period yields.

$$\tau_{avg} = \frac{\omega}{2\pi} \int_0^{\frac{2\pi}{\omega}} \alpha \sin(\omega t - \Phi) \cdot \mu \, dt \quad (3.1.7a)$$

$$\tau_{avg} = \frac{\omega}{2\pi}\int_{0}^{\frac{2\pi}{\omega}} \frac{\partial P}{\partial u}\Big|_{u=\hat{u}} \alpha^2 \sin(\omega t - \Phi)\cdot \sin(\omega t) \quad (3.1.7b)$$

$$\tau_{avg} = \frac{a^2}{2}\cdot \frac{\partial P}{\partial u}\Big|_{u=\hat{u}} \cos(\Phi) \quad (3.1.7c)$$

Therefore, it is easy to comprehend that in the case of plants with constant dynamics, the average signal τ_{avg} is proportional to the slope of the cost function *P* with respect to the input signal u.

The demodulated signal τ is then passing through an integrator block. Integration of signal τ results in $\hat{u}$ which is the best estimate of the optimal value u^* which maximizes (or minimizes) the objective function P.

$$\frac{d\hat{u}}{dt} = k\tau \quad (3.1.8)$$

Where k, is the integration gain. Integration gain determines how rapidly the actuation rises. However, selecting exceedingly high integration gain values may disrupt the scheme's stability.

In this section the proof of convergence of the perturbation based ES scheme for a static map is presented as in [9]. In order to perform the proof, the objective of the ES scheme is restated as the minimization of the estimation error denoted as:

$$\tilde{u} = u^* - \hat{u} \quad (3.1.9a)$$

$$\hat{u} = u^* + \tilde{u} \quad (3.1.9b)$$

Substituting equation (3.1.9b) into (3.1.2) gives

$$u - u^* = \text{asin}(\omega t) - \tilde{u} \quad (3.1.10)$$

Substituting equation (3.1.10) into (3.1.1) gives

$$P = P^* + \frac{P''}{2}(\tilde{u} - \text{asin}(\omega t))^2 \quad (3.1.11)$$

Expanding the squared term gives

$$P = P^* + \frac{P''}{2}\left(\tilde{u}^2 - 2\tilde{u}\cdot \text{asin}(\omega t) + a^2 sin^2(\omega t)\right) \quad (3.1.12a)$$

$$P = P^* + \frac{P''}{2}\tilde{u}^2 - P''\tilde{u}\cdot \text{asin}(\omega t) + \frac{P''}{2}a^2 sin^2(\omega t) \quad (3.1.12b)$$

Implementing the trigonometric identity $2sin^2(\omega t) = 1 - \cos(2\omega t)$ in equation (3.1.12) gives

$$P = P^* + \frac{P''}{4}a^2 + \frac{P''}{2}\tilde{u}^2 - aP''\tilde{u}\sin(\omega t) - \frac{P''}{4}a^2\cos(2\omega t) \quad (3.1.13)$$

Following the sequence of the block diagram of Figure (3.1), output signal P passes through the high pass filter. The Direct current terms, which in this case are the first two terms on the right side of equation (3.13), are removed by the high pass filter, thus giving

$$\frac{s}{s+\omega_h}[P] \approx \frac{P''}{2}\tilde{u}^2 - aP''\tilde{u}\sin(\omega t) - \frac{P''}{4}a^2\cos(2\omega t) \quad (3.1.14)$$

The high pass filtered signal is then multiplied by $\sin(\omega t)$ (Φ=0) giving

$$\tau \approx \frac{P''}{2}\tilde{u}^2\sin(\omega t) - aP''\tilde{u}\cdot sin^2(\omega t) - \frac{P''}{4}a^2\cos(2\omega t)\sin(\omega t) \quad (3.1.15)$$

Applying the following trigonometric identities

$$2sin^2(\omega t) = 1 - \cos(2\omega t) \text{ and } 2\cos(2\omega t)\sin(\omega t) = \sin(3\omega t) - \sin(\omega t)$$

gives

$$\tau \approx -a\frac{P''}{2}\tilde{u} + a\frac{P''}{2}\tilde{u}\cdot\cos(2\omega t) + a^2\frac{P''}{8}(\sin(\omega t) - \sin(3\omega t)) + \frac{P''}{2}\tilde{u}^2\sin(\omega t) \quad (3.1.16)$$

Since the plant is static, u^* is constant. Therefore,

$$\dot{\tilde{u}} = -\dot{\hat{u}} \quad (3.1.17)$$

The integration gives

$$\hat{u} \approx -\frac{k}{s}\tau \quad (3.1.18)$$

Substituting equations (3.1.16) and (3.1.17) in (3.1.18), one gets

$$\tilde{u} \approx \frac{k}{s}\left[-a\frac{P''}{2}\tilde{u} + a\frac{P''}{2}\tilde{u}\cdot\cos(2\omega t) + a^2\frac{P''}{8}(\sin(\omega t) - \sin(3\omega t)) + \frac{P''}{2}\tilde{u}^2\sin(\omega t)\right] \quad (3.1.19)$$

Since the conducted analysis is local, the last term which is quadratic in $\tilde{u}$ is neglected, thus giving

$$\tilde{u} \approx \frac{k}{s}\left[-a\frac{P''}{2}\tilde{u} + a\frac{P''}{2}\tilde{u}\cdot\cos(2\omega t) + a^2\frac{P''}{8}(\sin(\omega t) - \sin(3\omega t))\right] \quad (3.1.20)$$

The last two terms of the equation (3.1.20) are high frequency signals which are "attenuated" through integration. Therefore, they are neglected, giving

$$\dot{\tilde{u}} \approx -\frac{ka}{2}P''\tilde{u} \quad (3.1.21)$$

Where $kP'' > 0$, thus making the system stable.

3.2 Perturbation Based – Slope Seeking Control

Slope Seeking essentially is a generalization of the classical Extremum Seeking Control. In ESC the set slope of the objective function that the algorithm tracks, is the gradient of an extremum which is zero. However, on some applications operating on the extremum point, in presence of finite disturbances can destabilize the system, therefore the algorithm is commanded to track a non-zero gradient.

In the basic slope seeking scheme, a sinusoidal signal is added to the best estimate of the optimizing value $\hat{u}$ and the resulting signal passes through the plant as shown in Figure (3.3). The output of the plant is filtered by a high-pass filter and the resulting signal is multiplied by a sinusoid (demodulation) in order to extract the operating gradient information. Then, the reference slope is added to the demodulated signal and the output is integrated into $\hat{u}$. In the special case where the reference slope added is zero the algorithm tracks the extremum of the objective function.

Under Taylor's approximation, any C^2 function can be approximated locally by the following equation:

$$P = P^* + P'_{ref}(u - u^*) + \frac{P''}{2}(u - u^*)^2 \quad (3.2.1)$$

Where P'_{ref} is the gradient of the objective function in which the system is forced to operate at. For $P'' > 0$ we have negative integration gain $k < 0$, while for $P'' < 0$ we have positive $k > 0$. From Theorem 3.1 of [9] we know that the output error $y - P^*$ converges exponentially to an $O(a + \frac{1}{\omega})$ neighborhood of the origin given that: perturbation frequency ω is large enough and $\frac{1}{1+L(s)}$ is asymptotically stable

Where,

$$L(s) = \frac{kaP''}{2s} \quad (3.2.2)$$

and

$$r(P'_{ref}) = -\frac{aP'_{ref}}{2} Re\{\frac{j\omega}{j\omega + h}\} \quad (3.2.3)$$

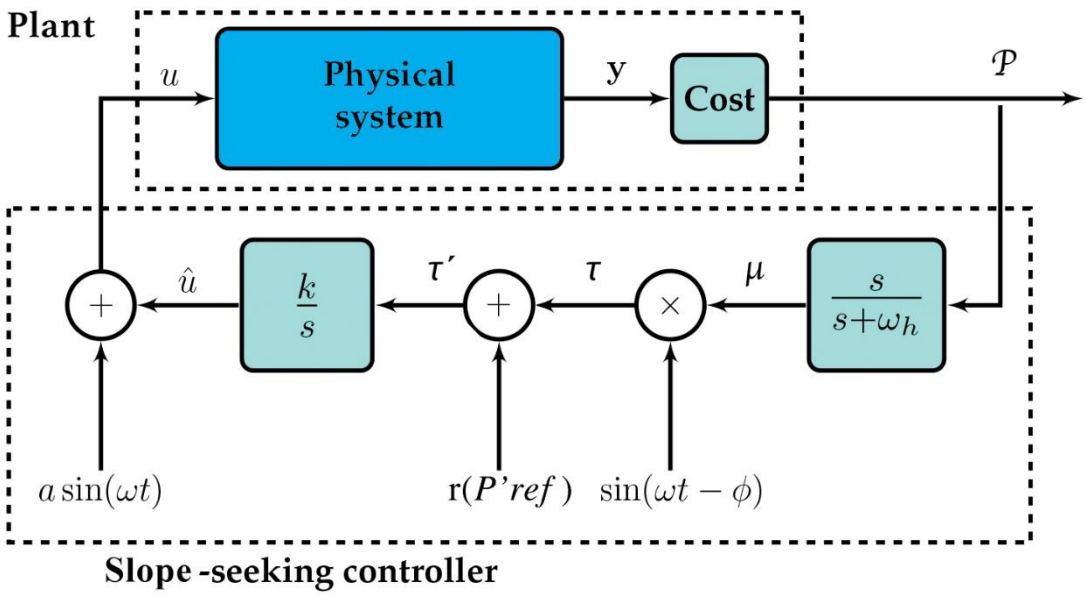

Figure 3. 3:Slope Seeking Control block diagram

4. APPLICATIONS

Simulation examples were conducted for both, the linear time invariant (LTI) and linear time variant (LTV) cases, showing the scheme's ability to track the optimal value even when it varies with time. Then, a generalization of the extremum seeking control, called slope seeking is presented accompanied by a simulation example. Then, a benchmark theoretical example of extremum seeking acting on a system with linear time variant dynamics is presented. Finally, the extremum seeking control technique is applied to the anti-lock braking system (ABS) of a unicycle vehicle model in order to track the optimum slip value that maximizes deceleration.

4.1 Extremum Seeking Control on LTI system

In this section the algorithm is demonstrated for a simple static quadratic cost function (the simplest possible problem) in order to showcase its function. By implementing the extremum seeking algorithm, the cost function's maximum is tracked. The quadratic objective function considered is the following:

$$P(u) = 60 - (4 - u)^2$$

Function P has a global maximum at $u^* = 4$, giving $P(u^*) = 60$. Extremum Seeking Control is applied with $u = 0$ as the initial value of the variable under optimization. Nonetheless the convergence of the proposed scheme is guaranteed, and it is independent of the initially selected value of u since there is only one extremum. Initial values of u furtherer from the optimal value prolong the convergence time. Perturbation amplitude is selected as $a = 0.2$ so that the peek seeking scheme's error, $y - P^*$ achieves local exponential convergence to within an $O(a^2 + \frac{1}{\omega^2})$ neighborhood of the origin, under Theorem 1.1 of [9]. Larger perturbation amplitude would result in larger residual error and faster tracking of the optimum value whilst smaller perturbation amplitudes would need more time to achieve convergence to an even smaller neighborhood of the optimum. Roughly speaking, the "accuracy" of the convergence and the fast tracking of the optimum are two antagonizing components that one should take into consideration while selecting the perturbation amplitude. Integration gain k is also controlling the speed of convergence thus it can compensate for the lack of "speed" that may be induced by the small amplitude. Therefore, integration gain is selected as $k = 3$. The perturbation frequency ω governs the distinction between the time scales of the integrator's estimation process and the additive and multiplicative perturbation's gradient estimation process. Sufficiently large frequencies, achieve more accurate slope estimation and less impact of the perturbations produced by higher order harmonics and the DC component $f(\theta^*)$. Therefore, perturbation frequency is selected as $\omega = 10Hz$, thus providing higher precision measurements of the gradient P' while being qualitatively large relative to the other design parameters (k, a, h, P''). As shown in [9] ω could even be a little larger than the plant time constants. The washout frequency of the high-pass filter should not be larger than ω in order

to attenuate the DC component in y, while the slope estimation $P'(u)$ passes through uncorrupted. A second order Butterworth high pass filter, with a cutoff frequency of $h = 2Hz$ is employed, so that only the output oscillations are passing. The simulation's results are plotted in Figure (4.1). The objective function P is oscillating while rising from 40 to 60 for about 3 seconds. It is essential to notice that although the actuation signal u is oscillating with an amplitude a throughout the entire simulation, the output signal is oscillating intensely when the input u is far from u^*, while the output perturbation is almost zero when the objective function reaches its peak. The ESC scheme manages to climb rapidly to the peak of the cost function and presents small deviations once it reaches the optimum value (as it was expected from the averaging analysis of signal τ).

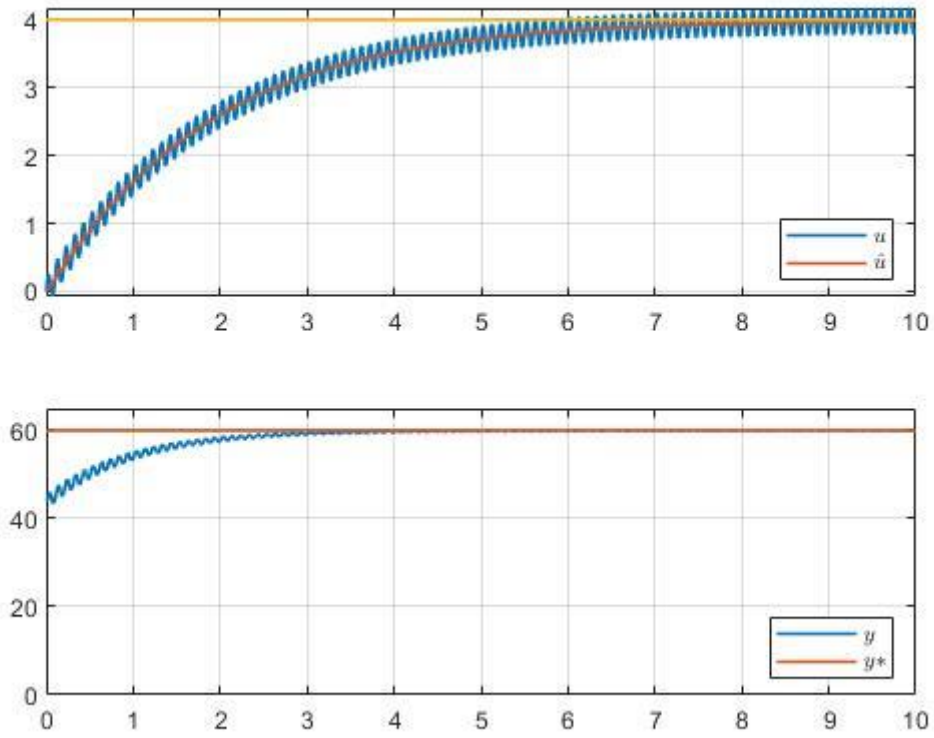

Figure 4. 1: Extremum Seeking Control response with a static objective function P(u)

The Butterworth filter was introduced by the British physicist and engineer Stephen Butterworth in 1930 in [41]. Butterworth filters have a maximally flat frequency response in the passband. The magnitude expression of a Butterworth high pass filter is:

$$|H(j\omega)| \triangleq \frac{1}{\sqrt{1+\omega^{2n}}} \quad (4.1.1)$$

Where ω is the angular frequency of the input signal to the high pass filter, and n is a positive integer, referring to the order of the corresponding filter. Assuming transfer function $H(s)$ is a rational function with real coefficients and rearranging gives:

$$|H(j\omega)|^2 = \frac{1}{1+\omega^{2n}} \quad (4.1.2)$$

Using the identity:

$$s = j\omega \leftrightarrow \omega = \frac{s}{j}$$

Gives:

$$H(s)H(-s) = \frac{1}{1+(\frac{s}{j})^{2n}} \quad (4.1.3)$$

Where $H(s)$ is the transfer function. The poles of equation (4.1.3) are given by:

$$s_k = e^{j2\pi\frac{2k+n+1}{4n}} \qquad , k \in \{0,1,\dots 2n-1\}$$

All these poles are points of the unit circle, $\frac{\pi}{n} rad$ apart from each other. Looking back at equation (4.1.3) it is evident that when the factor $H(s)$ has a root, the factor $H(s)$ has a root in the negative location. For a stable filter to be designed, it is necessary that $H(s)$ has all the poles in the left half of the s-plane. Stable poles are given by:

$$s_{k,stable} = e^{j2\pi\frac{2k+n+1}{4n}} \qquad , k \in \{0,1,\dots n-1\}$$

Therefore, the transfer function of a Butterworth low-pass filter is given by:

$$\mathrm{H(s)} = \frac{1}{B(s)}$$

Where:

$$B(s)\begin{cases} \prod_{k=0}^{\frac{n}{2}-1}\left(s^2 - 2\cos\left(2\pi\frac{2k+n+1}{4n}\right)s+1\right) & , even\ n \\ (s+1)\prod_{k=0}^{\frac{n-1}{2}-1}\left(s^2 - 2\cos\left(2\pi\frac{2k+n+1}{4n}\right)s+1\right) & , odd\ n \end{cases} \quad (4.1.4)$$

The poles of a high-pass Butterworth filter are given by the same expression as for the low-pass filter. The only difference is that the high-pass filter has n zeros. Its transfer function is given by:

$$H(s) = \frac{s^n}{B(s)}$$

Where $B(s)$ is given by equation (4.1.4), depending on the filter's order.

4.2 Slope Seeking Control on LTI system

Simulation.

An example of the slope seeking scheme acting on a linear time-invariant plant is illustrated here. The following quadratic static objective function is considered:

$$P(u,t) = 50 + (u-4) + (u-4)^2 \quad (4.2.1)$$

where $P'_{ref} = 1$, $u^* = 4$ and $P'' = 2$. We set perturbation frequency $\omega = 5Hz$, amplitude $a = 0.1$, integrator gain $k = 10$, washout high pass filter cutoff frequency $h = 5Hz$, $u = 0$ is selected as the initial guess and slope reference was calculated by substituting the above parameters in equation (3.2.2) thus giving:

$$r(P'_{ref}) = -0.025$$

. Substituting the parameters in $L(s)$ and calculating the poles of the characteristic polynomial $\frac{1}{1+L(s)}$ it is confirmed that the system attains stable gradient seeking.

$$L(s) = \frac{kaP''}{2s} = {}^1\!/_s$$

$$1 + L(s) = 0 \rightarrow s = -1$$

Derivation of equation (4.2.1) gives:

$$P' = -7 + 2u \quad (4.2.2)$$

Solving equation (4.2.2) in terms of u for the commanded slope: $P' = 1$ gives the optimal input value

$$-7 + 2u = 1$$

$$u = 4$$

And the objective function's value for the corresponding slope

$$P(4) = 50$$

The response graphs in figure (4.2) confirms that the system converges to the commanded values.

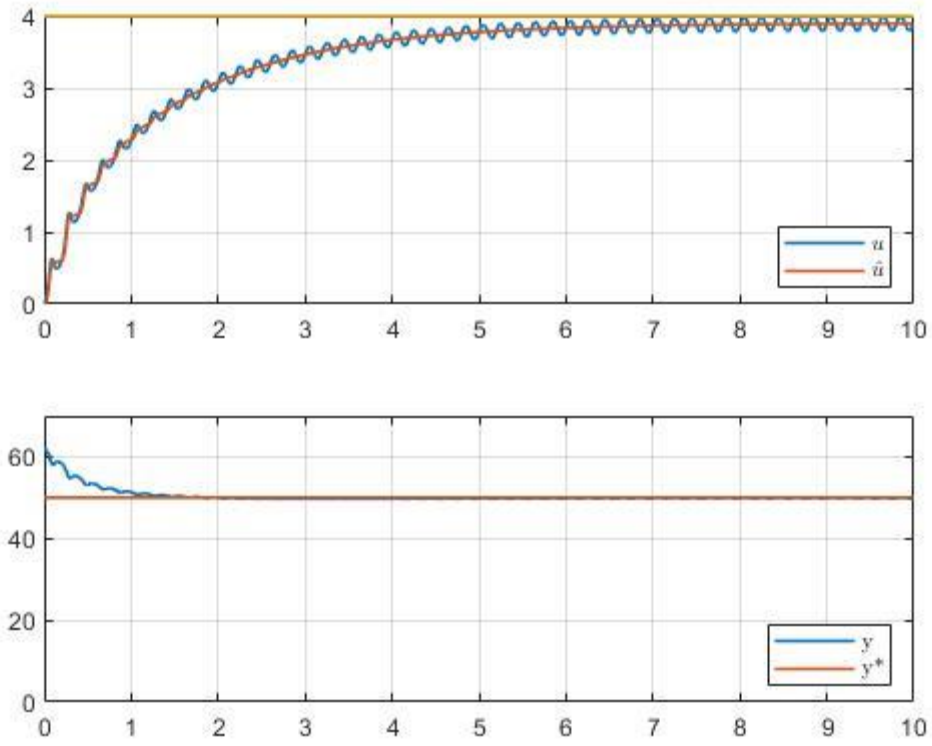

Figure 4. 2: Slope Seeking Control response with a static objective function P(u)

4.3 Extremum Seeking Control on LTV system

4.3.1 ESC on quadratic criterion

In this section the algorithm is employed in a linear time varying system in order to showcase its efficiency and its ability to track time-varying optimal values. Therefore, we consider the following quadratic time-dependent objective function

$$P(u,t) = 60 - \left(10 - u - 2\sin\left(\frac{t}{4}\right)\right)^2$$

The time-varying objective function P has a global maximum at $u^*(t) = 10 - 2\sin(\frac{t}{4})$ giving $P^* = 60$. Since the purpose of the algorithm is to track the varying parameter u^* with u, the perturbation frequency ω should be large enough to be considered fast compared to the varying parameters which oscillate at 1/8π Hz. Thus, perturbation frequency is selected as $\omega = 10$Hz. Since the objective function has one and only extremum, the selection of the initial value of u is

irrelevant with the quadratic function's convergence to the extremum. Therefore $u = 0$ is selected as the initial guess. For initial values furtherer away from the optimal value u^* the time of convergence is increasing. Integration gain is selected as $k = 4$, demodulation amplitude is selected as $A_d = 1$, and modulation amplitude is selected as $A_m = 0.2$. A first order Butterworth high pass filter, with a cutoff frequency of $h = 2$Hz is employed. By conducting the simulation in MATLAB and plotting the response of the extremum seeking control for the proposed dynamic plant it can be easily noticed that the ESC scheme maintains a near optimum performance for the quadratic cost criterion despite the lack of information about the varying parameter. The actuation signal has managed to approximately track the optimum value u^* which is oscillating around $u = 10$ with an amplitude of 2.

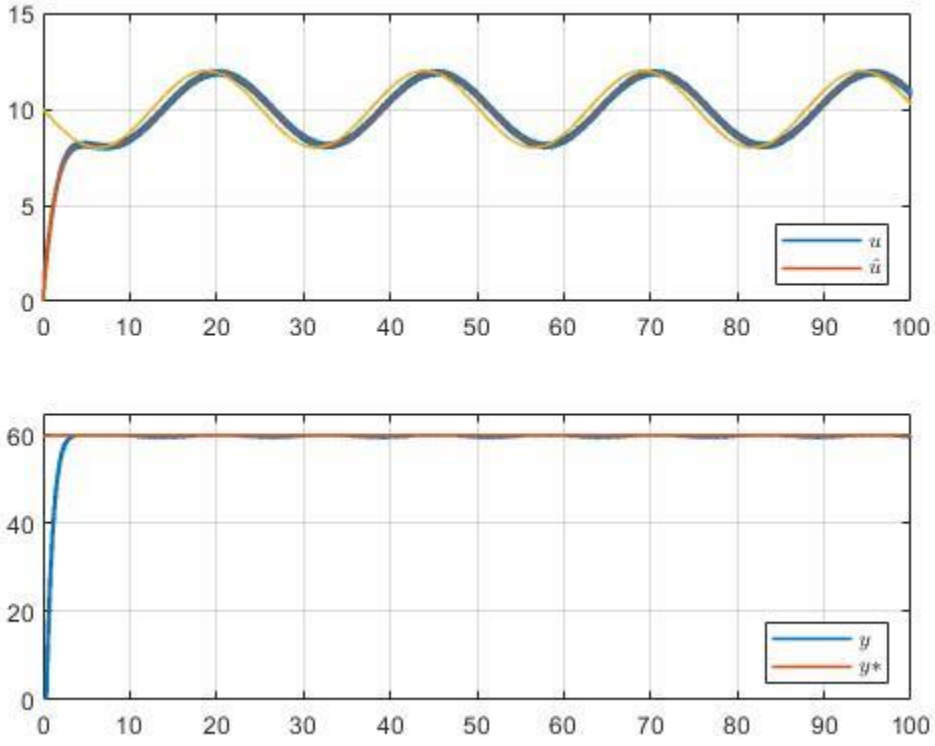

Figure 4. 3: Extremum Seeking Control response with a dynamic objective function P(u)

4.3.2 ESC on quadratic criterion with input/output dynamics

Inspired from example 1.3 as well as the proposed algorithm 1.2.1 in [9], the following rather challenging example is considered. Extremum Seeking Control is implemented on a dynamic plant according to the design algorithm 1.2.1 proposed in [9]. The input dynamics considered have a zero in the right half-plane, making them non-minimum phase dynamics. The product of input and output dynamics $F_i(s)F_o(s)$ has a large relative degree and the optimal values u^* and P^* are time variant, thus making the system difficult to control. Moreover, sensor noise is present in the simulation as a uniformly distributed random signal with minimum, $min = -0.05$, maximum, $max = 0.05$ and sample time, $T = 0.001$.

Input dynamics:

$$F_i(s) = \frac{(s-1)}{s^2 + 3s + 2} = \frac{(s-1)}{(s+2)(s+1)}$$

Output dynamics:

$$F_o(s) = \frac{1}{s+1}$$

Cost function:

$$P(u,t) = P^*(t) + 0.4\big(u - u^*(t)\big)^2$$

Therefore,

$$P'' = 0.2$$

Where:

$$P^*(t) = 0.02 \cdot \delta(t-15)$$

And:

$$u^*(t) = 0.005 \cdot e^{0.02 \cdot t}$$

Implementing the Laplace transform for $P^*(t)$, we arrive at:

$$\lambda_P \Gamma_P(s) = \frac{0.02e^{-15s}}{s}$$

Likewise, for $u^*(t)$ we get:

$$\lambda_u \Gamma_u(s) = \frac{0.005}{s - 0.02}$$

Following the procedure, as presented in algorithm 1.2.1 at [9] we first select perturbation frequency ω large enough and such that $\pm j\omega$ is unequal to any imaginary axis zero of the input dynamics $F_i(s)$. Furthermore, ω should not have the same frequency with any other noise. In case where $\pm j\omega$ is an imaginary axis zero of $F_i(s)$ the plant will remain unaffected from the sinusoidal forcing we implemented. Thus, $\omega = 5\, {rad}/{s}$ is chosen.

The perturbation amplitude α should be large enough to generate observable fluctuations in the plant's output, however large perturbation amplitude produces larger steady state output error $\tilde{y}$. This trade off was fine-tuned via trial and error and was finally set to be $\alpha = 0.05$.

Compensators design

For the compensators design the symbols of the block diagram of Figure (1.2) from [9] are employed.

We use one fast pole in $C_o(s)$ to compensate for the output dynamics $F_o(s)$, since $F_o(s)$ has one slow pole and $F_o(s)$ is strictly proper. If $\Gamma_P(s)$ has zeros that do not have asymptotic stability these zeros should also be used as zeros of $C_o(s)$. Furthermore, the compensator $C_o(s)$ should be designed asymptotically stable. $C_o(s) = \frac{1}{s+5}$ is satisfying the previously stated guidelines and therefore it is selected. Thus, the high-pass filter turns out to be:

$$\frac{C_o(s)}{\Gamma_P} = \frac{s}{s + 5}$$

$C_i(s)$ should be chosen to ensure that $C_i(s)\Gamma_u(s)$ is proper in order to attain robust control. Any poles of $\Gamma_u(s)$ that are not asymptotically stable, should not be utilized as zeros of $C_i(s)$. Finally, $C_i(s)$ should be designed such that:

$$\frac{1}{1 + L(s)}$$

Where:

$$L(s) = \frac{aP''|F_i(j\omega)|}{4} H_i(s)$$

And:

$$H_i(s) = C_i(s)\Gamma_u(s)F_i(s)$$

Attains asymptotic stability.

In order to simplify the design procedure of $C_i(s)$, phase shift of the demodulation sinusoid is taken by:

$$\Phi = -\angle F_i(j\omega)$$

Solving for the parameters above results in:

$$\Phi = -\angle F_i(5j) = 0.7955$$

Compensator C_i is set to be:

$$C_i(s) = s - 4$$

And the "integrator" block is set to be:

$$C_i(s)\Gamma_u(s) = 25\frac{s-4}{s-0.02}$$

Replacing the terms above in the characteristic polynomial gives:

$$L(s) = \frac{0.05 \cdot 0.2|F_i(5j)|}{4} H_i(s) = 0.0025|F_i(5j)|H_i(s)$$

Where:

$$|F_i(5j)| = \left|\frac{5j-1}{15j-23}\right| = \left|\frac{49}{377} - \frac{50}{377}j\right| = \frac{1}{\sqrt{29}} \cong 0.1857$$

And:

$$H_i(s) = \frac{25s^2 - 125s + 100}{s^3 + 2.98s^2 + 1.94s - 0.04}$$

So,

$$L(s) = 0.00046425H_i(s)$$

The roots of $1 + L(s) = 0$ are the poles of the characteristic polynomial:

$$L(s) = -1$$

Multiplying on both sides with the denominator of $H_i(s)$ and rearranging gives the final form of the characteristic equation:

$$s^3 + 2.99160625s^2 + 1.88196875s + 0.006425 = 0$$

The roots of the above equation were given by MATLAB as follows:

$$s_1 = -0.0034$$

$$s_2 = -0.8936$$

$$s_3 = -2.0946$$

Since all three poles have negative real parts, the system attains stable extremum seeking.

The Simulink model built, to simulate the problem stated above is presented in Figure (4.4)

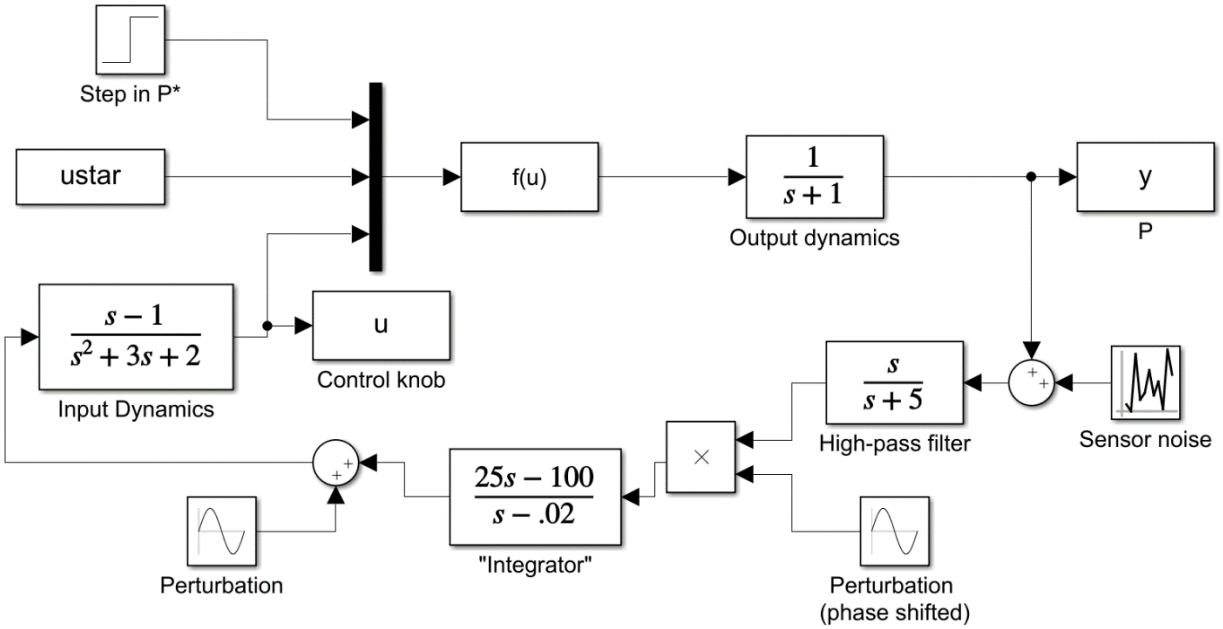

Figure 4. 4: Extremum Seeking Control simulation for a system with non-minimum phase dynamics

The simulation's results are shown in Figure (4.5) and Figure (4.6). Figure (4.5) shows the control variable u which is oscillating about the time variant optimal value u^* with success, thus, producing rapid and precise tracking of the optimal output value y^* as shown in Figure (4.6).

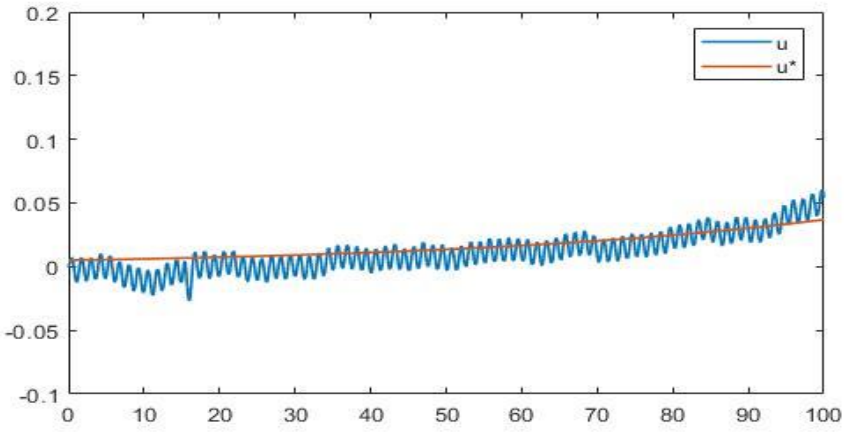

Figure 4. 5: Extremum Seeking Control input response for a system with non-minimum phase dynamics

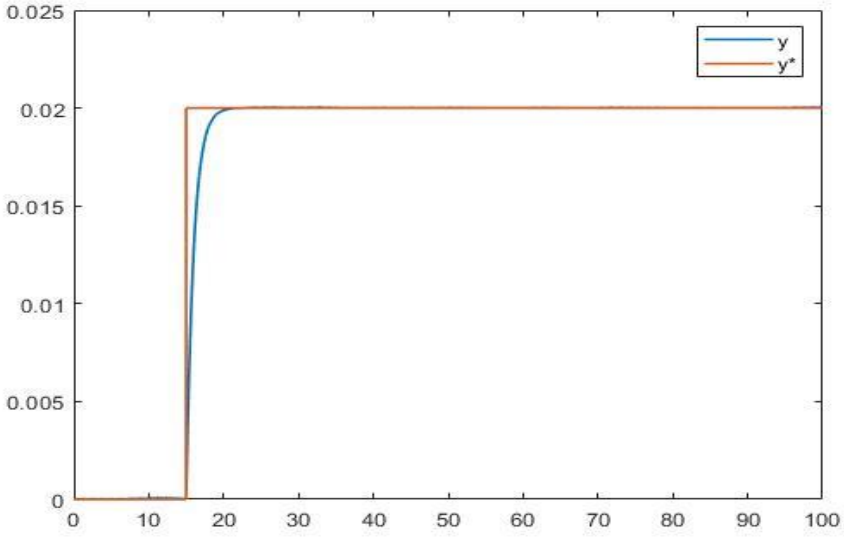

Figure 4. 6: Extremum Seeking Control output response for a system with non-minimum phase dynamics

4.4 Extremum Seeking Control on Anti-lock Braking system

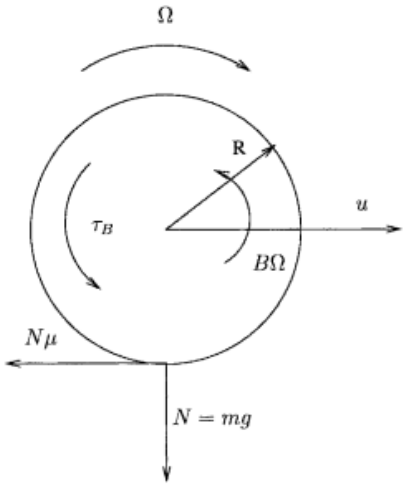

Figure 4. 7: Model of a slipping wheel

We consider a single wheel (the unicycle model) which may be replicated two or four times, to compose a model for a two-wheel or a four-wheel vehicle. Tire dynamics under braking situations are described by the following equations:

$$m\dot{v} = -N\mu(\lambda) \quad (4.4.1)$$

And,

$$I\dot{\omega} = -B\omega + NR\mu(\lambda) \quad (4.4.2)$$

where $N = mg$ is the weight of the wheel, $\dot{\omega}$ is the angular acceleration, $\dot{v}$ is the linear acceleration, R is the wheel's radius, I is the moment of inertia of the wheel, τ_b is the torque from braking, B is the bearing friction torque coefficient, and ω, $\dot{\omega}$ are the wheel's angular velocity and acceleration respectively and $\mu(\lambda)$ the friction force coefficient and the wheel slip ratio denoted as λ are shown in Figure (4.8). A simple function which qualitatively matches the friction force's coefficient is utilized as in [9] for the purpose of simulation.

$$\mu(\lambda) = 2\mu^* \frac{\lambda^* \lambda}{\lambda^{*2} + \lambda^2} \quad (4.4.3)$$

Equation (4.4.3) is shown, for two different wheel slip values in Figure (4.8).

The wheel slip is defined as:

$$\lambda(v, \omega) = \frac{v - R\omega}{v} = 1 - \frac{R\omega}{v} \quad (4.4.4)$$

It is observed that when $R\omega = v$ the wheel slip drops to zero $\lambda(v, v) = 0$ since the tire is not skidding on the road. When the wheel "locks" the angular velocity of the wheel is $\omega = 0$ and therefore wheel slip is $\lambda(v, 0) = 0$. In figure(μ) the friction force coefficient is presented for

various road conditions. It is easily noticed that the friction force coefficient has an extremum (maximum) point μ^* for

some wheel slip value λ^*. The optimum value μ^* is different for every one of the three road conditions of the graph, as well as the optimizing wheel slip value λ^*.

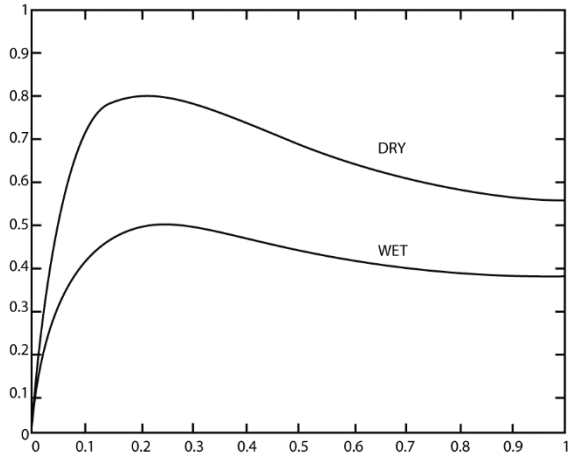

Figure 4. 8: Schematic illustration of Equation 4.4.3 for dry and wet road conditions

To formulate the ABS problem in the extremum seeking control format, let us introduce the relative error $\tilde{\lambda} = \lambda - \lambda_0$ where λ_0 is an unknown constant. The derivative of $\tilde{\lambda}$ gives:

$$\dot{\tilde{\lambda}} = \dot{\lambda} = \left(\frac{R\omega}{v^2} + \frac{mR^2}{Iv}\right)\dot{v} + \frac{RB}{Iv}\omega + \frac{R}{Iv}\tau_b \quad (4.4.5)$$

Since linear acceleration $\dot{u}$ measurements are provided through the accelerometer (which is a sensor commonly used in today's vehicles for triggering airbag inflation), the feedback linearizing controller is formulated as:

$$\tau_b = -\frac{dIv}{R}(\lambda - \lambda_0) - B\omega - \frac{I\omega}{v}\dot{v} - mR\dot{v} \quad (4.4.6)$$

Where d is a positive constant, introduced, for the system (4.4.5) to be exponentially stable.

By rearranging equation (4.4.6) and formulating it into the extremum seeking control a cascade of input dynamics and a static map:

$$-\lambda + \lambda_0 = \frac{1}{d}\dot{\lambda} \quad (4.4.7)$$

$$y = \mu(\lambda) \quad (4.4.8)$$

The Simulink model of the Anti-lock Braking system shown in Figure (4.9), is comprised of four subsystems. The wheel model, shown in Figure (4.10) is built based on the equations (4.4.1) and (4.4.2). The lower saturation limit of the integrator resulting in the linear velocity is set to be zero and it is connected to a "stop simulation" block in order to end the simulation when the vehicle is immobilized. The wheel model calculates the angular velocity, the linear velocity and the linear acceleration (which is measured via accelerometer in real vehicles). Angular and linear velocities

are used from the coefficient of friction subsystem Mi shown in Figure (4.11) in order to calculate the current value of $\mu(\lambda)$ which is then fed back to the wheel model. Linear acceleration is promoted to the Extremum Seeking Control subsystem which is shown in Figure (4.13). By substituting the vertical force N with mass times gravitational acceleration mg in equation (4.4.1) we get $\dot{u}$. Since μ(λ) is the objective function of the problem, $\dot{u}$ is divided with (-g) so that the perturbation-Based Extremum Seeker tracks with λ_0 the optimal slip value λ^*. Signal λ_0 from the ESC subsystem and signals v, $\dot{v}$ and ω from the wheel model subsystem are utilized by the controller according to the equation (4.4.5) as shown in Figure (4.12). This results in the braking torque, which is forwarded to the wheel model, thus completing the control loop.

Simulation Parameters

Two simulations were conducted, both on Simulink. In the first case the optimal wheel slip value is $\lambda^* = 0.2$ and the optimal coefficient of friction is $\mu^* = 0.8$, simulating a dry road, while $\lambda^* = 0.15$ and $\mu^* = 0.5$, are simulating a wet road. Conducting two simulations, enables the investigation to consider a wider spectrum of possible road conditions, while evaluating the algorithm's performance and robustness. The rest of the parameters are common for both cases. The vehicle in the simulation starts braking with an initial linear speed v=33.33m/s and an angular speed of the wheel $w = \frac{v}{R} = 111.11\,{}^{m}/_{s}$. Therefore, the initial value of wheel slip λ is $\lambda = 0$. $\lambda^* = 0.2$ and $\mu^* = 0.8$ are chosen as the optimum values for maximizing the deceleration, the controller's gain is chosen as $d = 1$ and $g = 9.81\,{}^{m}/_{s^2}$ is the gravitational acceleration.

The wheel's parameters are chosen as $m = 400kg$, $B = 0.01$ and $R = 0.3m$, $I = 1.4kgm^2$.

Maximum deceleration for dry road conditions is: $\dot{v} = -\mu g = -7.848$

Maximum deceleration for wet road conditions is $\dot{v} = -4.905$

The ES controller's parameters are chosen as $\omega = 2.7\,{}^{rad}/_{s}$ the frequency of the sinusoidal excitation, integration gain $k = 2$, amplitude of the demodulation sinusoid $A = 1$, amplitude of the additive sinusoid $a = 0.05$ and high pass filter cutoff frequency $p = 2.6\,{}^{rad}/_{s}$. The simulation for dry conditions stopped after $5.88sec$, when the vehicle was immobilized while the simulation for wet conditions stopped after $8.2345sec$. In Figure (4.15) it is shown that the vehicle is immobilized after $117.9m$ in dry conditions, compared to $157.47m$ in wet conditions as shown in Figure (4.19). The Extremum Seekers' output is shown in Figure (4.14) in dry conditions and in Figure (4.18) in wet conditions, with respect to the optimal value λ^* for which the controller has non priori knowledge. Linear velocity together with angular velocity multiplied by the wheel's radius for dry and wet conditions are plotted in Figure (4.16) and in Figure (4.20) respectively. The proposed scheme can track the optimal value that maximizes the friction coefficient sufficiently well in both cases, thus achieving maximum deceleration (minimum acceleration) as shown in both Figure (4.17) and Figure (4.21). Therefore, the proposed scheme seems robust enough to track the unknown varying parameter λ_0, despite its unpredictable behavior.

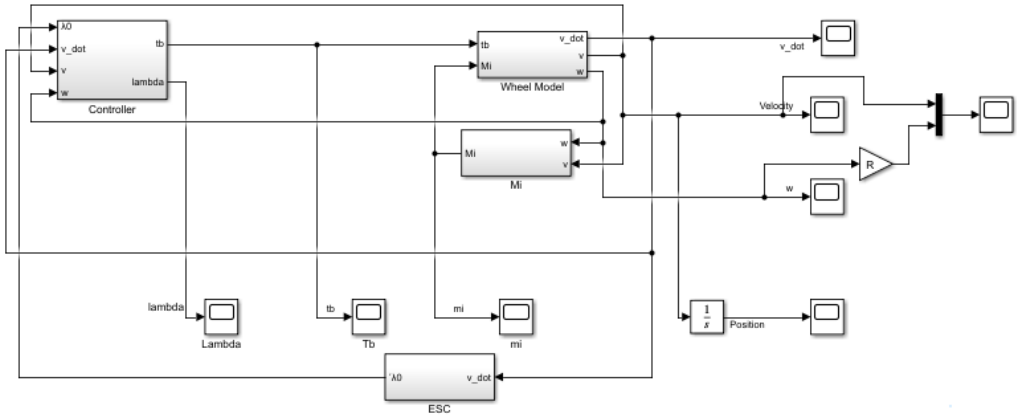

Figure 4. 9: Simulink model of Anti-lock Braking system

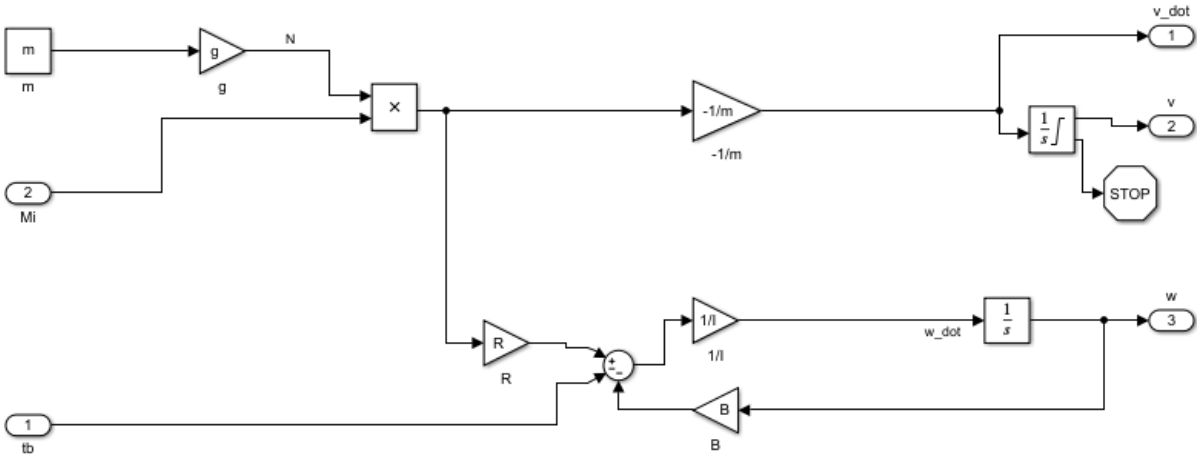

Figure 4. 10: Wheel sub-model

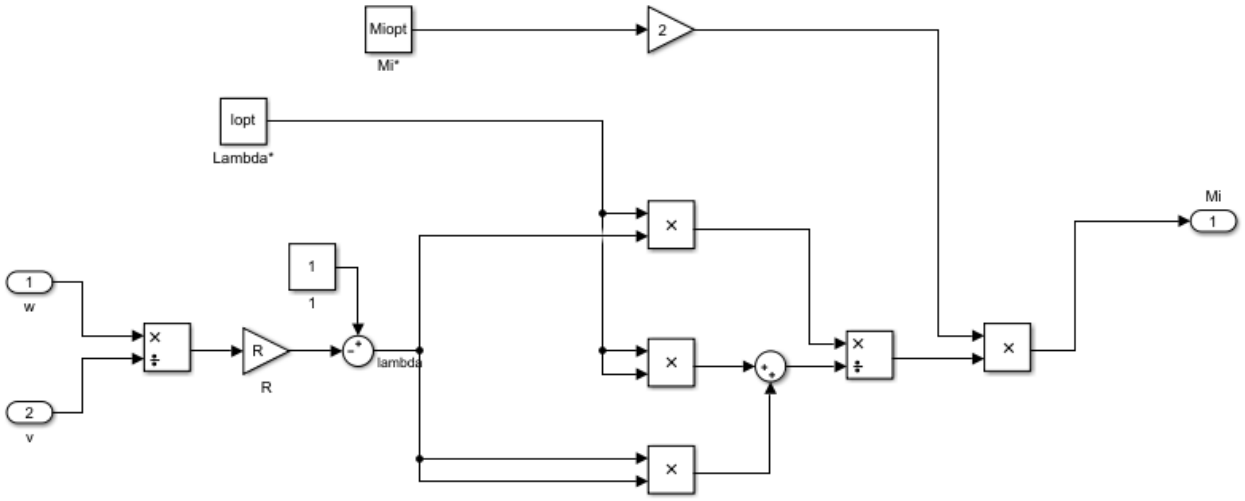

Figure 4. 11: Coefficient of friction sub-model

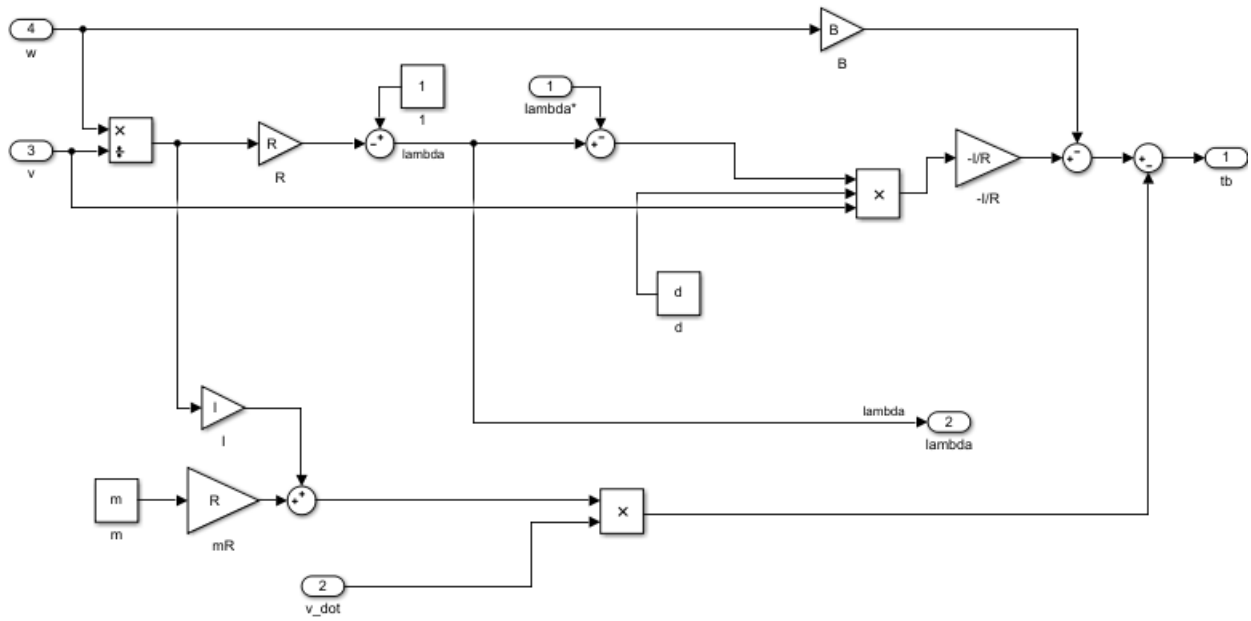

Figure 4. 12: Controller's sub-model

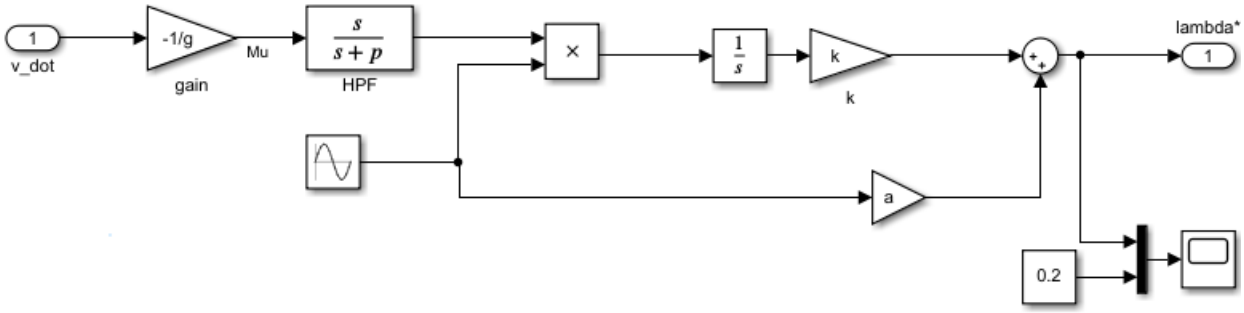

Figure 4. 13: Extremum Seeking Control sub-model

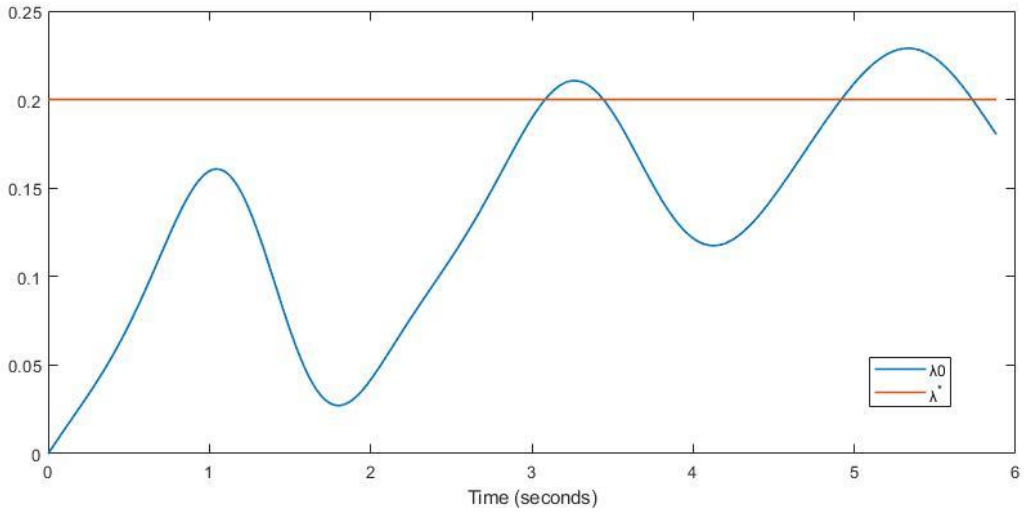

Figure 4. 14: Extremum Seeker tracking λ_0 (dry conditions)

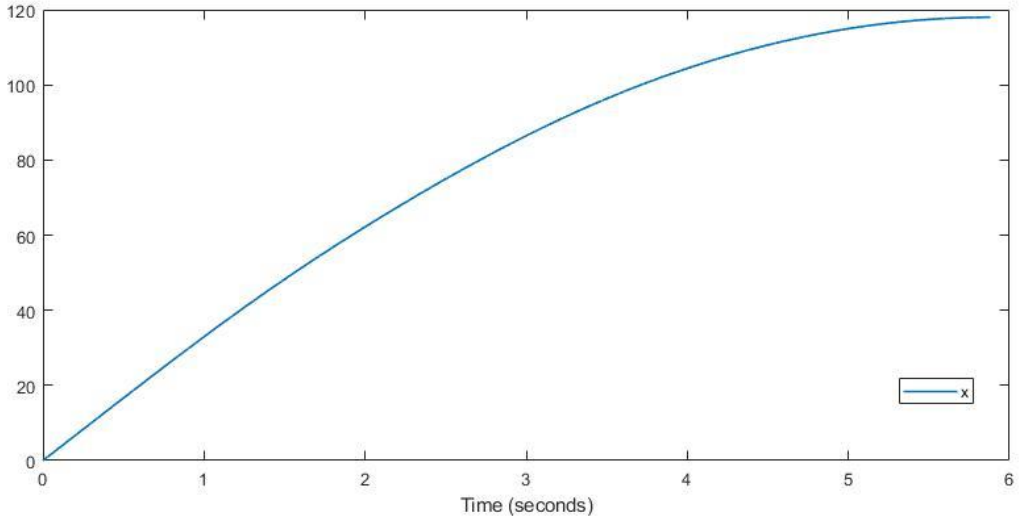

Figure 4. 15: Braking distance (dry conditions)

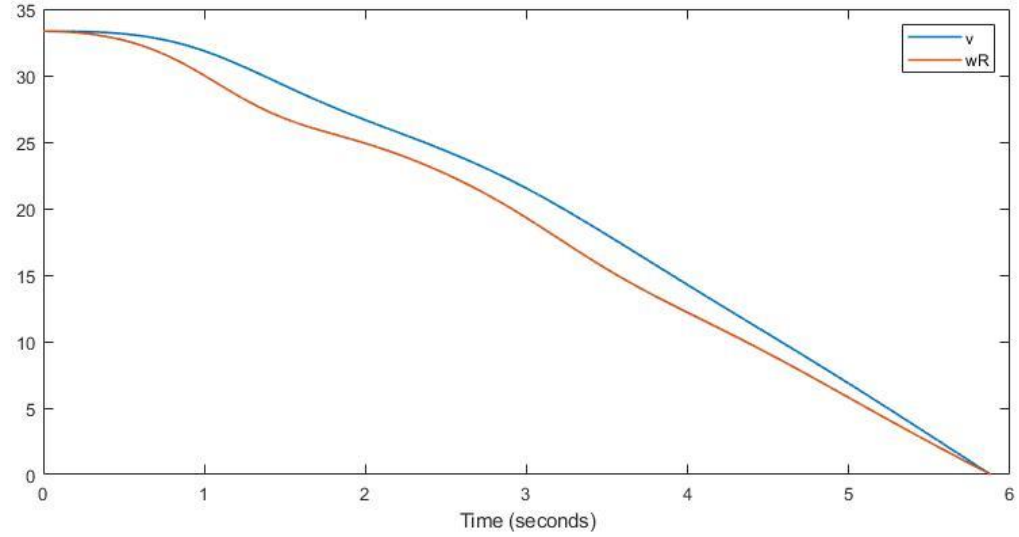

Figure 4. 16: Linear velocity and angular velocity multiplied by the wheel's radius (dry conditions)

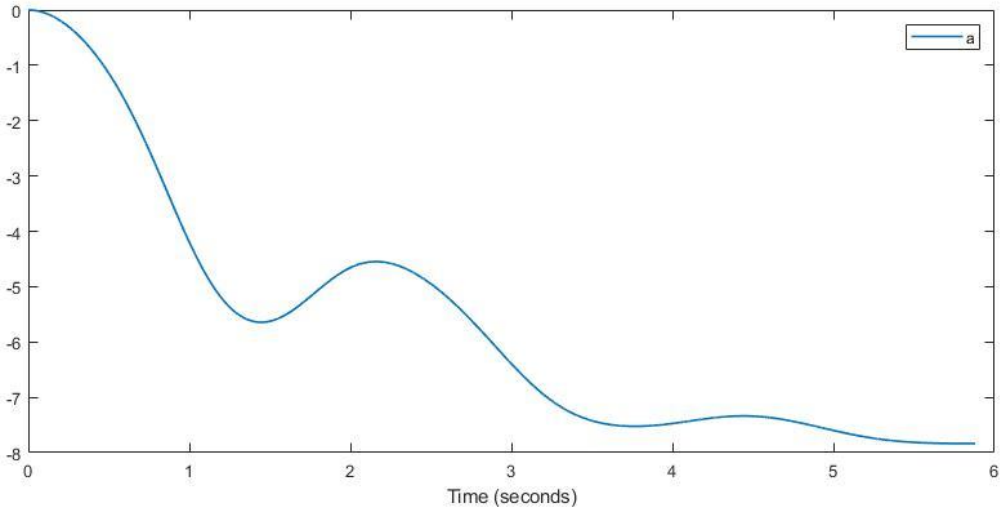

Figure 4. 17: Vehicle's deceleration (dry conditions)

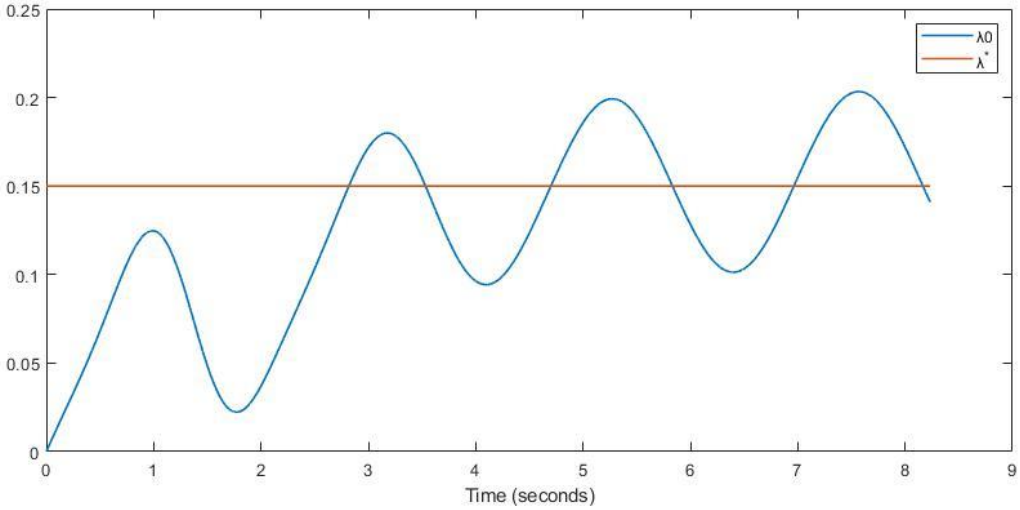

Figure 4. 18: Extremum Seeker tracking λ_0 (wet conditions)

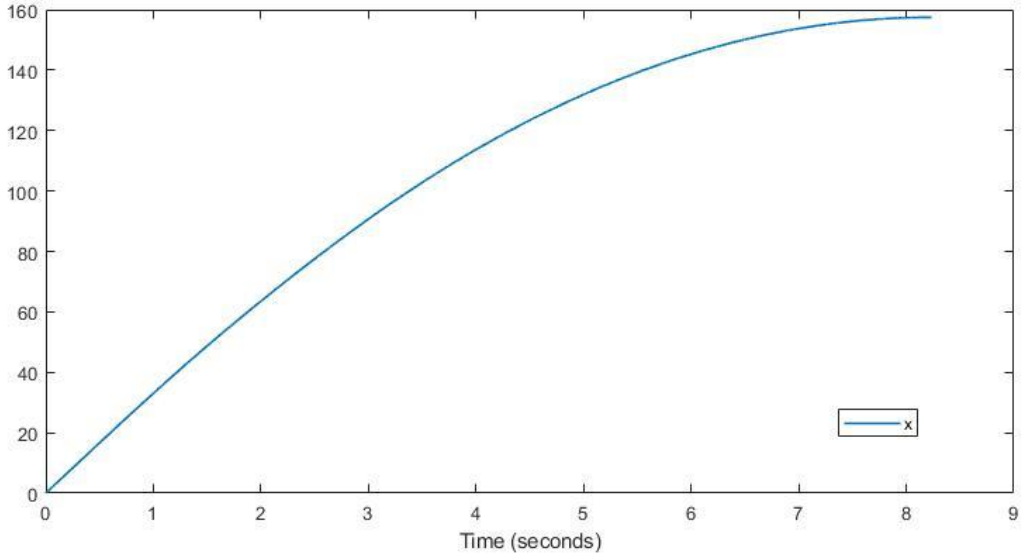

Figure 4. 19: Braking distance (wet conditions)

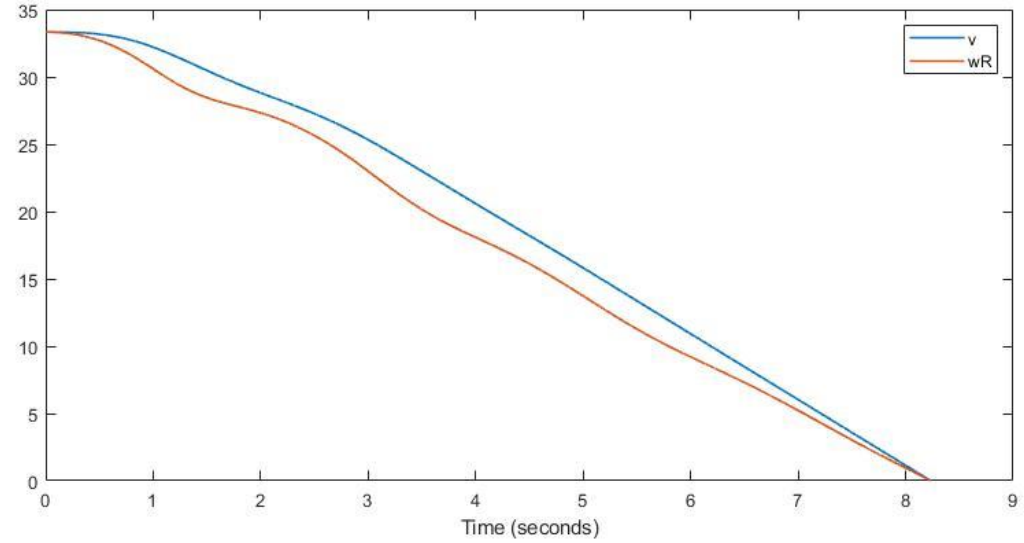

Figure 4. 20: Linear velocity and angular velocity multiplied by the wheel's radius (wet conditions)

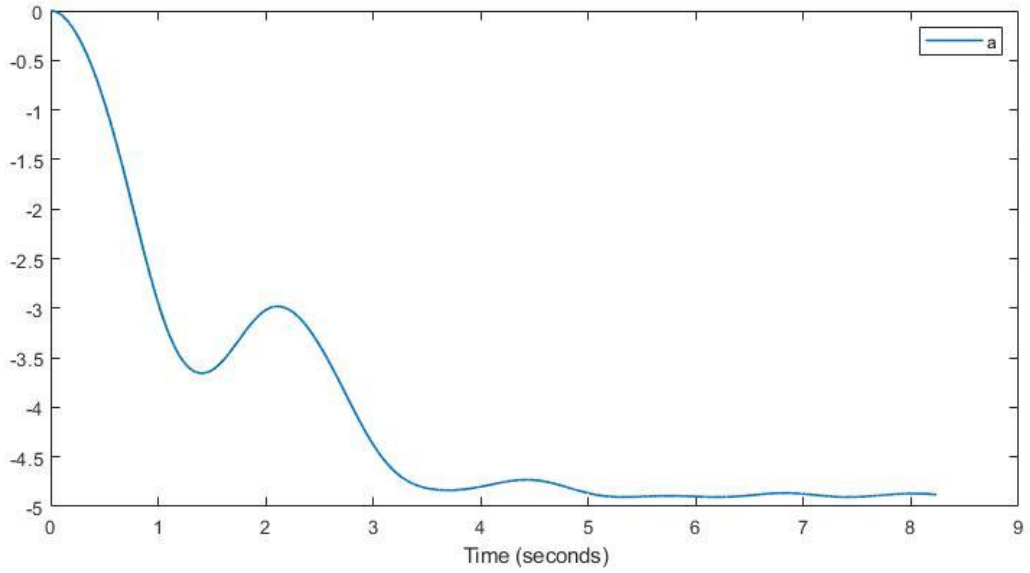

Figure 4. 21: Vehicle's deceleration (wet conditions)

4.5 ESC on traffic congestion

4.5.1 Data presentation

Data description

The experimental data with which the ES scheme will be tested, are collected during the operation of the TASS strategy by Siemens in the central business district (CBD) of Chania, utilizing 70 sensors from June 5 to June 11, 2006 [8]. TASS is a semi-real-time signal control strategy, that includes six different, fixed signal plans. Every 15 min, TASS evaluates the traffic conditions in the network, based on measurements of 17 "strategically" located sensors, and selects which signal plan is suitable to be adopted for the next 15 min period. The CBD of Chania, as it is defined in [8], consists of 71 links of various lengths and 24 junctions. The experimental data includes measurements of flow and occupancy (%) values every 90 seconds.

Data analysis

The data are depicted in Figure (4.22-4.28) for each one of the seven days of the week in terms of flow time series, occupancy time series and their corresponding Network Fundamental Diagrams (NFDs). The NFD or MFD (Macroscopic Fundamental Diagram) [4] model of urban road networks depends on the hypothesis that traffic dynamics of an urban area (like Chania), can be considered as a single-region dynamic system with vehicle occupancy n as a state variable. The NFD figures (on the top of each day's Figure) indeed verify that there exists an NFD for the CBD

of Chania across the 7 days of the test week. Following a thorough examination of the Figures produced from the data, the remarks stated below were highlighted:

- It can be observed that flow capacity is about 800 (vehicles/cycle) for every day except Sunday where the demand is lower than it should be in order to fully form region B, as defined in [8], in the NFD figure (Sunday). Therefore, on Sunday the network only reaches to an occupancy of $x \cong 20\%$, as shown in Figure (4.28).
- On Monday, not only region B is fully formed, but also the congested regime region C is partially formed as shown in Figure (4.22). Congested regime region C is described by negative slope in the NFD. This is because of the uneven spatiotemporal distribution of congestion throughout the protected network, combined with the imposed signal plan that (TASS) selected. Flow capacity is observed at $x \cong 20\%$.
- On Wednesday, as shown in Figure (4.24) region B has fully formed in the NFD and flow capacity is observed at a range of occupancies (20-25%).
- On Tuesday, Thursday and Friday, where shops are open in the evening, flow capacity is observed over a wide spectrum of occupancies (18-35%, 22-30% and 20-25% respectively). The NFDs of these weekdays, Figure (4.23), Figure (4.25) and Figure (4.26), indicate that TASS control strategy achieves to maintain high values of flow, however on Friday the network enters the congested regime region in the NFD of Figure (4.26) thus failing to retain network's maximum throughput. This is attributed to the spatiotemporal distribution of congestion inside the network
- On Saturday, flow capacity is observed at x=~22%. The congested regime region C has only slightly been formed as shown in the NFD of Figure (4.27).
- Even though the CBD exhibits an NFD, it is observed that the critical accumulation of vehicles in the network $x^*(t)$ cannot be precisely specified, since the traffic patterns from day-to-day traffic are subject to uncertainties and the imposed control signal may be any of the six fixed signal plans. Therefore, this problem calls for an adaptive control technique, that will track the critical occupancy in real-time by exploiting real-time sensor measurements without requiring knowledge of the plant's dynamics.

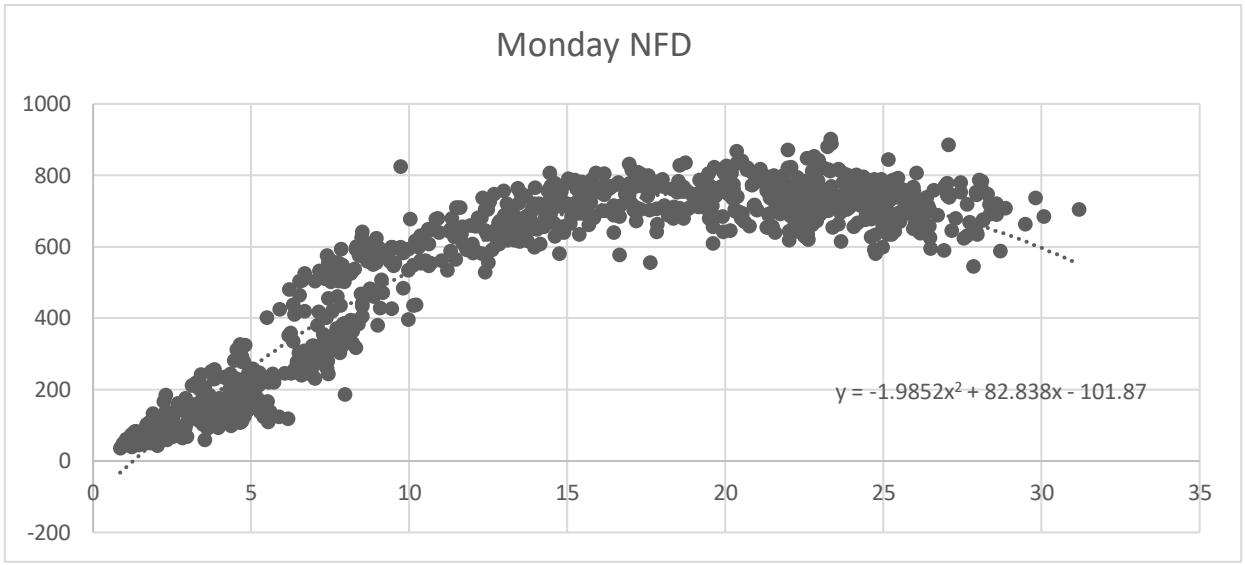

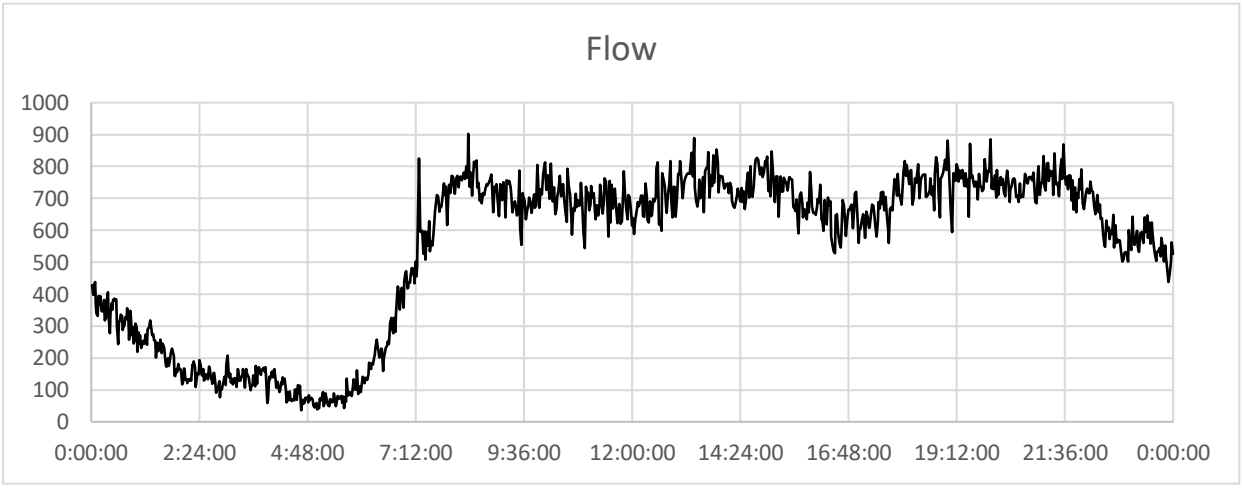

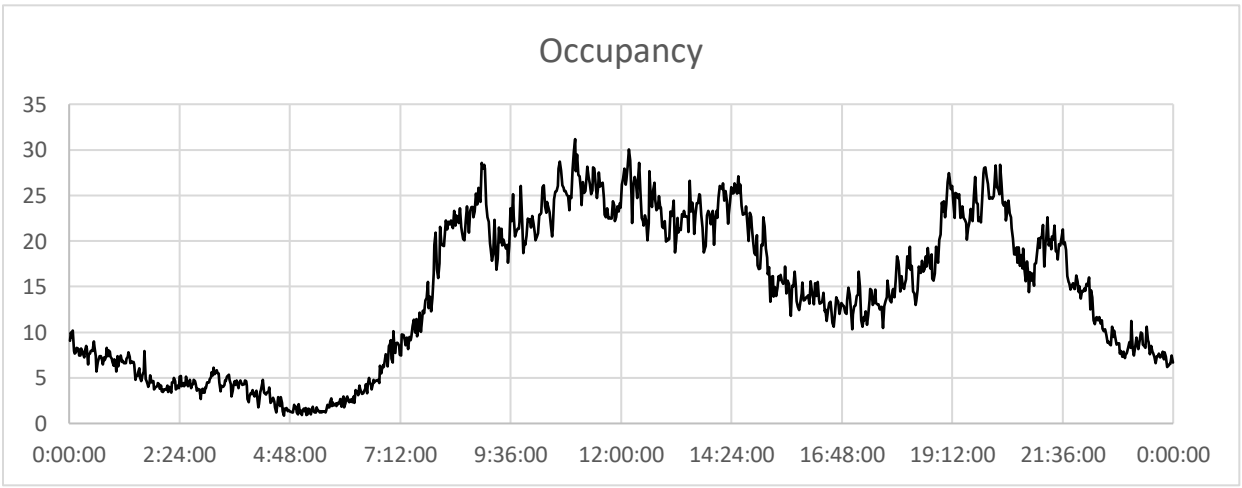

Figure 4. 22: Network Fundamental Diagram, Flow and Occupancy time series on Monday, June 5, 2006

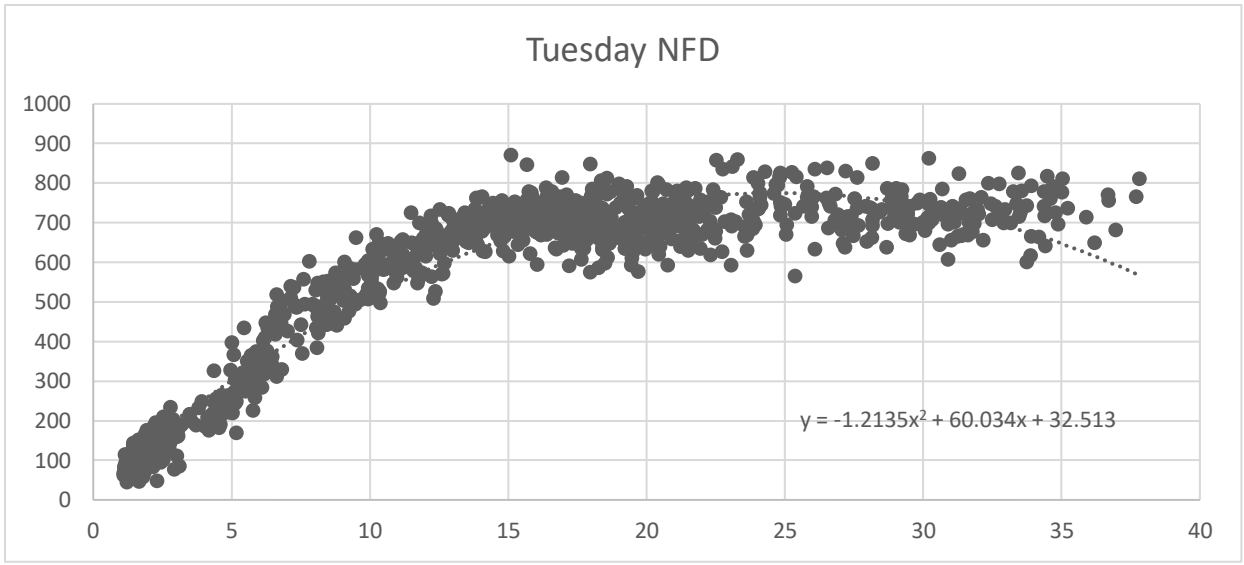

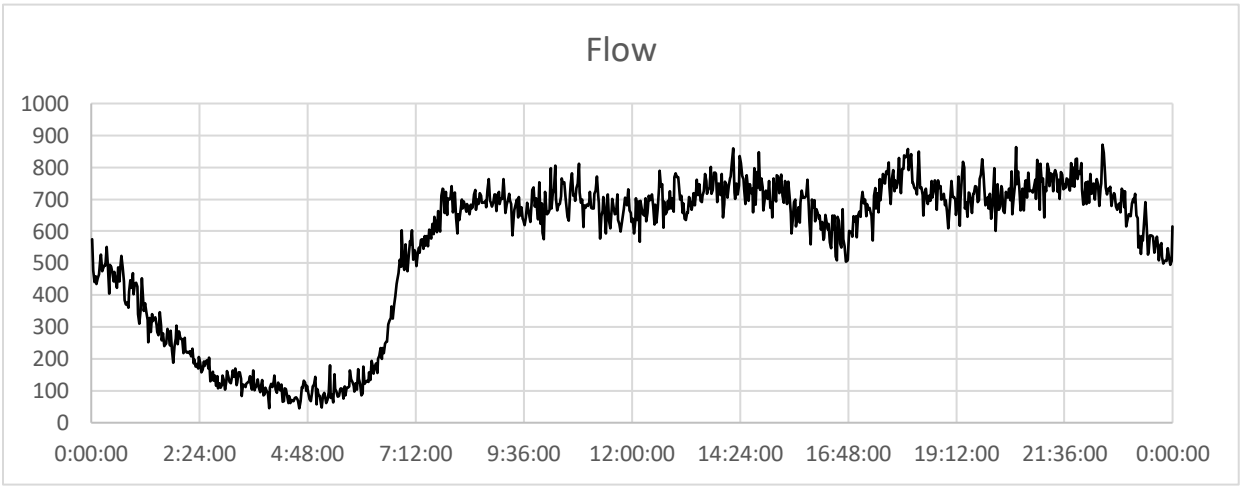

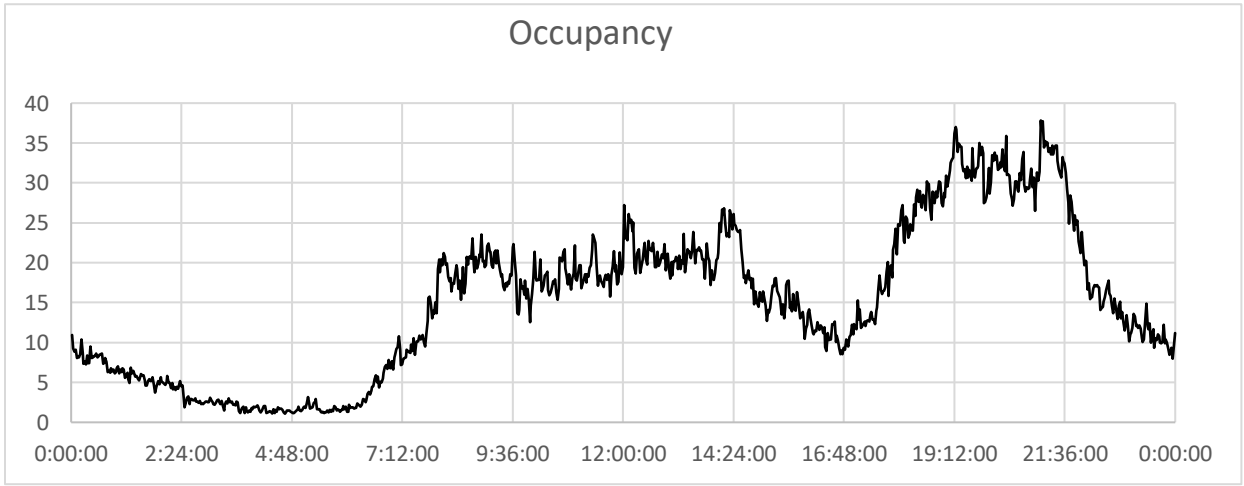

Figure 4. 23: Network Fundamental Diagram, Flow and Occupancy time series on Tuesday, June 6, 2006

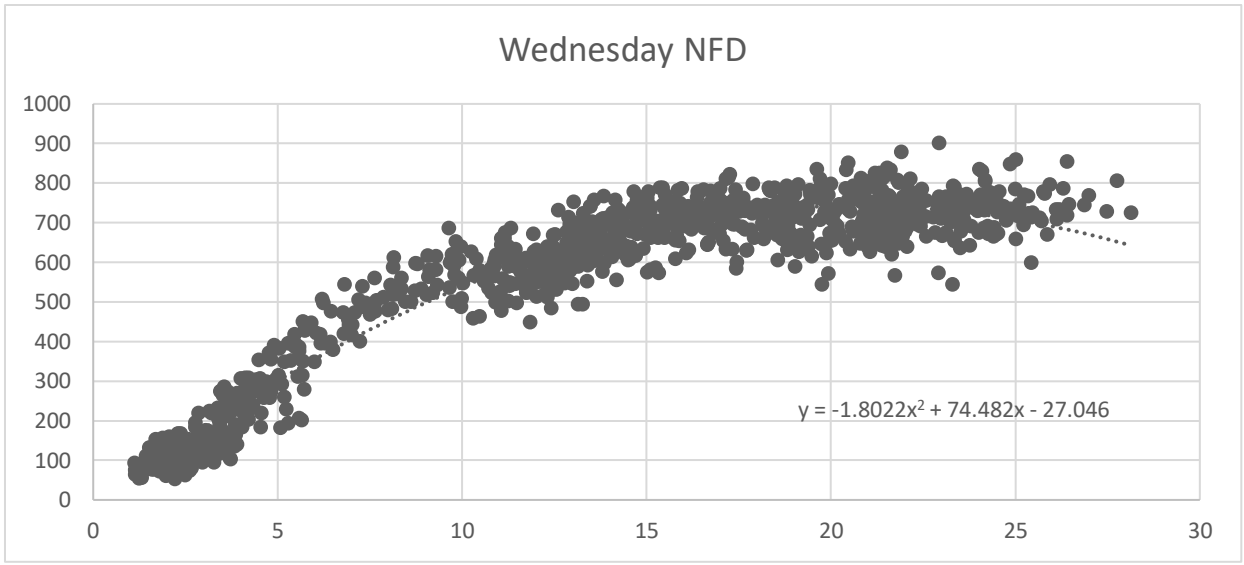

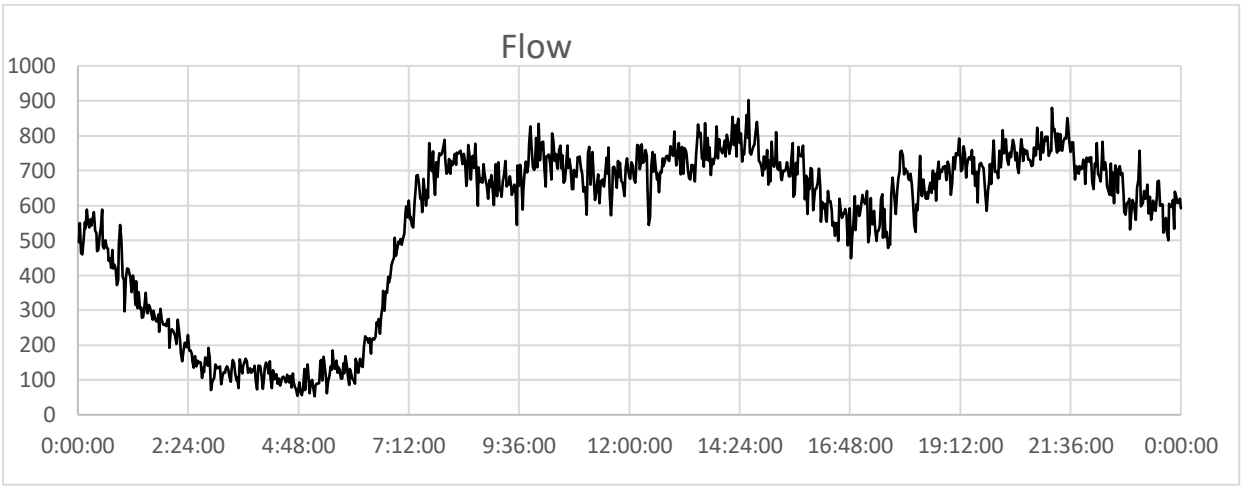

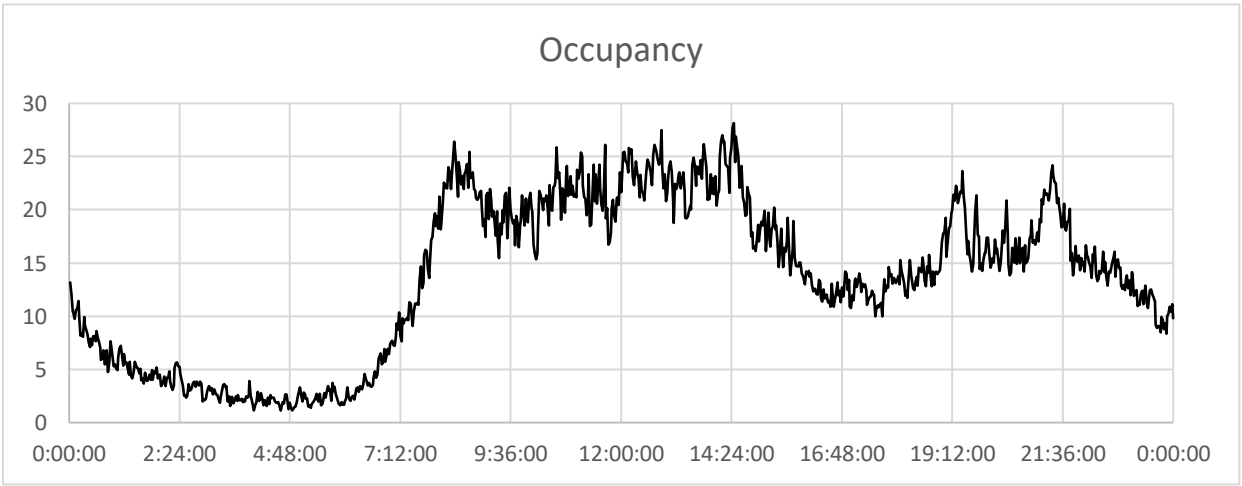

Figure 4. 24: Network Fundamental Diagram, Flow and Occupancy time series on Wednesday, June 7, 2006

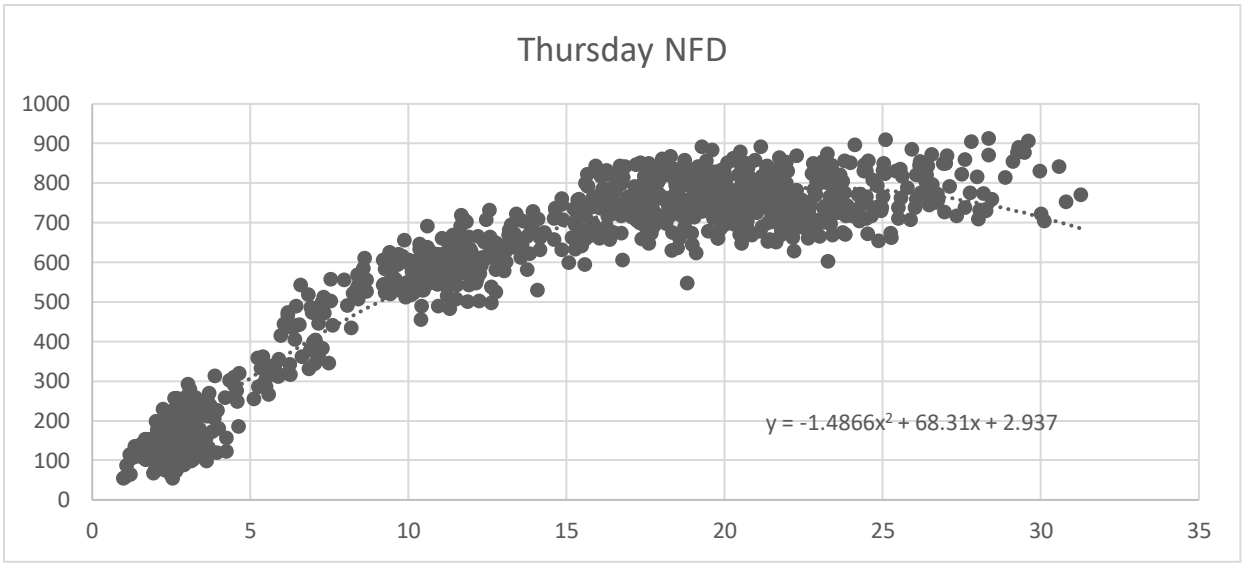

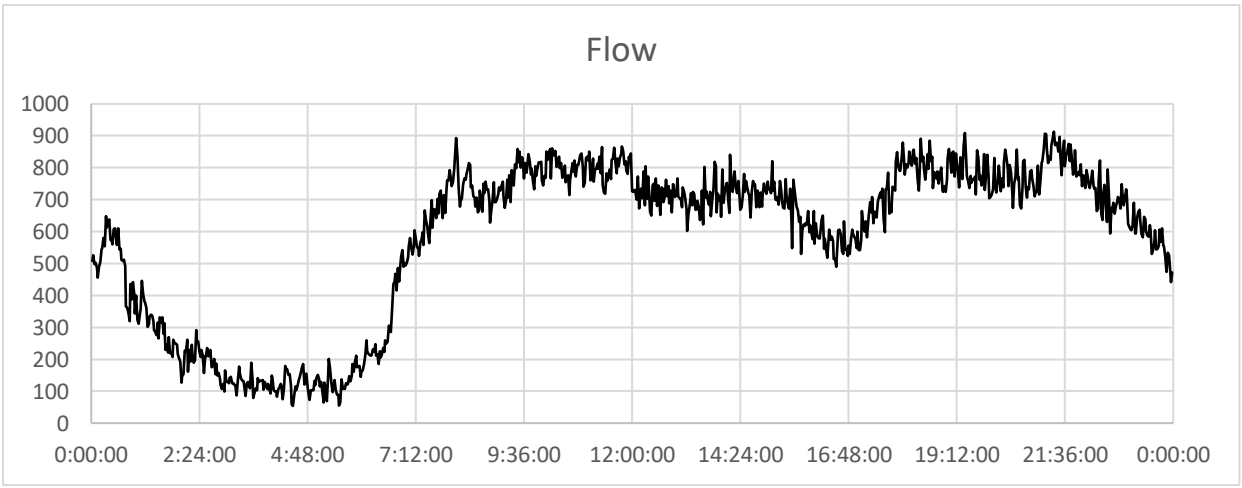

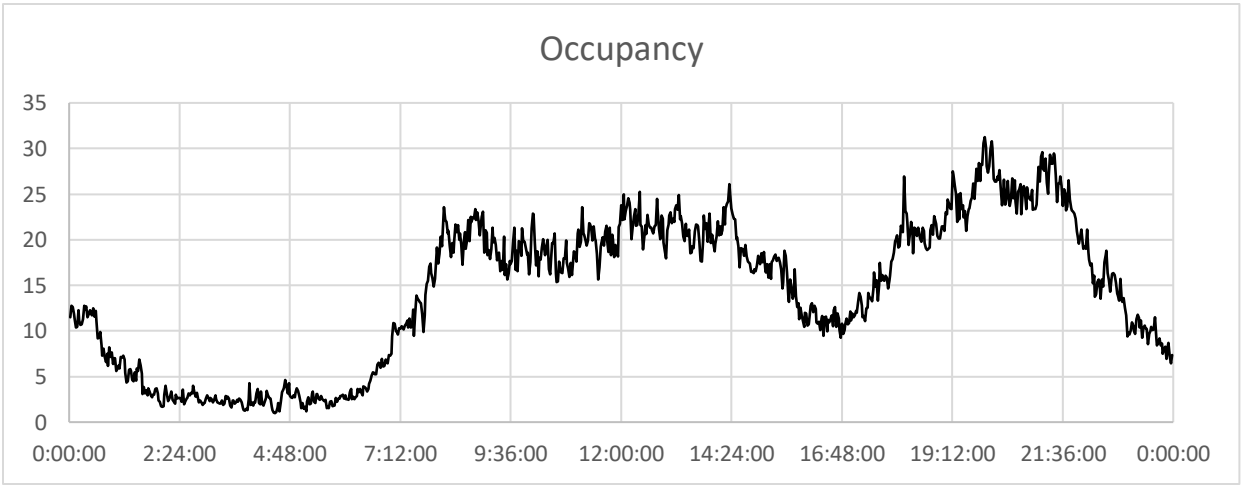

Figure 4. 25: Network Fundamental Diagram, Flow and Occupancy time series on Thursday, June 8, 2006

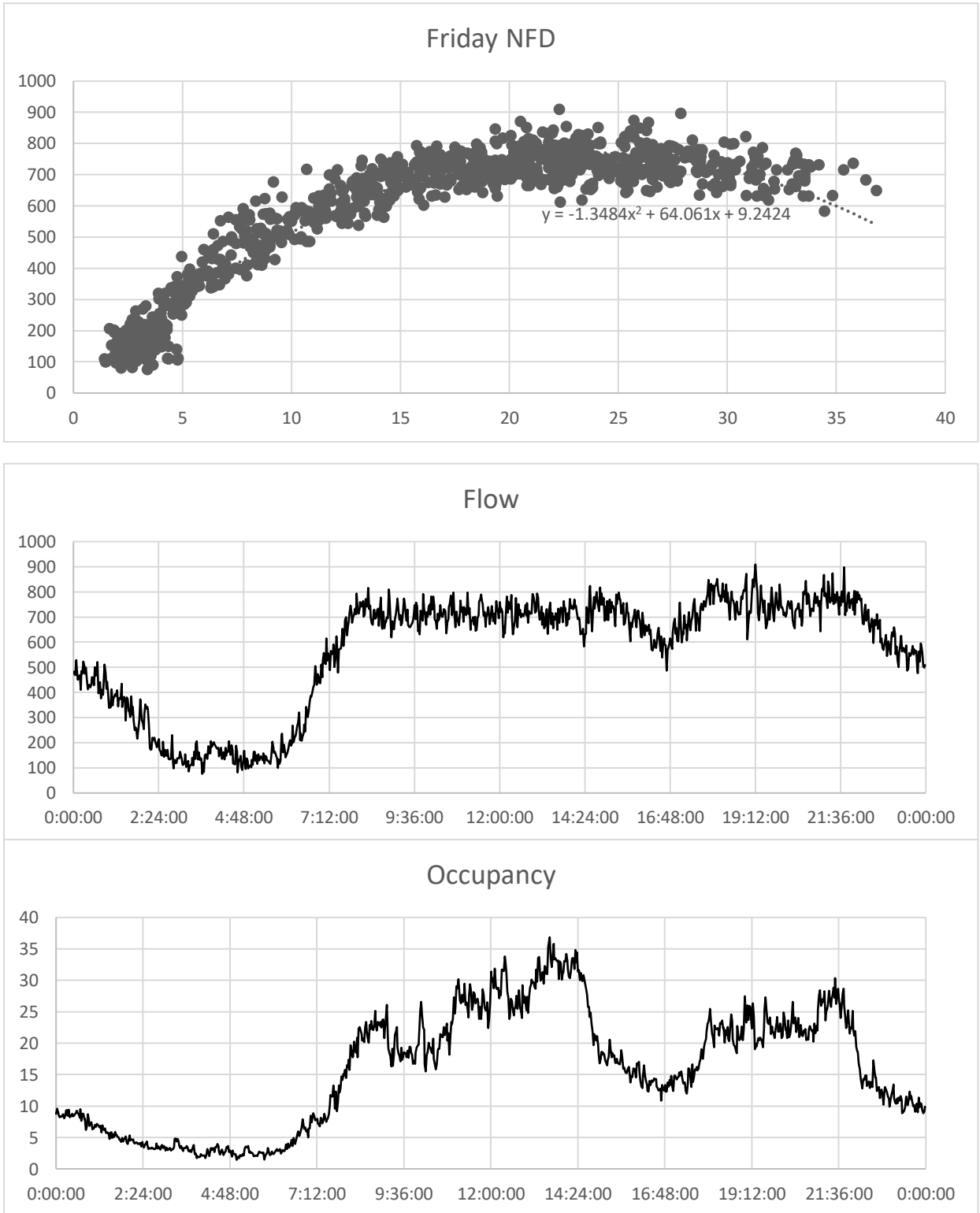

Figure 4. 26: Network Fundamental Diagram, Flow and Occupancy time series on Friday, June 9, 2006

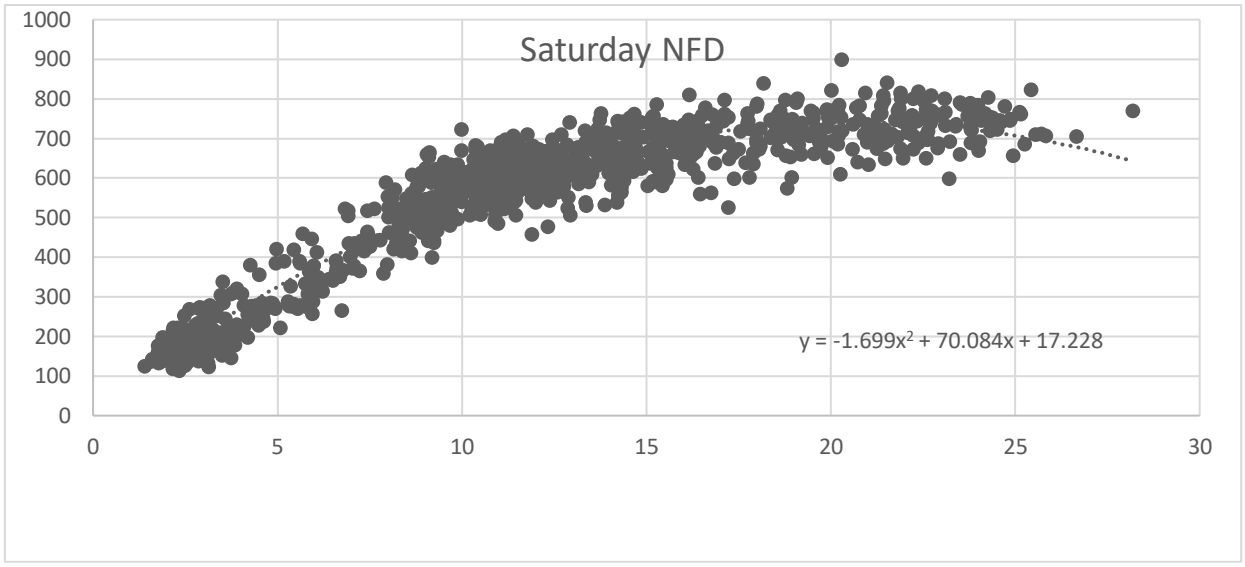

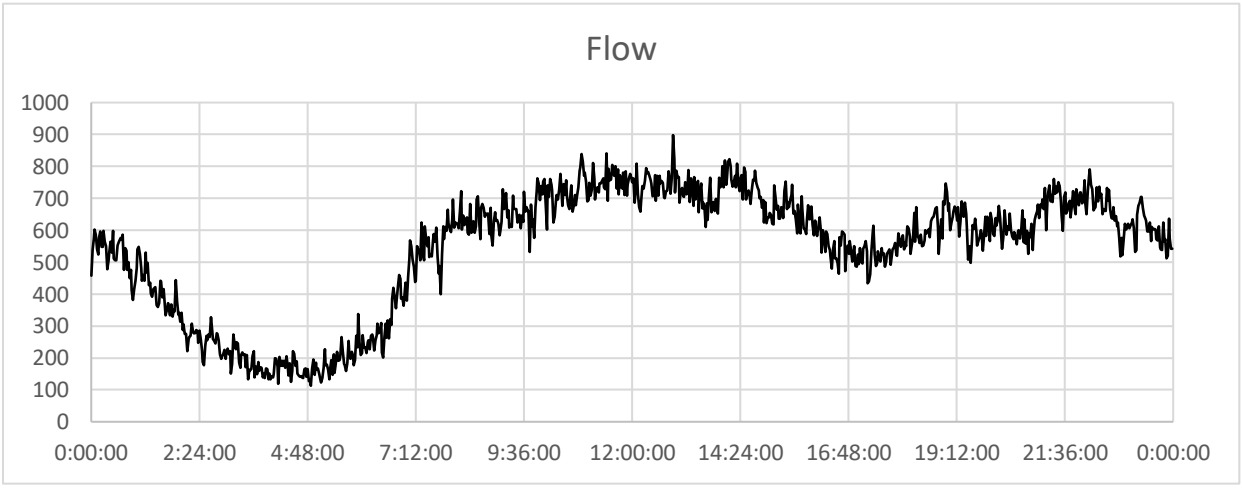

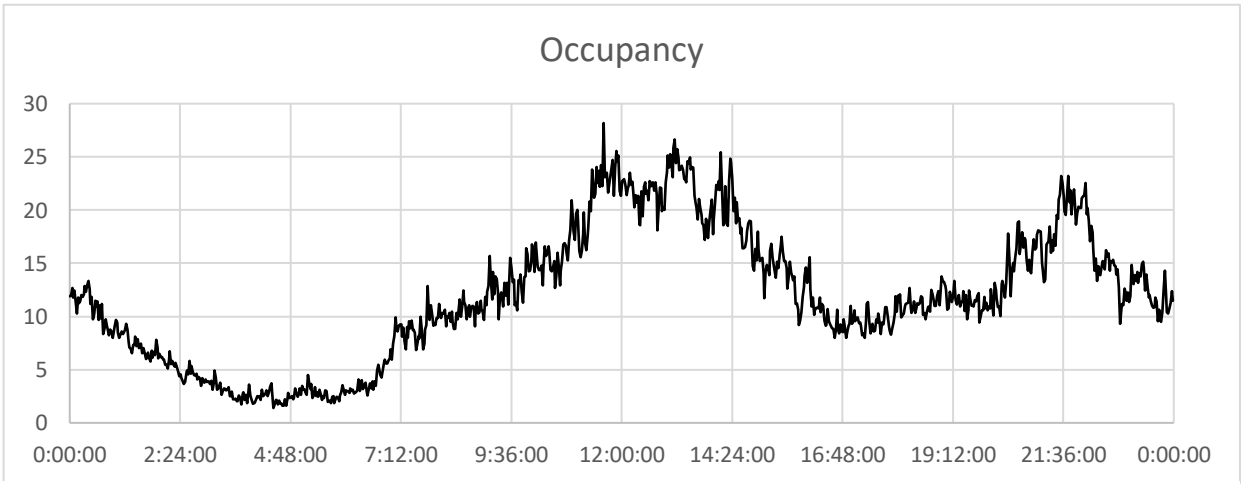

Figure 4. 27: Network Fundamental Diagram, Flow and Occupancy time series on Saturday, June 10, 2006

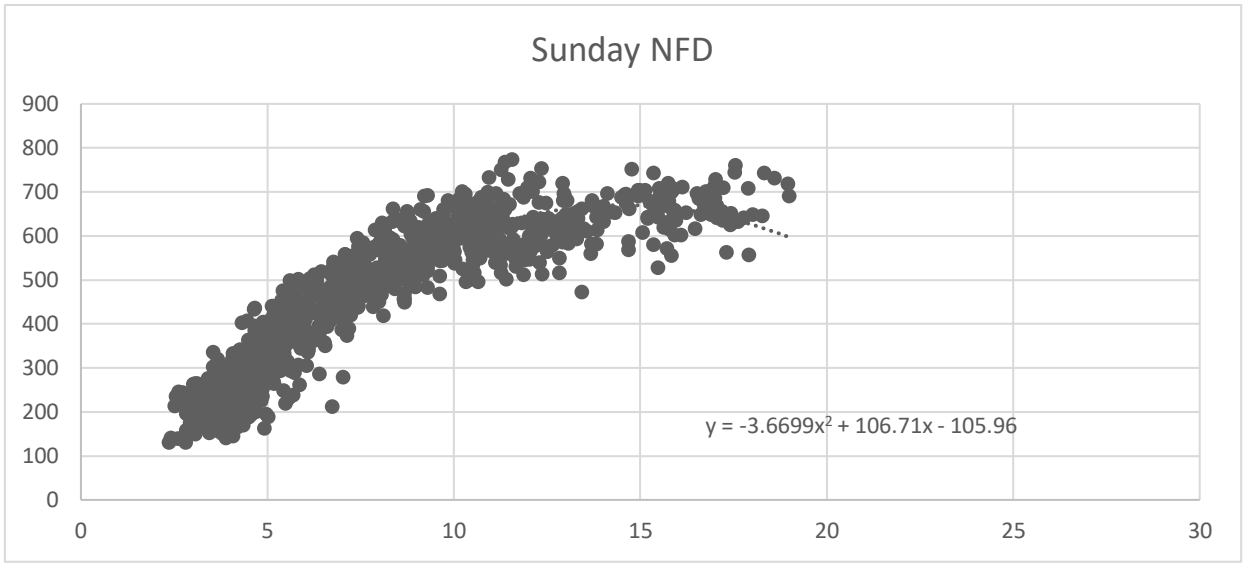

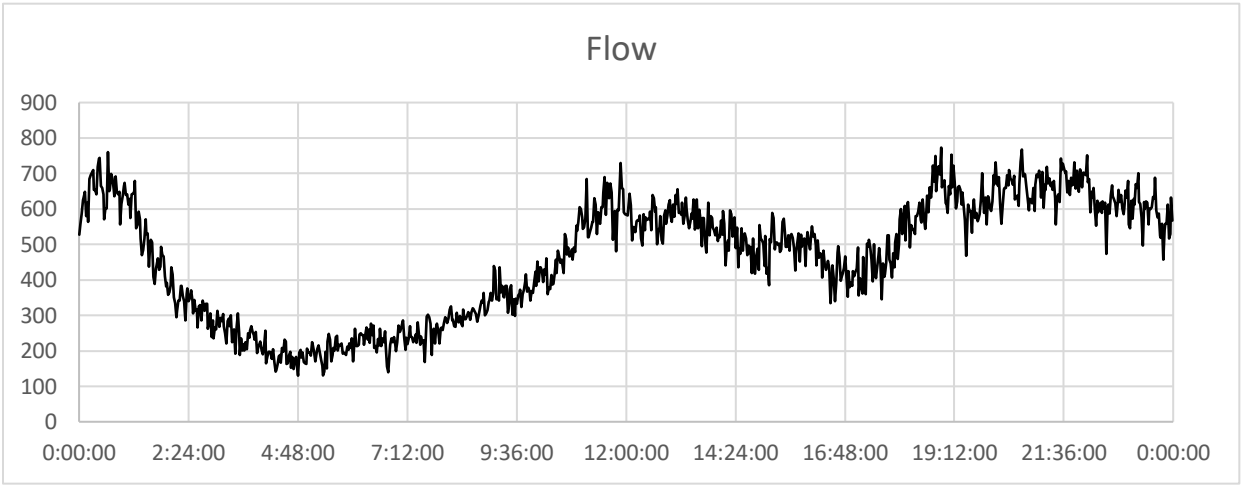

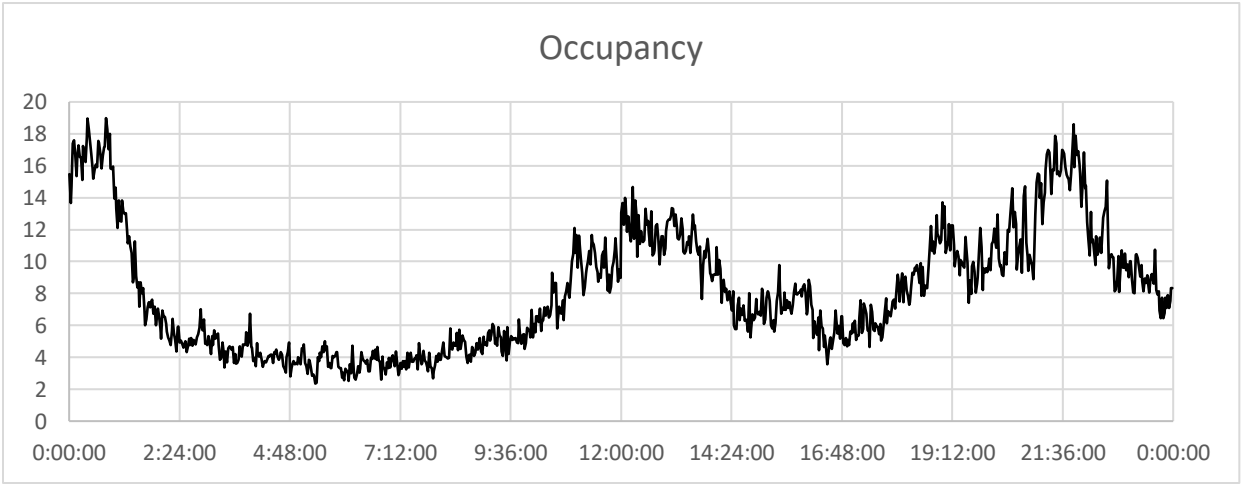

Figure 4. 28: Network Fundamental Diagram, Flow and Occupancy time series on Sunday, June 11, 2006

4.5.2 Solving the static problems

Next a preliminary evaluation test is conducted. The algorithm will be evaluated in tracking the optimal values of seven second order polynomials (one for each day) which were produced using the trendlines command in excel and they are shown in the NFD Figures in Figure (4.22-4.28). The resulting polynomials are then formulated via Taylor approximation to posit a static map form. The Quadratic Taylor approximation of y(x) around point x=a satisfies:

$$y(x) = \sum_{n=0}^{2} \frac{y^{(n)}(a)}{n!}(x-a)^n \quad (4.5.1)$$

Since point x=a is the extremum, the formulated polynomials will posit the following form:

$$P(x) = y(a) + \frac{y''(a)}{2}(x-a)^2$$

Implementing equation (4.5.1) in polynomials y_i, for $i = 1,2,3,4,5,6,7$ results in the following objective functions for each day respectively.

Monday: $P_1 = 762.292 - 1.9852(x - 20.864)^2$

With $x^* = 20.864$ and $P_1(x^*) = 762.292$

Tuesday: $P_2 = 775.01 - 1.2135(x - 24.736)^2$

With $x^* = 24.736$ and $P_2(x^*) = 775.01$

Wednesday: $P_3 = 742.509 - 1.8022(x - 20.664)^2$

With $x^* = 20.664$ and $P_3(x^*) = 742.509$

Thursday: $P_4 = 787.656 - 1.4866(x - 22.975)^2$

With $x^* = 22.975$ and $P_4(x^*) = 787.656$

Friday: $P_5 = 770.109 - 1.3484(x - 23.754)^2$

With $x^* = 23.754$ and $P_5(x^*) = 770.109$

Saturday: $P_6 = 739.972 - 1.699(x - 20.625)^2$

With $x^* = 20.625$ and $P_6(x^*) = 739.972$

Sunday: $P_7 = 669.744 - 3.67(x - 14.538)^2$

With $x^* = 14.538$ and $P_7(x^*) = 669.744$

A perturbation-based extremum seeking control scheme, as discussed in Chapter 3, is implemented seven times for each of the static maps produced by the linearization and the parameters of it are chosen as follows: perturbation frequency $\omega = 10Hz$, demodulation amplitude $d = 1$, modulation amplitude $a = 0.05$, a 1st order Butterworth filter with a cutoff frequency $h = 5Hz$ and integration gain $k = 2$. The initial occupancy is considered as $x = 0$. In Figure (4.29) for Monday, it takes about 25 time units for the system to achieve its maximum output. Approximately the same time is needed for Wednesday, as shown in Figure (4.30), while for Sunday to reach its optimal occupancy, only 20 time units passed as shown in Figure (4.35). For Thursday, Friday, and Saturday it takes about 30 time units to reach the peak as shown in Figures (4.32), (4.33) and (4.34) respectively. For Tuesday, where its NFD exhibited an extremum for the highest occupancy value than the other days' NFDs, 35 time units passed until the system reaches optimality. The proposed algorithm achieves optimum tracking for each one of the seven static maps produced by the collected data. It is evident that initiating the system's input value, far from the optimum value, rises the time needed for the system to extremize its output. Nonetheless, in every case, the system's output converged asymptotically to the optimal

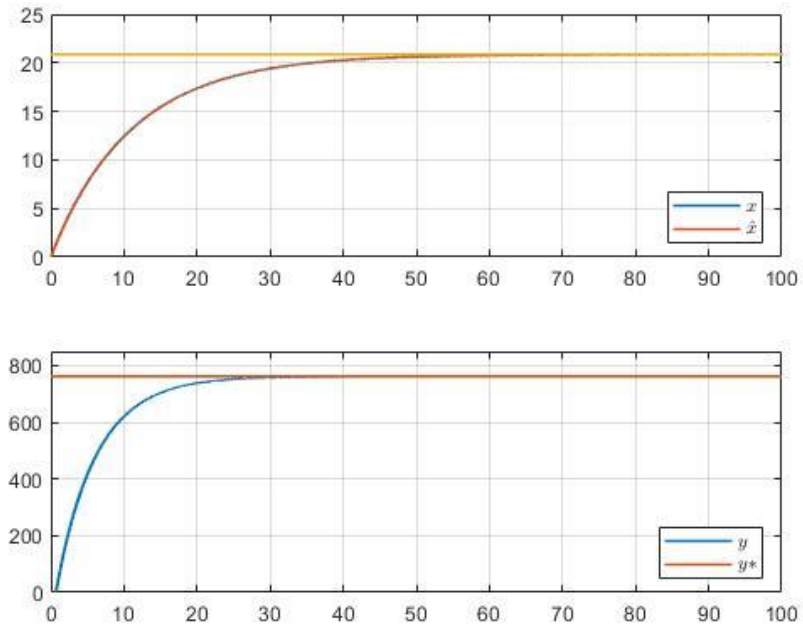

Figure 4. 29: Extremum Seeking Control response graphs for Monday

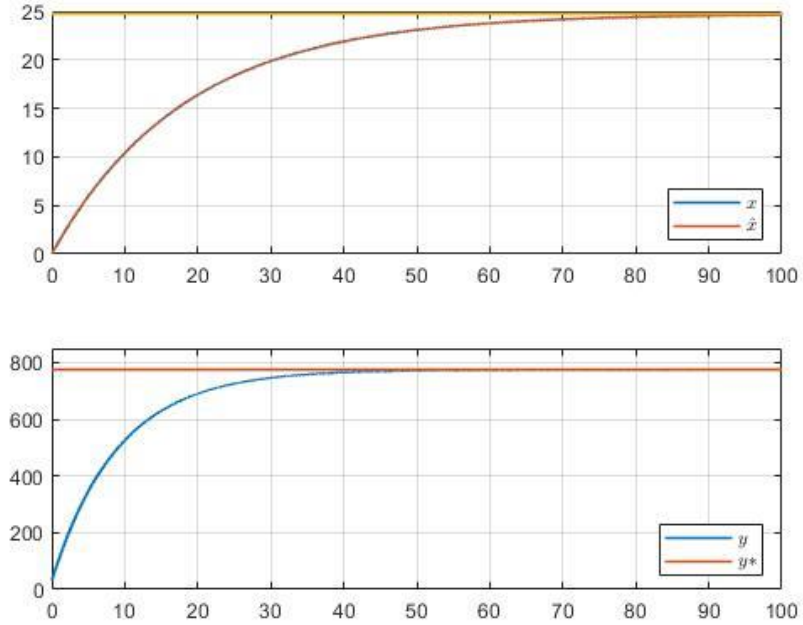

Figure 4. 30: Extremum Seeking Control response graphs for Tuesday

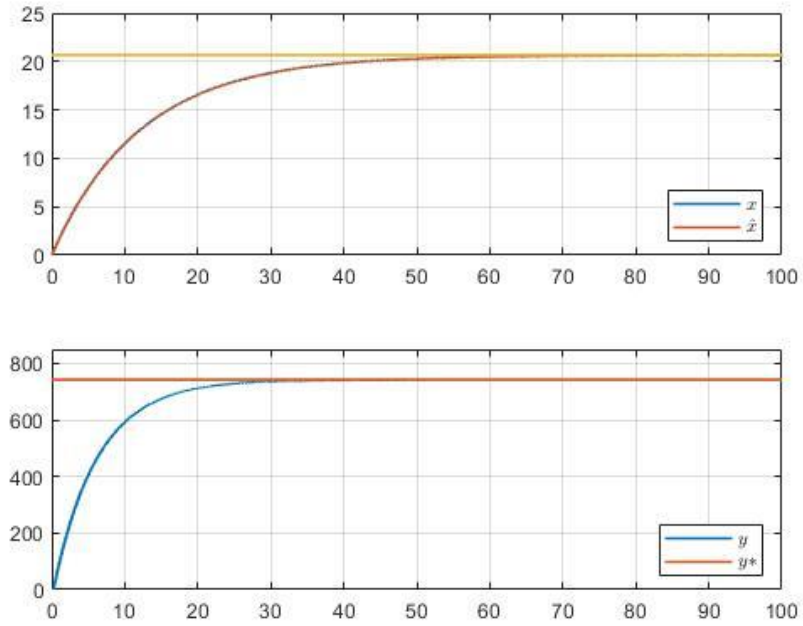

Figure 4. 31: Extremum Seeking Control response graphs for Wednesday

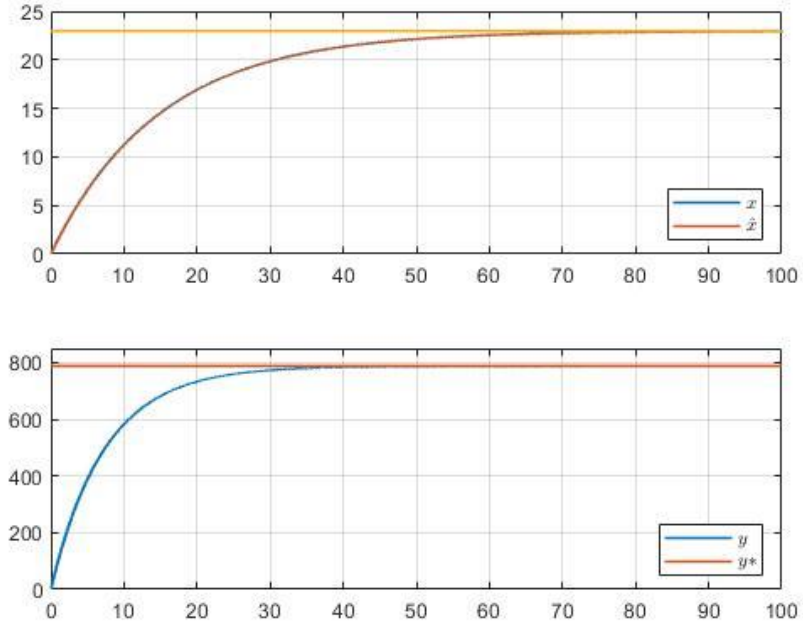

Figure 4. 32: Extremum Seeking Control response graphs for Thursday

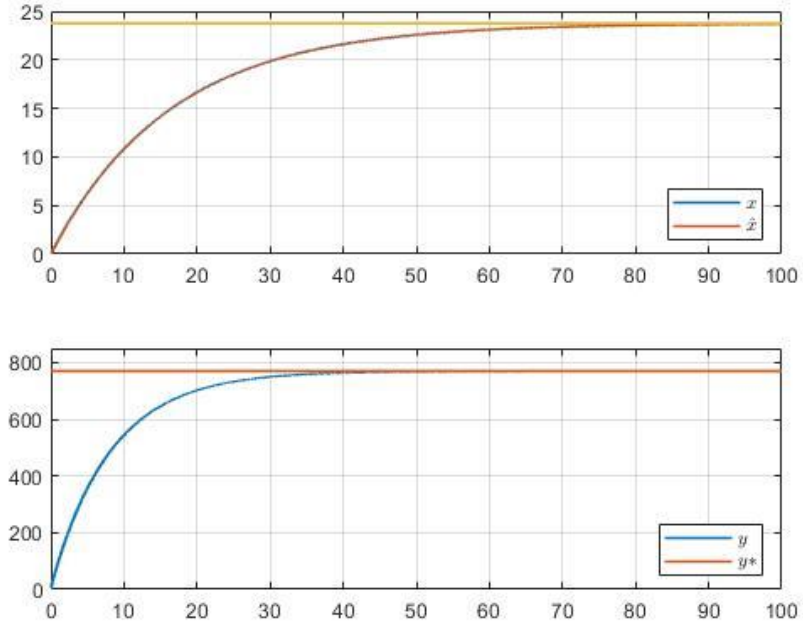

Figure 4. 33: Extremum Seeking Control response graphs for Friday

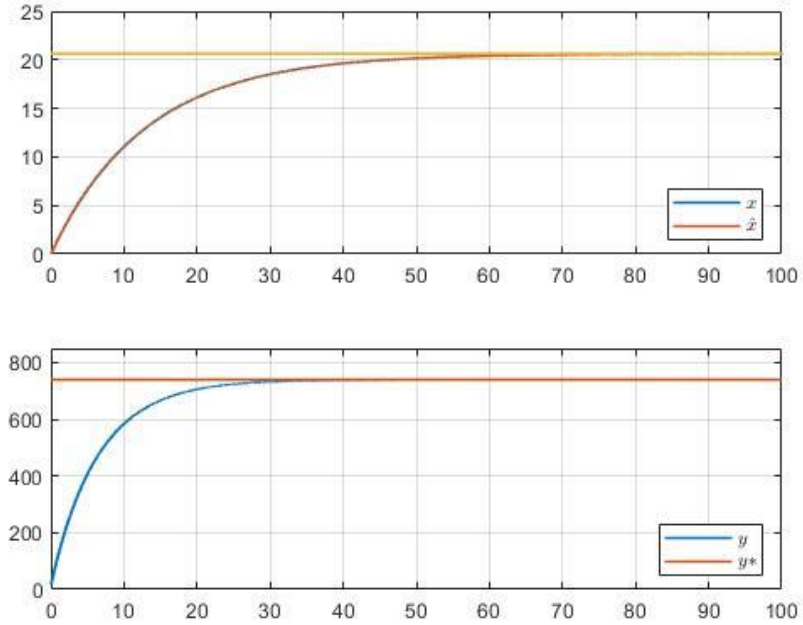

Figure 4. 34: Extremum Seeking Control response graphs for Saturday

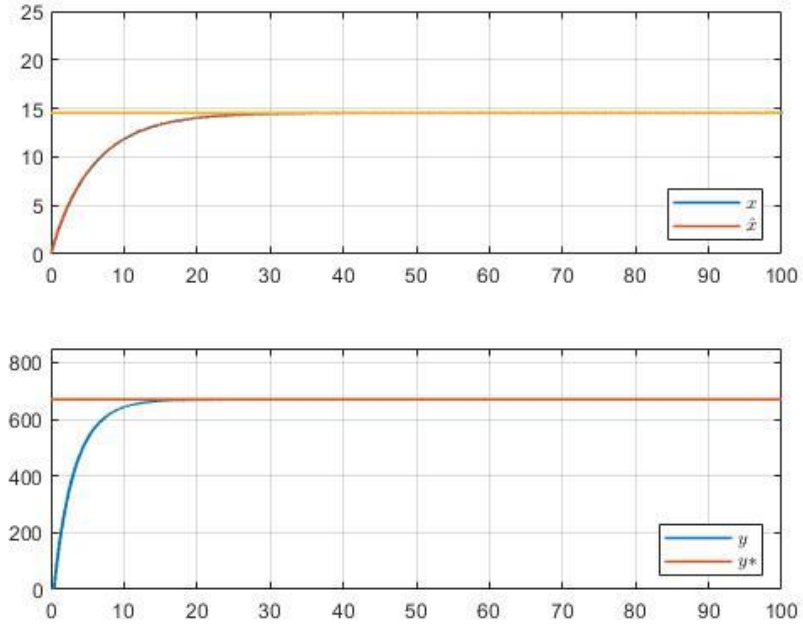

Figure 4. 35: Extremum Seeking Control response graphs for Sunday

It is observed that the proposed algorithm manages to track the unknown optimal occupancy value in all the seven days' NFDs.

4.5.3 ESC as an estimation algorithm

In this section an Extremum Seeking Control estimator is proposed for real time implementation. The proposed algorithm will be evaluated in terms of its ability to monitor the prevailing critical occupancy of an adaptive perimeter control flow strategy as proposed in [4], but instead of a Kalman filter based estimator, an Extremum Seeker is utilized for tracking the varying critical occupancy. The corresponding block diagram of the proposed scheme is shown in Figure (4.36).

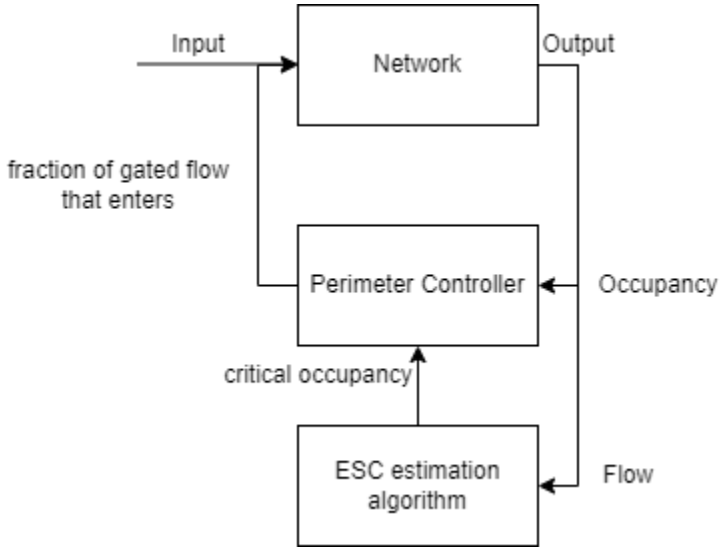

Figure 4. 36: Adaptive perimeter control flow strategy on a network

Sensor measurements of occupancy and flow are collected from the network and are forwarded to the perimeter controller and the Extremum Seeker. Utilizing these measurements, the ESC estimation algorithm, forwards the prevailing critical occupancy to the perimeter controller. The discretized perimeter controller's, state feedback control law is given by:

$$\theta(m) = \theta(m-1) - K_p\big(X(m) - X(m-1)\big) - K_I(X(m) - X^*)$$

Where, θ is the fraction of the gated flow that is allowed to enter the network in the present time step. K_P is the proportional gain, K_I is the integrational gain, X is the measured occupancy and X^* is the prevailing critical occupancy, estimated by the Extremum Seeker. From the estimation algorithm's perspective, the plant consists of the network and the perimeter controller. To evaluate the proposed scheme an open loop scheme is constructed in which the values of flow and occupancy from the collected data are fed to the ES controller as shown in Figure (4.37). The evaluation of the proposed scheme in this section, concerns its ability to estimate the underlying critical occupancy values, during the operation of the TASS signal control strategy in the CBD of Chania from June 5 to June 11, 2006. It is noted that the proposed algorithm does not track the current operating occupancy of the data, but the critical occupancy values of the prevailing NFDs. The ES controller's output is its estimate of the unknown critical occupancy X^*.

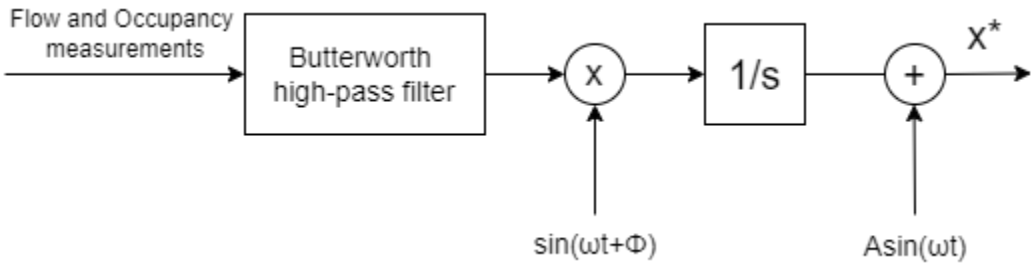

Figure 4. 37: ESC scheme for estimation of critical occupancy

Algorithmic Scheme: (Initial values $\boldsymbol{X_0^* = 20}$ and $\boldsymbol{Y_0 = 600}$)

1. New measurements of Flow $Y(m-1)$ and Occupancy $X(m-1)$ are entering the algorithm.
2. The measurements are then filtered by a Butterworth high-pass filter.
3. The filtered signal is multiplied by a phase shifted sinusoid, to extract the operating gradient information.
4. The produced signal is then integrated into the estimate of the unknown critical occupancy.
5. The same sinusoid, but this time not phase shifted, is additively injected into the estimated critical occupancy.

The algorithm is set to inactivity for as long as $X \leq 10$, because there is no need for perimeter control if there is not sufficient demand on the entrance links. The critical occupancy estimation is restricted by lower and upper boundaries: $10 \leq X^* \leq 30$. The parameters of the Extremum Seeker are chosen as follows: Perturbation frequency: $\omega = 0.001Hz$, Amplitude: $A = 0.2$, Phase: $\Phi = -\pi$ rad, integration gain: $k = 0.0001$ and a second order Butterworth high-pass filter with a cutoff frequency $h = 0.0009Hz$. The applied filter serves at removing the low frequency noise from the measurements before the operating gradient is estimated from the product of the filtered and the sinusoidal signals (demodulation).

The constructed algorithm is evaluated using the data shown in Figures (4.22 - 4.28) for each day of the week and then, the high pass filtered signal, the gradient's estimate and the critical occupancy estimation are plotted (Figures 4.38-4.44). In Figure (4.38), in which the estimation algorithm's results for Monday are shown, it is observed that during the morning peak (8:00-12:00) the critical occupancy estimate of the algorithm is about $X^* = 22\%$. The actual occupancy during that period on Monday as shown in Figure (4.22) was about $X = 25\%$ thus, presenting small deviation from the obtained estimate. This algorithm's estimate suggests that the actual occupancy during that period, was right of the peak of the prevailing NFD, thus decreasing the network's

throughput. After the morning peak the algorithm climbs gradually and reaches critical occupancies around $X^* = 28\%$ and maintains them during the evening peak (18:00-22:00) when the actual occupancy was between $X = 20\%$ and $X = 25\%$. This means that the obtained measurements for that period exhibit a positive derivative of the NFD (left of the peak), therefore the algorithm steers the critical occupancy towards higher values to achieve better performance. The filtered signal and the gradient's estimate tend to oscillate with high frequency, which is attributed to the presence of noise in the experimental data. The actual occupancy for Tuesday's morning peak is observed from Figure (4.23) to be about $X = 20\%$ and the critical occupancy estimate for the same period is $X^* = 22\%$ (not posing a threat for oversaturation) as shown in Figure (4.39). The estimate drops slightly during the off-peak and begins rising steadily in the evening peak. The first hours of Wednesday, as shown in Figure (4.40) (and of most days) the algorithm mainly remains inactive, since the actual occupancy is not surpassing the declared threshold value. During the morning peak the algorithm maintains its output at about $X^* = 20\%$ which is a little lower than the actual measured occupancy for that time. The estimate quickly drops to $X^* = 16\%$ during the off-peak and it then rises to $X^* = 24\%$ to track the critical occupancy during the evening peak. The critical occupancy estimated for Thursday is shown in Figure (4.41) and it is observed that the estimation values are about the same with the actual values in the morning peak. However, in the evening peak the algorithm estimates the critical occupancy at about $X^* = 25\%$ compared to the actual value which even reaches $X = 30\%$. This comparison suggests that the imposed control (TASS) led the network's operation to the congested regime since it estimated critical occupancy values lower than the actual values. In Figure (4.42) it is evident that the algorithm quickly tracks the rising critical occupancy during both peaks (morning and evening) of Friday, while settling to a lower $X^* = 20\%$ in the off-peak between them. The estimate for Saturday is shown in Figure (4.43). In the morning (8:00-12:00) the critical occupancy estimation is close to $X^* = 22\%$ while the corresponding actual occupancy shown in Figure (4.27) is climbing from $X = 10\%$ to $X = 25\%$. During the off-peak the estimate drops to $X^* = 17\%$ and even $X^* = 15\%$ in the evening, thus exhibiting slight deviation from the actual occupancy values obtained from the measurements. During Sunday the occupancy hardly surpasses the threshold value therefore the algorithm is only activated for three short periods throughout the day as shown in Figure (4.44). The adaptive perimeter controller is not needed if the demand in vehicles waiting to enter the protected area does not pose the threat of congestion.

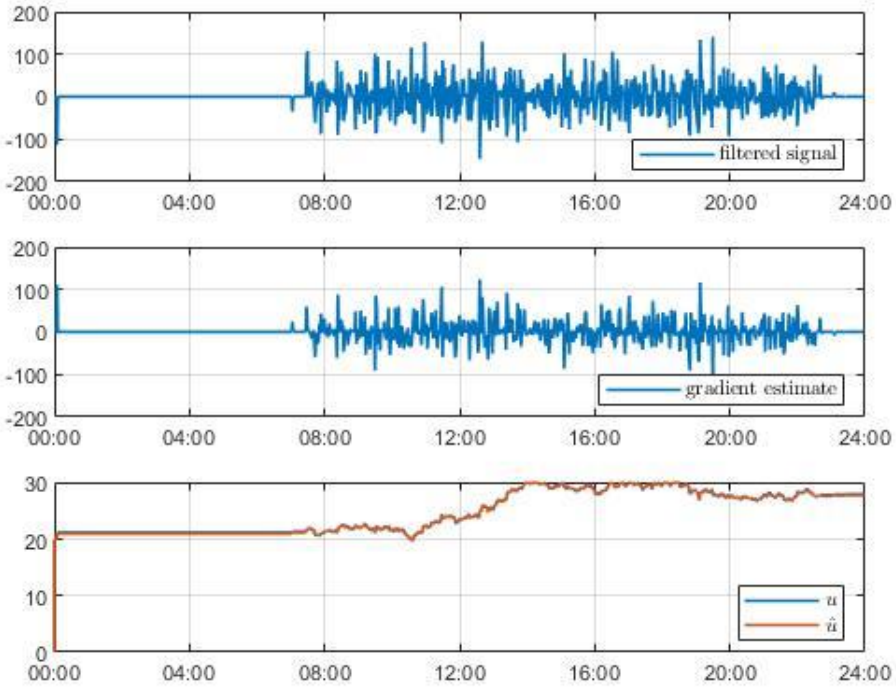

Figure 4. 38: High pass filtered measurements, Derivative estimate and Critical occupancy estimate for Monday

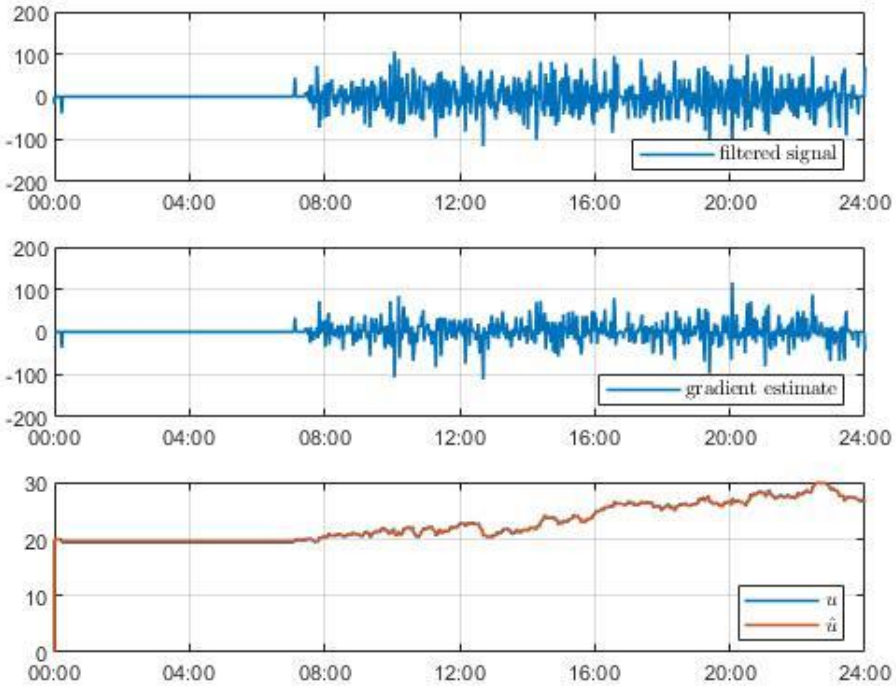

Figure 4. 39: High pass filtered measurements, Derivative estimate and Critical occupancy estimate for Tuesday

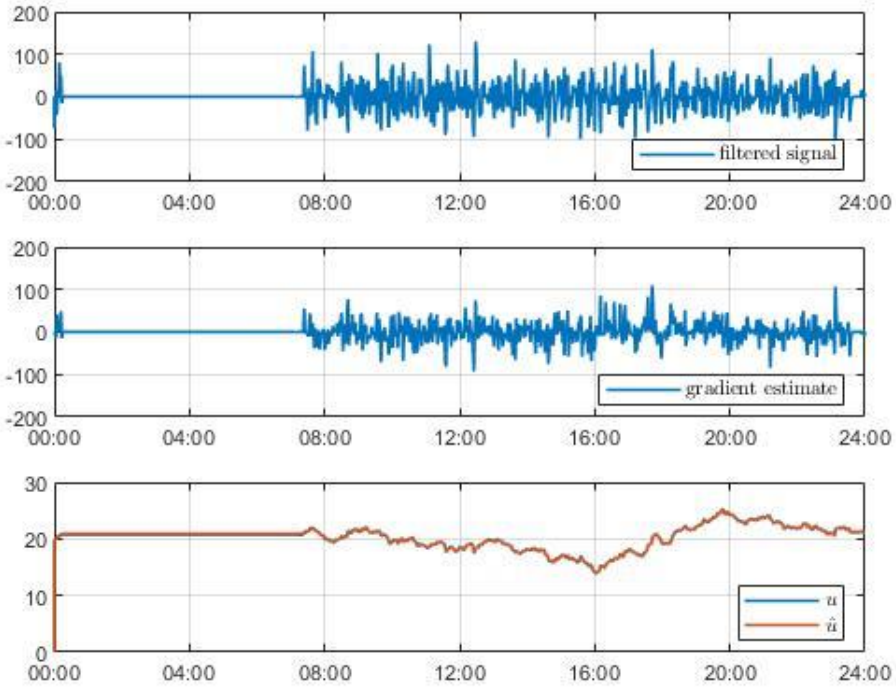

Figure 4. 40: High pass filtered measurements, Derivative estimate and Critical occupancy estimate for Wednesday

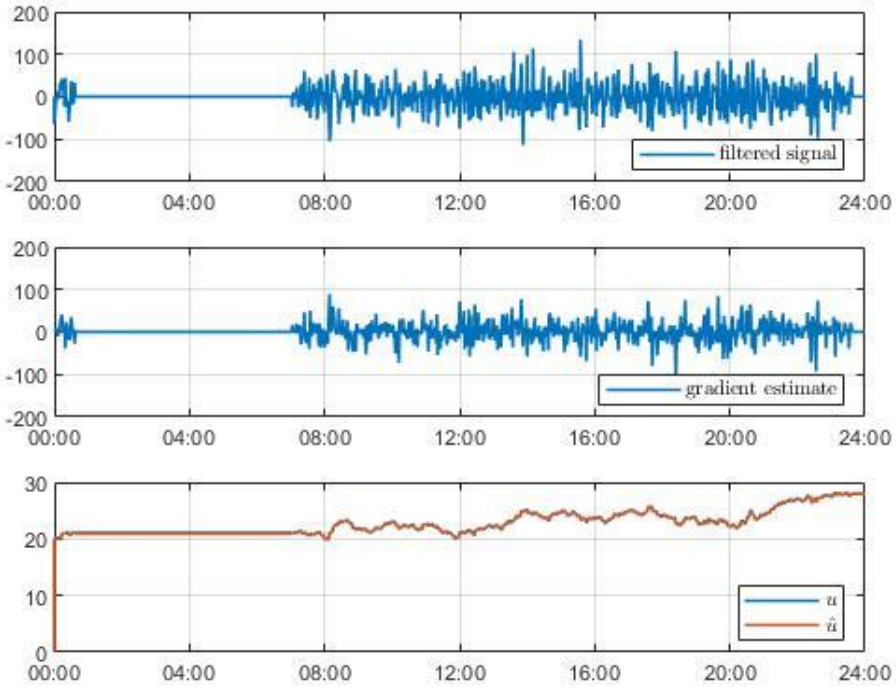

Figure 4. 41: High pass filtered measurements, Derivative estimate and Critical occupancy estimate for Thursday

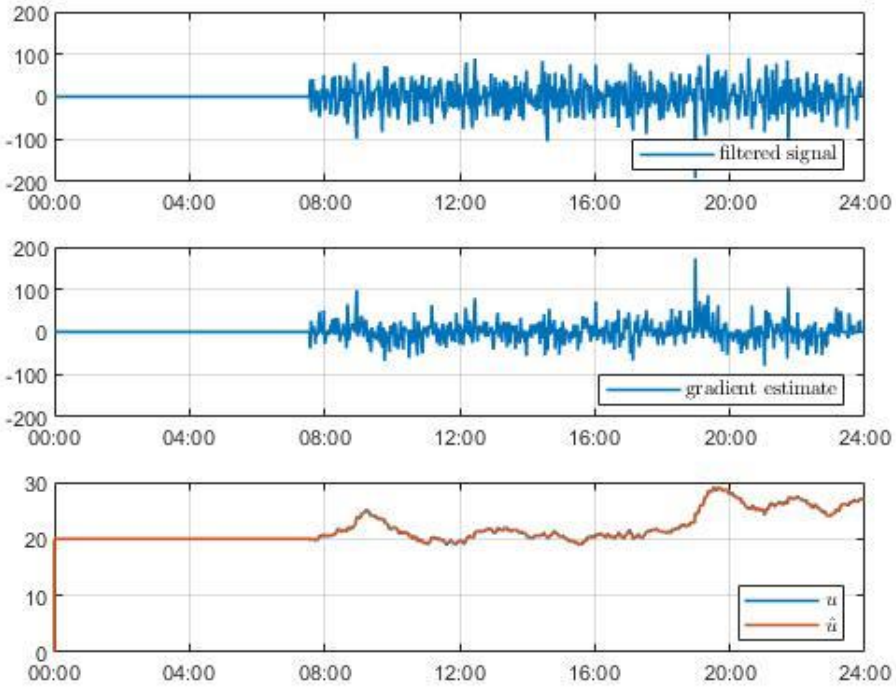

Figure 4. 42: High pass filtered measurements, Derivative estimate and Critical occupancy estimate for Friday

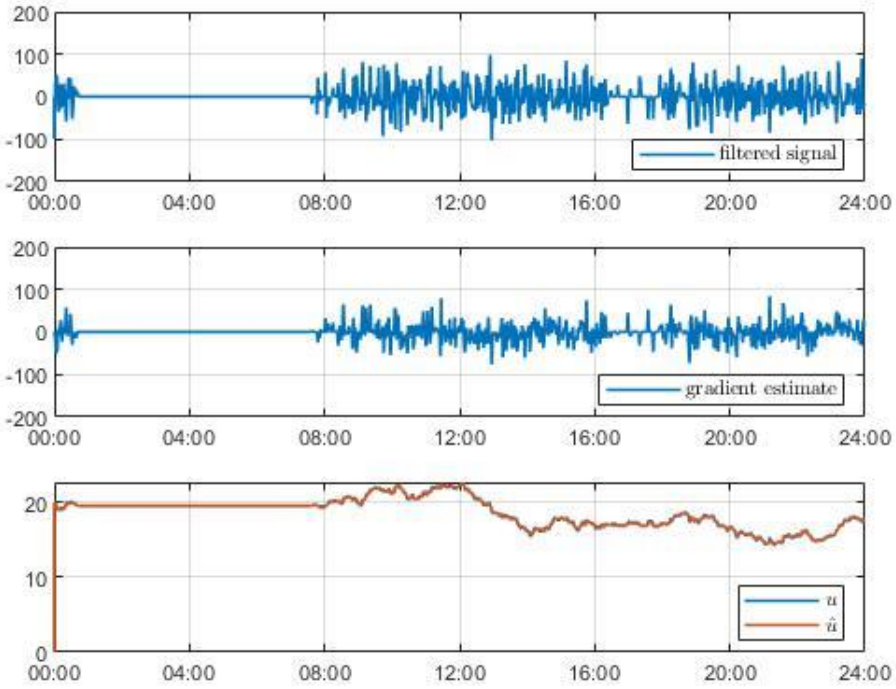

Figure 4. 43: High pass filtered measurements, Derivative estimate and Critical occupancy estimate for Saturday

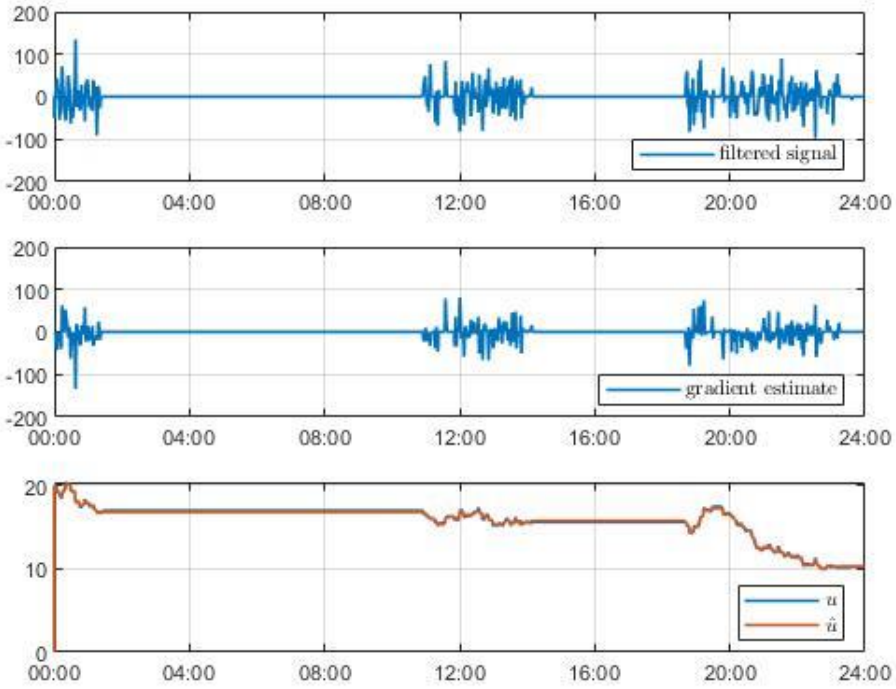

Figure 4. 44: High pass filtered measurements, Derivative estimate and Critical occupancy estimate for Sunday

5. CONCLUSIONS AND FURTHER WORK

This thesis has investigated the implementation of Extremum Seeking Control as a real time estimation algorithm, utilizing sensor measurements to produce the current critical occupancy value for which the network's flow is maximized. These measurements were collected from the CBD of Chania under the operation of TASS from June 5 to June 11, 2006, and they were shown, in section 4.5.1, to exhibit seven NFDs one for each of the seven days with relatively low scatter. The produced NFDs were approximated by seven linearized static maps. Then the estimation algorithm was implemented on the static maps to preliminary evaluate its tracking ability. The results were promising, showcasing the algorithm's ability to quickly and precisely converge to the optimum in every case. The proposed algorithm combined with the perimeter controller seems able to track the critical occupancy on real time even when the NFD of the network is not well defined. The evaluation conducted in the last chapter highlighted that the proposed ESC algorithm tracks the varying optimal operation point quickly and accurately. Therefore, the proposed adaptive perimeter control scheme coupled with SOTL (which promotes even spatial distribution and therefore well-defined NFDs) for the internal intersections' control, seems to be a solid alternative for traffic light control in urban areas.

The investigation conducted in this thesis, produced the following research opportunities:

1. To solidify the conclusions of this thesis, the proposed scheme should also be evaluated in a realistic simulation with varying demands. In [17], a simulation is conducted for the proposed scheme, however the manually constructed network is small and does not include enough sudden events that may occur in a real life network, like car crushes, pedestrians crossing the streets etc. A simulation including the aforementioned, would produce robust evidence for the proposed scheme's ability to track in real-time the critical occupancy and therefore, alleviate the congestion.

2. Different approaches on ESC implementation for urban traffic control should also be investigated. Using a faster convergence, enhanced ESC scheme, directly optimizing the offsets and cycle lengths could even be possible. ESC could also be applied to other urban or even highway traffic light controllers for optimizing their throughput by perturbing the parameters of the controller.

3. The adaptive perimeter control flow could also be constructed, using various other adaptive control techniques for the real-time estimation of the unknown critical occupancy. Enhanced ESC schemes could also be applied in order to achieve faster convergence.

BIBLIOGRAPHY

[1] R. Arnott and K. Small, "The Economics of Traffic Congestion," *American Scientist*, vol. 82, no. 5, pp. 446–455, 1994.

[2] F. Laden, L. M. Neas, D. W. Dockery, and J. Schwartz, "Association of fine particulate matter from different sources with daily mortality in six U.S. cities.," *Environmental Health Perspectives*, vol. 108, no. 10, p. 7, 2000.

[3] H. R. Bae, "Adverse effects of air pollution-derived fine particulate matter on cardiovascular homeostasis and disease," p. 12.

[4] R. M. Jusoh and K. Ampountolas, "Multi-gated perimeter flow control of monocentric cities," p. 25.

[5] K. Aboudolas and N. Geroliminis, "Perimeter and boundary flow control in multi-reservoir heterogeneous networks," *Transportation Research Part B: Methodological*, vol. 55, pp. 265–281, Sep. 2013, doi: 10.1016/j.trb.2013.07.003.

[6] L. Zhang, T. M. Garoni, and J. de Gier, "A comparative study of Macroscopic Fundamental Diagrams of arterial road networks governed by adaptive traffic signal systems," *Transportation Research Part B: Methodological*, vol. 49, pp. 1–23, Mar. 2013, doi: 10.1016/j.trb.2012.12.002.

[7] J. de Gier, T. M. Garoni, and O. Rojas, "Traffic flow on realistic road networks with adaptive traffic lights," *J. Stat. Mech.*, vol. 2011, no. 04, p. P04008, Apr. 2011, doi: 10.1088/1742-5468/2011/04/P04008.

[8] K. Ampountolas and A. Kouvelas, "Real-time estimation of critical vehicle accumulation for maximum network throughput," in *2015 American Control Conference (ACC)*, Chicago, IL, USA, Jul. 2015, pp. 2057–2062. doi: 10.1109/ACC.2015.7171036.

[9] K. B. Ariyur and M. Krstić, *Real time optimization by extremum seeking control*. Hoboken, NJ: Wiley Interscience, 2003.

[10] M. Krstic and H.-H. Wang, "Stability of extremum seeking feedback for general nonlinear dynamic systems&," p. 7, 2000.

[11] E. Dinçmen, T. Acarman, and B. A. Güvenç, "ABS Control Algorithm via Extremum Seeking Method with Enhanced Lateral Stability," *IFAC Proceedings Volumes*, vol. 43, no. 7, pp. 19–24, Jul. 2010, doi: 10.3182/20100712-3-DE-2013.00017.

[12] M. Gerard, W. Pasillas-Lépine, E. de Vries, and M. Verhaegen, "Adaptation of hybrid five-phase ABS algorithms for experimental validation," *IFAC Proceedings Volumes*, vol. 43, no. 7, pp. 13–18, Jul. 2010, doi: 10.3182/20100712-3-DE-2013.00021.

[13] N. Bizon, "Global Maximum Power Point Tracking (GMPPT) of Photovoltaic array using the Extremum Seeking Control (ESC): A review and a new GMPPT ESC scheme," *Renewable*

and Sustainable Energy Reviews, vol. 57, pp. 524–539, May 2016, doi: 10.1016/j.rser.2015.12.221.

[14] M. A. Rotea, "Logarithmic Power Feedback for Extremum Seeking Control of Wind Turbines," *IFAC-PapersOnLine*, vol. 50, no. 1, pp. 4504–4509, Jul. 2017, doi: 10.1016/j.ifacol.2017.08.381.

[15] H. Fathabadi, "Novel high efficient speed sensorless controller for maximum power extraction from wind energy conversion systems," *Energy Conversion and Management*, vol. 123, pp. 392–401, Sep. 2016, doi: 10.1016/j.enconman.2016.06.046.

[16] O. Trollberg, "Akademisk avhandling som med tillstånd av Kungliga Tekniska högskolan framläg- ges till offentlig granskning för avläggande av doktorsexamen 15 September 2017 i F3, Lindstedtsvägen 26, Kungliga Tekniska högskolan, Stockholm.," p. 173.

[17] R. J. Kutadinata, "Nash Equilibrium Seeking for Augmentation of Urban Traffic Light Control," p. 147.

[18] H. Yu, S. Koga, T. R. Oliveira, and M. Krstic, "Extremum Seeking for Traffic Congestion Control with a Downstream Bottleneck," *arXiv:1904.04315 [math]*, Apr. 2019, Accessed: May 11, 2022. [Online]. Available: http://arxiv.org/abs/1904.04315

[19] S. J. Garvey, "Engineering Cybernetics. H. S. Tsien. McGraw–Hill, New York, 1954. 289 pp. Diagrams. 46s. 6d.," *J. R. Aeronaut. Soc.*, vol. 59, no. 535, pp. 511–511, Jul. 1955, doi: 10.1017/S036839310011956X.

[20] L. Hu *et al.*, "Sliding mode extremum seeking control based on improved invasive weed optimization for MPPT in wind energy conversion system," *Applied Energy*, vol. 248, pp. 567–575, Aug. 2019, doi: 10.1016/j.apenergy.2019.04.073.

[21] S. J. Moura and Y. A. Chang, "Lyapunov-based switched extremum seeking for photovoltaic power maximization," *Control Engineering Practice*, vol. 21, no. 7, pp. 971–980, Jul. 2013, doi: 10.1016/j.conengprac.2013.02.009.

[22] I. Munteanu, A. I. Bratcu, and E. Ceangă, "Wind turbulence used as searching signal for MPPT in variable-speed wind energy conversion systems," *Renewable Energy*, vol. 34, no. 1, pp. 322–327, Jan. 2009, doi: 10.1016/j.renene.2008.03.001.

[23] N. Bizon, "Searching of the extreme points on photovoltaic patterns using a new Asymptotic Perturbed Extremum Seeking Control scheme," *Energy Conversion and Management*, vol. 144, pp. 286–302, Jul. 2017, doi: 10.1016/j.enconman.2017.04.065.

[24] L. Wang, S. Chen, and K. Ma, "On stability and application of extremum seeking control without steady-state oscillation," *Automatica*, vol. 68, pp. 18–26, Jun. 2016, doi: 10.1016/j.automatica.2016.01.009.

[25] S. L. Brunton, X. Fu, and J. N. Kutz, "Extremum-Seeking Control of a Mode-Locked Laser," *IEEE J. Quantum Electron.*, vol. 49, no. 10, pp. 852–861, Oct. 2013, doi: 10.1109/JQE.2013.2280181.

[26] Y. Li and Z. Tong, “Development of real-time adaptive model-free extremum seeking control for CFD-simulated thermal environment,” *Sustainable Cities and Society*, vol. 74, p. 103166, Nov. 2021, doi: 10.1016/j.scs.2021.103166.

[27] E. Hellstrom, D. Lee, L. Jiang, A. G. Stefanopoulou, and H. Yilmaz, “On-Board Calibration of Spark Timing by Extremum Seeking for Flex-Fuel Engines,” *IEEE Trans. Contr. Syst. Technol.*, vol. 21, no. 6, pp. 2273–2279, Nov. 2013, doi: 10.1109/TCST.2012.2236093.

[28] R. van der Weijst, T. van Keulen, and F. Willems, “Constrained multivariable extremum-seeking for online fuel-efficiency optimization of Diesel engines,” *Control Engineering Practice*, vol. 87, pp. 133–144, Jun. 2019, doi: 10.1016/j.conengprac.2019.03.008.

[29] D. Zhou, A. Ravey, A. Al-Durra, and F. Gao, “A comparative study of extremum seeking methods applied to online energy management strategy of fuel cell hybrid electric vehicles,” *Energy Conversion and Management*, vol. 151, pp. 778–790, Nov. 2017, doi: 10.1016/j.enconman.2017.08.079.

[30] S. L. Brunton and J. N. Kutz, “Data Driven Science & Engineering,” p. 572, 2017.

[31] C. Yin, B. Stark, Y. Chen, and S. Zhong, “Adaptive minimum energy cognitive lighting control: Integer order vs fractional order strategies in sliding mode based extremum seeking,” *Mechatronics*, vol. 23, no. 7, pp. 863–872, Oct. 2013, doi: 10.1016/j.mechatronics.2013.09.004.

[32] C. Centioli *et al.*, “Maximization of the lower hybrid power coupling in the Frascati Tokamak Upgrade via extremum seeking,” *Control Engineering Practice*, vol. 16, no. 12, pp. 1468–1478, Dec. 2008, doi: 10.1016/j.conengprac.2008.04.008.

[33] J. Zhao, W. Jing, and J. Wang, “An indirect optimization scheme for tuning a fractional order PI controller using extremum seeking,” *Mechatronics*, vol. 56, pp. 146–156, Dec. 2018, doi: 10.1016/j.mechatronics.2018.11.003.

[34] H. De las Casas, H. Warner, and H. Richter, “Real-time optimization of an ellipsoidal trajectory orientation using muscle effort with Extremum Seeking Control,” *Medical Engineering & Physics*, vol. 91, pp. 19–27, May 2021, doi: 10.1016/j.medengphy.2021.03.009.

[35] N. Beniich, B. Abouzaid, and D. Dochain, “Extremum seeking control for a mass structured cell population balance model in a bioreactor,” *IFAC-PapersOnLine*, vol. 53, no. 2, pp. 11392–11397, 2020, doi: 10.1016/j.ifacol.2020.12.573.

[36] S. L. Brunton, C. W. Rowley, S. R. Kulkarni, and C. Clarkson, “Maximum Power Point Tracking for Photovoltaic Optimization Using Ripple-Based Extremum Seeking Control,” *IEEE Trans. Power Electron.*, vol. 25, no. 10, pp. 2531–2540, Oct. 2010, doi: 10.1109/TPEL.2010.2049747.

[37] Y. Xiao, Y. Li, and M. Rotea, “Experimental Evaluation of Extremum Seeking Based Region-2 Controller for CART3 Wind Turbine,” presented at the 34th Wind Energy Symposium, San Diego, California, USA, Jan. 2016. doi: 10.2514/6.2016-1737.

[38] G. Michellone, “54 ANTI-SKID BRAKING SYSTEMS,” p. 6.

[39] P. W. A. Zegelaar, *The dynamic response of tyres to brake torque variations and road unevennesses*. Delft: Delft Univ. of Technology, 1997.

[40] P. Frihauf, M. Krstic, and T. Basar, "Nash Equilibrium Seeking for Dynamic Systems with Non-Quadratic Payoffs," *IFAC Proceedings Volumes*, vol. 44, no. 1, pp. 3605–3610, Jan. 2011, doi: 10.3182/20110828-6-IT-1002.00232.

[41] S. Butterworth, "On the Theory of Filter Amplifiers," *Experimental Wireless and the Wireless Engineer*, 1930.

[42] J. Shi, L. Hu, F. Xue, Z. Qin, L. Ling, and L. Ma, "IIWO Based Sliding Mode Extremum Seeking Control for MPPT in Wind Energy Conversion System," *Energy Procedia*, vol. 158, pp. 85–90, Feb. 2019, doi: 10.1016/j.egypro.2019.01.050.

APPENDIX

All codes used for the simulations of Chapter 4 are presented in this appendix, written in the Matlab programming environment. Code for example 4.1

```
P = @(u,t)(60-(4-(u)).^2);
u = 0;
y0 = P(u,0);
ustar = @(t)(4);
ystar = @(t)(60);
% Parameters of ESC
freq = 100; % sample frequency
dt = 1/freq;
T = 10; % total period of simulation (in seconds)
A = .2;  % amplitude
omega = 10*2*pi; % 10 Hz
phase = 0;
K = 3;   % integration gain

% high pass filter
butterorder=1;
butterfreq=2;  % in Hz for 'high'
[b,a] = butter(butterorder,butterfreq*dt*2,'high')
ys = zeros(1,butterorder+1)+y0;
HPF=zeros(1,butterorder+1);

uhat=u;
for i=1:T/dt
    t = (i-1)*dt;
    time(i) = t;
    yvals(i) = P(u,t);
    ustars(i) = ustar(t);
    ystars(i) = ystar(t);
    for r=1:butterorder
        ys(r) = ys(r+1);
        HPF(r) = HPF(r+1);
    end
    ys(butterorder+1) = yvals(i);
    HPFnew = 0;
    for r=1:butterorder+1
       HPFnew = HPFnew + b(r)*ys(butterorder+2-r);
    end
    for r=2:butterorder+1
       HPFnew = HPFnew - a(r)*HPF(butterorder+2-r);
    end
    HPF(butterorder+1) = HPFnew;


    xi = HPFnew*sin(omega*t + phase);


    uhat = uhat + xi*K*dt;
    u = uhat + A*sin(omega*t + phase);
    uhats(i) = uhat;
    uvals(i) = u;
```

```
end

%%
figure
subplot(2,1,1)
plot(time,uvals,time,uhats,time,ustars,'LineWidth',1.2)
l1=legend('$u$','$\hat{u}$')
set(l1,'interpreter','latex','Location','SouthEast')
grid on
subplot(2,1,2)
plot(time,yvals,time,ystars,'LineWidth',1.2)
ylim([-0.1 65])
l1=legend('$y$','$y*$')
set(l1,'interpreter','latex','Location','SouthEast')
grid on
```

Code used in example 4.2

```
P = @(u,t)(50+((u)-4)+(4-(u)).^2);
u = 0;
y0 = P(u,0);  % u = 0

% ESC Parameters
freq = 100; % sample frequency
dt = 1/freq;
T = 10; % total period of simulation (in seconds)
A = .1;  % amplitude
omega = 10*pi; % 5 Hz
phase = 0;
K = 10;   % integration gain

% High pass filter (Butterworth filter)
butterorder=1;
butterfreq=5;  % in Hz for 'high'

[b,a] = butter(butterorder,butterfreq*dt*2,'high')
ys = zeros(1,butterorder+1)+y0;
HPF=zeros(1,butterorder+1);

uhat=u;



for i=1:T/dt
    t = (i-1)*dt;
    time(i) = t;
    yvals(i)=P(u,t);
```

```
    for r=1:butterorder
        ys(r) = ys(r+1);
        HPF(r) = HPF(r+1);
    end
    ys(butterorder+1) = yvals(i);
    HPFnew = 0;
    for r=1:butterorder+1
        HPFnew = HPFnew + b(r)*ys(butterorder+2-r);
    end
    for r=2:butterorder+1
        HPFnew = HPFnew - a(r)*HPF(butterorder+2-r);
    end
    HPF(butterorder+1) = HPFnew;

    xi = HPFnew*sin(omega*t + phase);
    xi = xi-0.025;

    uhat = uhat - xi*K*dt;
    u = uhat + A*sin(omega*t + phase);
    uhats(i) = uhat;
    uvals(i) = u;
    uset(i) = 4;
    yset(i) = 50;
end

%%
figure
subplot(2,1,1)
plot(time,uvals,time,uhats,time,uset,'LineWidth',1.2)
l1=legend('$u$','$\hat{u}$')
set(l1,'interpreter','latex','Location','SouthEast')
grid on
subplot(2,1,2)
plot(time,yvals,time,yset,'LineWidth',1.2)
l1=legend('y','y*')
set(l1,'interpreter','latex','Location','SouthEast')
ylim([0 70])
grid on
```

Code used in 4.3.1

```
P = @(u,t)(60-(10-(u)-2*sin(t/4)).^2);
u = 0;
y0 = P(u,0);
ustar = @(t)(10-2*sin(t/4));
ystar = @(t)(60);
% Parameters of ESC
freq = 100; % sample frequency
dt = 1/freq;
T = 100; % total period of simulation (in seconds)
A = .2;  % amplitude
omega = 10*2*pi; % 10 Hz
phase = 0;
K = 4;   % integration gain

% high pass filter
```

```
butterorder=1;
butterfreq=2;  % in Hz for 'high'
[b,a] = butter(butterorder,butterfreq*dt*2,'high')
ys = zeros(1,butterorder+1)+y0;
HPF=zeros(1,butterorder+1);

uhat=u;
for i=1:T/dt
    t = (i-1)*dt;
    time(i) = t;
    yvals(i) = P(u,t);
    ustars(i) = ustar(t);
    ystars(i) = ystar(t);
    for r=1:butterorder
        ys(r) = ys(r+1);
        HPF(r) = HPF(r+1);
    end
    ys(butterorder+1) = yvals(i);
    HPFnew = 0;
    for r=1:butterorder+1
       HPFnew = HPFnew + b(r)*ys(butterorder+2-r);
    end
    for r=2:butterorder+1
       HPFnew = HPFnew - a(r)*HPF(butterorder+2-r);
    end
    HPF(butterorder+1) = HPFnew;


    xi = HPFnew*sin(omega*t + phase);


    uhat = uhat + xi*K*dt;
    u = uhat + A*sin(omega*t + phase);
    uhats(i) = uhat;
    uvals(i) = u;
end

%%
figure
subplot(2,1,1)
plot(time,uvals,time,uhats,time,ustars,'LineWidth',1.2)
l1=legend('$u$','$\hat{u}$')
set(l1,'interpreter','latex','Location','SouthEast')
grid on
subplot(2,1,2)
plot(time,yvals,time,ystars,'LineWidth',1.2)
l1=legend('$y$','$y*$')
set(l1,'interpreter','latex','Location','SouthEast')
ylim([-0.1 65])
grid on
```

Supplementary code for example in 4.3.2

```
t = 0:.001:100;
 ustar(:,1) = t;
```

```
 ustar(:,2) = .005*exp(.02*t);
```

Supplementary Code for parameters declaration, for example in 4.4

```
% vehicle parameters
I = 1.4;
m = 400;
R = 0.3;
g = 9.81;
B = 0.01;
% initial conds
Miopt = 0.5;
lopt = 0.15;
v_0 = 33.33; %m/s
w_0 = v_0/R; %?=0
%ESC Parameters
freq = 2.7;
phase = 0;
k = 2;
amp = 1;
a = 0.05;
d = 1;
p = 2.6;
```

Code for the static problems in 4.5.2

```
% (from TAYLOR)monday
%P = @(u,t)(762.292-1.9852*(20.864-(u)).^2);

% tuesday
%P = @(u,t)(775.01-1.2135*(24.736-(u)).^2);

%   wednesday
%P = @(u,t)(742.509-1.8022*(20.664-(u)).^2);

%    thursday
%P = @(u,t)(787.656-1.4866*(22.975-(u)).^2);

%   friday
%P = @(u,t)(770.109-1.3484*(23.754-(u)).^2);

%  saturday
%P = @(u,t)(739.972-1.699*(20.625-(u)).^2);

%   sunday
P = @(u,t)(669.744-3.67*(14.538-(u)).^2);



u = 0;
y0 = P(u,0);

% Extremum Seeking Control Parameters
freq = 100; % sample frequency
```

```
dt = 1/freq;
T = 100; % total period of simulation (in seconds)
A = .05;  % amplitude
d = 1 ;  %demodulation amplitude
omega = 10*2*pi; % 10 Hz
phase = 0;
K = 1;   % integration gain

% high pass filter
butterorder=1;
butterfreq=5;  % in Hz for 'high'
[b,a] = butter(butterorder,butterfreq*dt*2,'high')
ys = zeros(1,butterorder+1)+y0;
HPF=zeros(1,butterorder+1);

uhat=u;
for i=1:T/dt
    t = (i-1)*dt;
    time(i) = t;
    yvals(i)=P(u,t);

    for k=1:butterorder
        ys(k) = ys(k+1);
        HPF(k) = HPF(k+1);
    end
    ys(butterorder+1) = yvals(i);
    HPFnew = 0;
    for k=1:butterorder+1
        HPFnew = HPFnew + b(k)*ys(butterorder+2-k);
    end
    for k=2:butterorder+1
        HPFnew = HPFnew - a(k)*HPF(butterorder+2-k);
    end
    HPF(butterorder+1) = HPFnew;

    xi = HPFnew*d*sin(omega*t + phase);
    uhat = uhat + xi*K*dt;
    u = uhat + A*sin(omega*t + phase);
    xhats(i) = uhat;
    xvals(i) = u;

    %moday
   % fdef(i) = 762.292;
    %ndef(i) = 20.864;

    %tues
%    ftri(i) = 775.01;
 %   ntri(i) = 24.736;

 %wed
%   ftet(i) = 742.509;
 %   ntet(i) = 20.664;

 %thurs
   % fpem(i) = 787.656;
```

```
    %npem(i) = 22.975;

    %fri
%   fpar(i) = 770.109;
 %   npar(i) = 23.754;

 %satur
%    fsav(i) = 739.972;
 %   nsav(i) = 20.625;

 %sun
    fkyr(i) = 669.744;
    nkyr(i) = 14.538;
end

%monday
%figure
%subplot(2,1,1)
%plot(time,xvals,time,xhats,time,ndef,'LineWidth',1.2)
%l1=legend('$x$','$\hat{x}$')
%ylim([0 25])
%set(l1,'interpreter','latex','Location','SouthEast')
%grid on
%subplot(2,1,2)
%plot(time,yvals,time,fdef,'LineWidth',1.2)
%ylim([0 850])
%l1=legend('$y$','$y*$')
%set(l1,'interpreter','latex','Location','SouthEast')
%grid on

%tuesday
%figure
%subplot(2,1,1)
%plot(time,xvals,time,xhats,time,ntri,'LineWidth',1.2)
%l1=legend('$x$','$\hat{x}$')
%ylim([0 25])
%set(l1,'interpreter','latex','Location','SouthEast')
%grid on
%subplot(2,1,2)
%plot(time,yvals,time,ftri,'LineWidth',1.2)
%ylim([0 850])
%l1=legend('$y$','$y*$')
%set(l1,'interpreter','latex','Location','SouthEast')
%grid on

%wednesday
%figure
%subplot(2,1,1)
%plot(time,xvals,time,xhats,time,ntet,'LineWidth',1.2)
%l1=legend('$x$','$\hat{x}$')
%ylim([0 25])
%set(l1,'interpreter','latex','Location','SouthEast')
%grid on
%subplot(2,1,2)
%plot(time,yvals,time,ftet,'LineWidth',1.2)
%ylim([0 850])
```

```
%l1=legend('$y$','$y*$')
%set(l1,'interpreter','latex','Location','SouthEast')
%grid on

%thursday
%figure
%subplot(2,1,1)
%plot(time,xvals,time,xhats,time,npem,'LineWidth',1.2)
%l1=legend('$x$','$\hat{x}$')
%ylim([0 25])
%set(l1,'interpreter','latex','Location','SouthEast')
%grid on
%subplot(2,1,2)
%plot(time,yvals,time,fpem,'LineWidth',1.2)
%ylim([0 850])
%l1=legend('$y$','$y*$')
%set(l1,'interpreter','latex','Location','SouthEast')
%grid on

%friday
%figure
%subplot(2,1,1)
%plot(time,xvals,time,xhats,time,npar,'LineWidth',1.2)
%l1=legend('$x$','$\hat{x}$')
%ylim([0 25])
%set(l1,'interpreter','latex','Location','SouthEast')
%grid on
%subplot(2,1,2)
%plot(time,yvals,time,fpar,'LineWidth',1.2)
%ylim([0 850])
%l1=legend('$y$','$y*$')
%set(l1,'interpreter','latex','Location','SouthEast')
%grid on

%saturday
%figure
%subplot(2,1,1)
%plot(time,xvals,time,xhats,time,nsav,'LineWidth',1.2)
%l1=legend('$x$','$\hat{x}$')
%ylim([0 25])
%set(l1,'interpreter','latex','Location','SouthEast')
%grid on
%subplot(2,1,2)
%plot(time,yvals,time,fsav,'LineWidth',1.2)
%ylim([0 850])
%l1=legend('$y$','$y*$')
%set(l1,'interpreter','latex','Location','SouthEast')
%grid on

%sunday
figure
subplot(2,1,1)
plot(time,xvals,time,xhats,time,nkyr,'LineWidth',1.2)
l1=legend('$x$','$\hat{x}$')
ylim([0 25])
set(l1,'interpreter','latex','Location','SouthEast')
```

```
grid on
subplot(2,1,2)
plot(time,yvals,time,fkyr,'LineWidth',1.2)
ylim([0 850])
l1=legend('$y$','$y*$')
set(l1,'interpreter','latex','Location','SouthEast')
grid on
```

Code used for application in 4.5.3

```
%load('Monday.mat')
%load('tuesday.mat')
load('wednesday.mat')
%load('thursday.mat')
%load('friday.mat')
%load('saturday.mat')
%load('sunday.mat')

y0 = 600;
u = 20;
% Parameters of ESC
dt = 90; %seconds
omega = 0.001*2*pi; % 0.001 Hz
Ap = 0.2;
phase = -pi;
K = 0.0001;   % integration gain

% high pass filter
butterorder=2;
butterfreq=0.0009;  % in Hz for 'high'
[b,a] = butter(butterorder,butterfreq*dt*2,'high');
ys = zeros(1,butterorder+1)+y0;
HPF = zeros(1,butterorder+1);

%initial values
Time(1) = 0;
uhat = u;
xi(1) = 0;
ro(1) = 0;

for i=2:961

%for Monday, for i=2:1022



    t = Time(i-1)*86400;   %Time: in seconds
    Ti(i) = t/3600;  %Time in hours for the plots
    yvals(i)=Flow(i-1);

    %inactivity when occupancy<10%
    if Occupancy(i-1)<10
     uvals(i) = u;
     uhats(i) = uhat;
```

```
      xi(i) = 0;
      ro(i) = 0;
      continue
     end

     for r=1:butterorder
         if Occupancy(i-1)<10
             continue
         end
         ys(r) = ys(r+1);
        HPF(r) = HPF(r+1);
    end
    ys(butterorder+1) = yvals(i);
    HPFnew = 0;
    for r=1:butterorder+1
         if Occupancy(i-1)<10
            continue
       end
      HPFnew = HPFnew + b(r)*ys(butterorder+2-r);
    end
    for r=2:butterorder+1
        if Occupancy(i-1)<10
          continue
    end
     HPFnew = HPFnew - a(r)*HPF(butterorder+2-r);
    end
    HPF(butterorder+1) = HPFnew;
    ro(i)=HPFnew;

     %gradient estimate, signal xi
     xi(i) = HPFnew*sin(omega*t + phase);


     uhat = uhat + xi(i)*K*dt;
     u = uhat + Ap*sin(omega*t);

     %upper lower boundaries
     if u >= 30;
        u = 30;
        uhat = u;
    elseif u <= 10;
        u = 10;
        uhat = u;
     end
     uvals(i) = u;
     uhats(i) = uhat;
end
%%
figure
subplot (5,1,1)
plot(24*Time,Flow,'LineWidth',1.2)
ylim([0 1000])
xlim([0 24])
grid on

subplot(5,1,2)
```

```
plot(24*Time,Occupancy,'LineWidth',1.2)
ylim([0 40])
xlim([0 24])
grid on

subplot(5,1,3)
plot(Ti,ro,'LineWidth',1.2)
ylim([-200 200])
l1=legend('filtered');
set(l1,'interpreter','latex','Location','SouthEast')
xlim([0 24])
grid on


subplot(5,1,4)
plot(Ti,xi,'LineWidth',1.2)
ylim([-200 200])
l1=legend('xi');
set(l1,'interpreter','latex','Location','SouthEast')
xlim([0 24])
grid on

subplot (5,1,5)
plot(Ti,uvals,Ti,uhats,'LineWidth',1.2);
l1=legend('$u$','$\hat{u}$');
set(l1,'interpreter','latex','Location','SouthEast')
xlim([0 24])
grid on
```